T2R2 東京科学大学 リサーチリポジトリ
Science Tokyo Research Repository

論文 / 著書情報
Article / Book Information

題目(和文)	
Title(English)	Role of bismuth at the interface between bismuth layered ferroelectric thin film and platinum electrode for ferroelectric memory applications
著者(和文)	渡部浩司
Author(English)	Koji Watanabe
出典(和文)	学位:博士(工学), 学位授与機関:東京工業大学, 報告番号:甲第11602号, 授与年月日:2020年9月25日, 学位の種別:課程博士, 審査員:若林 整,筒井 一生,舟窪 浩,渡辺 正裕,大見 俊一郎,角嶋 邦之
Citation(English)	Degree:Doctor (Engineering), Conferring organization: Tokyo Institute of Technology, Report number:甲第11602号, Conferred date:2020/9/25, Degree Type:Course doctor, Examiner:,,,,,
学位種別(和文)	博士論文
Type(English)	Doctoral Thesis

Powered by T2R2 (Science Tokyo Research Repository)

Doctoral Thesis

Role of bismuth at the interface between bismuth layered ferroelectric thin film and platinum electrode for ferroelectric memory applications

Koji Watanabe

Supervisor: Professor Hitoshi Wakabayashi

Date: August 27, 2020

Department of Electrical and Electronic Engineering,
School of Engineering,
Tokyo Institute of Technology, Japan

Signature of Autor ______________________________

Department of Electrical and Electronic Engineering, August 27, 2020

Certified by ______________________________

Hitoshi, Wakabayashi, Professor, Thesis Supervisor

Role of bismuth at the interface between bismuth layered ferroelectric thin film and platinum electrode for ferroelectric memory applications

Department of Electrical and Electronic Engineering
Koji Watanabe

Abstract

Electrical properties and electronic structures of ferroelectric strontium bismuth tantalate ($SrBi_2Ta_2O_9$: SBT) thin films, sandwiched between Pt electrodes, have been studied. The Schottky emission dominated the leakage current at voltages above the Ohmic conduction regime, while space charges limited by currents, for which the observed temperature dependence is correctly predicted in the Rose's theory, appeared to dominate the leakage current in the SBT thin films with high conductivity including Bi-excess SBT films. The X-ray photoemission spectroscopy (XPS) depth profiling indicated that Bi has diffused into the ferroelectric–metal interface and also influenced the electronic conduction mechanism of the ferroelectric capacitors. Ultraviolet photoelectron spectroscopy (UPS) and XPS were used to determine the electronic structure near the band-edge of SBT thin films. The spectra for Bi-excess SBT film indicate additional density of states (DOS) in the wide bandgap of the SBT film. These electronic structural data are used to explain the observed dependency of the electrical properties of the SBT/electrode junction on the Bi concentration. Then, an optimal composition ratio of the SBT thin film is proposed, which is expected to have high ferroelectric properties and stable contact properties with the electrode material. Finally, the recent research trend of ferroelectric memories and the possibility of future application development will be mentioned.

Thesis Supervisor: Hitoshi Wakabayashi
Title: Professor

Koji Watanabe
August 27, 2020

Acknowledgements

First, I would like to thank Professor Hitoshi Wakabayashi in Tokyo Institute of Technology for providing a great deal of guidance in completing this study.

I would like to thank Professor Kazuo Tsutsui, Professor Hiroshi Funakubo, Associate Professor Masahiro Watanabe, Associate Professor Shunichiro Ohmi, and Asociate Professor Kuniyuki Kakushima of Tokyo Institute of Technology for providing me with useful advice on this research and writing the dissertation.

This research was originally conducted as a part of the research and development activities of Sony Corporation. I would like to thank the boss and members of the FeRAM project at Sony Corporation for supporting my research at that time.

Part of this research was done when I stayed at the University of New South Wales in Australia. I would like to thank Professors James F. Scott and Robert N. Lamb for teaching at the university at that time (Professor James. F. Scott is still active at the University of St Andrews, UK and Professor Robert N. Lamb is still active at the University of Melbourne, Australia).

Contents

Chapter 1 Introduction of this thesis 14

1.1 Background 14

1.2 Ferroelectric memory 17

1.3 Aurivillius- structure layered bismuth compounds 21

1.4 Structure and approach of this thesis 24

Chapter 2 The effect of Bi contents on the crystallization of SBT thin film .. 27

2.1 Introduction 27

2.2 Experiments 29

2.3 The effect of Bi contents for ferroelectric SBT thin film formation 34

2.4 Evaluation of Bi contents in SBT film 42

2.5 Summary 46

Chapter 3 The effect of Bi contents on current-voltage characteristics of SBT thin film capacitor 47

3.1 Introduction 47

3.2 Experiments 48

3.3 Current-voltage characteristics dependence of Bi contents 50

3.4 Evaluation of contact in Pt/SBT/Pt capacitor....52

3.5 Summary....60

Chapter 4 Electronic Structures dependence on Bi contents of SBT thin film

....61

4.1 Introduction....61

4.2 Experiments....62

4.3 Electronic structures evaluated by XPS and UPS....64

4.4 Evaluation of bandgap states....67

4.5 Summary....70

Chapter 5 Energy band model for SBT thin film capacitor....71

5.1 Introduction....71

5.2 Energy band model....72

5.3 Summary....82

Chapter 6 Consideration on optimum composition ratio of SBT thin film....85

6.1 Introduction....85

6.2 Consideration on optimum composition ratio of SBT thin film....86

6.3 Summary....92

Chapter 7 Recent advances in ferroelectric materials for ferroelectric memory research 93

7.1 Introduction 93

7.2 Research progress of SBT 95

7.3 New ferroelectric material 97

7.4 Benchmark of various ferroelectric thin films and memory devices using them 100

7.5 Future application development 111

7.6 Summary 114

Chapter 8 Conclusions 117

8.1 Summary of this thesis 117

8.2 Conclusions of this thesis 123

8.3 Future direction 125

List of Figures

Figure 1.1 Excerpt from the explanatory material for Society 5.0 prepared by the Cabinet Office. 15

Figure 1.2 Excerpt from the explanatory document of the Science and Technology Basic Plan related to Society 5.0 prepared by the Ministry of Education, Culture, Sports, Science and Technology. 16

Figure 1.3 Typical structure of Ferroelectric Random Access Memory (FeRAM). 19

Figure 1.4 Crystal structure for perovskite-type ferroelectric $Pb(Zr,Ti)O_3$ (PZT) and typical hysteresis curve. 19

Figure 1.5 Repetition properties of residual polarization (Pr) for $Pt/Pb(Zr,Ti)O_3/Pt$ thin film capacitor and $Pt/SrBi_2Ta_2O_9/Pt$ thin film capacitor. 23

Figure 1.6 Crystal structure of bismuth-layered perovskite. 23

Figure 1.7 Structure of this thesis. 26

Figure 2.1 Film formation process for SBT film. 31

Figure 2.2 Schematic image of the RTA system. 32

Figure 2.3 Sawyer-Tower circuit for measuring the hysteresis curve of ferroelectrics. 33

Figure 2.4 XRD patterns for SBT after RTA Process.................................36

Figure 2.5 SEM images for SBT after RTA Process..................................37

Figure 2.6 Schematic diagram of the Sr-Bi-Ta-O fluorite structure quoted from ref. 39...37

Figure 2.7 SEM images of the surface of the SBT films after the crystallization annealing at 800 ℃ with RTA temperatures at (a) 690 and (b) 760 ℃, respectively. 38

Figure 2.8 Comparison of main X-ray diffraction peaks around 2θ=29° for SBT films of 0.8/2.4/2.0 precursor with and without the heat treatment at 800 ℃ for 1 hour in oxygen atmosphere after RTA...38

Figure 2.9 Hysteresis curves of the SBT capacitors with 0.8/2.4/2.0 solution composition and RTA at 760 ℃ / annealed at 800 ℃.............................40

Figure 2.10 Applied voltage dependence of the remanent polarization of SBT thin film capacitors with solution compositions of 0.8/2.4/2.0 and 0.8/2.0/2.0. 41

Figure 2.11 RTA temperature dependence of Bi contents of the SBT films measured by EPMA..45

Figure 3.1 Image of voltage application sequence for leak current (current-voltage dependence) measurement. 49

Figure 3.2 Variation of the leakage current density, *J*, of (a) the Bi-stoichiometric and (b) the Bi-excess samples. 51

Figure 3.3 Variation of $log(J/T^2)$ as a function of the square root of the applied voltage (V) in the 1.8–3.0 V range at different measuring temperatures in the Bi-stoichiometric Pt/SBT/Pt capacitor (a) shown in figure 3.2...........53

Figure 3.4 The Schottky plot of the Bi-stoichiometric Pt/SBT/Pt capacitor. ..53

Figure 3.5 Variation of $log(J/T^2)$ as a function of the square root of the applied voltage (V) at different measuring temperatures in the Bi-excess Pt/SBT/Pt capacitor (b) shown in Figure 3.2. 54

Figure 3.6 The Schottky plot of the Bi-excess Pt/SBT/Pt capacitor.............55

Figure 3.7 Linear plot of J-V curves in the Bi-excess Pt/SBT/Pt capacitor. ..56

Figure 3.8 Current-temperature dependence of the quadratic regime at the different applied voltages in the Bi-excess Pt/SBT/Pt capacitor. 58

Figure 3.9 XPS depth profiles of the both (a) Bi-stoichiometric and (b) Bi-excess SBT capacitors. 59

Figure 4.1 XPS valence-band spectra for Bi-stoichiometric and Bi-excess SBT thin films. 64

Figure 4.2 Total and partial density of state of SBT film taken from ref. 52. .65

Figure 4.3 He I (21.2 eV)-UPS valence-band spectra for Bi-stoichiometric and

Bi-excess SBT thin films. 66

Figure 4.4 Valence-band edge of the SBT thin film measured by He I (21.2 eV)-UPS. 66

Figure 4.5 Bi 4f-XPS spectra for Bi-stoichiometric SBT thin film at (a) normal incidence emission; (b) 60 degree sample tilt. 69

Figure 5.1 UV-visible absorption measurement for SBT thin film on platinum coated substrate (thick line) and platinum coated substrate only (thin line). 73

Figure 5.2 XPS measurement data showing the region near the Fermi level of SBT and Pt. 74

Figure 5.3 Energy-band match-up at the SBT/Pt interface obtained from XPS data and band gap estimated from UV absorption data. 75

Figure 5.4 Expected energy-band match-up at the SBT/$PtBi_2$ interface. 77

Figure 5.5 Expected energy-band match-up at the SBT/Bi interface. 78

Figure 5.6 Expected energy-band match-up at the SBT/Bi_2O_3/Pt interface. 79

Figure 6.1 Voltage dependence of the remanent polarization value obtained by adding the results of the composition ratio of the periphery to Figure 2.10. 89

Figure 6.2 The same data as in Figure 6.1, but the voltage dependence of

the remanent polarization value when the composition ratio was expressed by the film composition measured by EPMA. 90

Figure 6.3 Relationship between the composition ratio of Sr and the composition ratio of Bi by EPMA and the residual polarization value 2Pr at 5 V of the film shown in Figure 6.2 91

Figure 6.4 Schematic diagram of a film structure proposed by the author as an optimal SBT thin film composition for changing the Bi composition ratio in the film thickness direction. 91

Figure 7.1 Schematic figure of the FeFET with MIFS stack take from ref. 72.96

Figure 7.2 Crystal structures of HfO_2 based ferroelectrics and perovskite-based ferroelectrics taken from ref. 78. 99

Figure 7.3 Relationship between the film thickness of the ferroelectric and its remanent polarization value P_r. 103

Figure 7.4 Relationship between the remanent polarization value P_r of the ferroelectric and its coercive electric field E_c. 104

Figure 7.5 Relationship between the area and film thickness of the ferroelectric used in the prototype memory device shown in the lower part of Table 7.1.. 104

Figure 7.6 Estimated lower limit of film thickness and area for SBT and PZT.

.... 107

Figure 7.7 Relationship between the remanent polarization value P_r of the ferroelectric and its coercive electric field E_c including the lines of the necessary coercive electric field derived under certain preconditions. 109

Figure 7.8 Diagram in which the author adds the use cases to Figure 1.2.112

List of Tables

Table 1.1 Characteristics of ferroelectrics and application examples utilizing them. 18

Table 1.2 Performance comparison between FeRAM and other semiconductor memories created in 2000 with reference to ref. 10. 20

Table 2.1 Composition ratios of precursor solutions analyzed by ICP-MS, in the thin films by EPMA and at the surface of the films by XPS. 45

Table 6.1 Comparison of the composition ratio of the precursor solution (starting composition ratio) measure by ICP, the film composition ratio measured by EPMA, and the surface composition ratio measured by XPS obtained by adding the results of the composition ratio of the periphery to Table 2.1. 90

Table 7.1 Comparison of characteristics of ferroelectric materials and characteristics of recent ferroelectric memory devices using them. 101

Table 7.2 Simple comparison table of semiconductor nonvolatile memory extracted from ref. 94. 113

Chapter 1 Introduction of this thesis

1.1 Background

The evolution of the IoT (Internet of Things) in recent years has been remarkable towards the realization of the so-called Society 5.0 world. Along with this, the environment surrounding semiconductor devices including semiconductor memories is also changing drastically. Figure 1.1 is an excerpt from the explanatory material for Society 5.0 prepared by the Cabinet Office[1]. In the information society so far, we have accessed the cloud from the physical space and obtained and used the necessary information. On the other hand, Society 5.0 in the future will create a world in which cyberspace and physical space are highly integrated through artificial intelligence (AI). Figure 1.2 is an excerpt from the explanatory document of the Science and Technology Basic Plan related to Society 5.0 prepared by Ministry of Education, Culture, Sports, Science and Technology[2]. This figure explains the technology required for the integration of cyberspace and physical space and the world that will be realized. From these figures, it is clear that transmitting, storing, and processing large-scale data at high speed, low power consumption, and low cost are necessary and important technologies in Society 5.0. And the point that the importance of edge devices with real-time processing increases can be said to be a feature of Society 5.0. Therefore, a non-volatile memory with low power consumption and high speed is inevitably required. A semiconductor non-volatile

memory using a ferroelectric material has exactly that feature and is suitable for these applications. In addition to this, there are increasing expectations for the application of memory using ferroelectrics to neuromorphic devices. The neuromorphic device is an essential element of the neural network which is the basic configuration of machine learning. In-memory computing has been attracting attention for efficient processing of neural networks. The ideal form from the viewpoint of energy efficiency is an analog AI chip[3)]. Studies have been intensively investigated for using a non-volatile memory using ferroelectric arranged at a cross point in an analog AI chip[4)-7)]. Therefore, it is very meaningful that the materials for the ferroelectric memory and their basic characteristics are discussed.

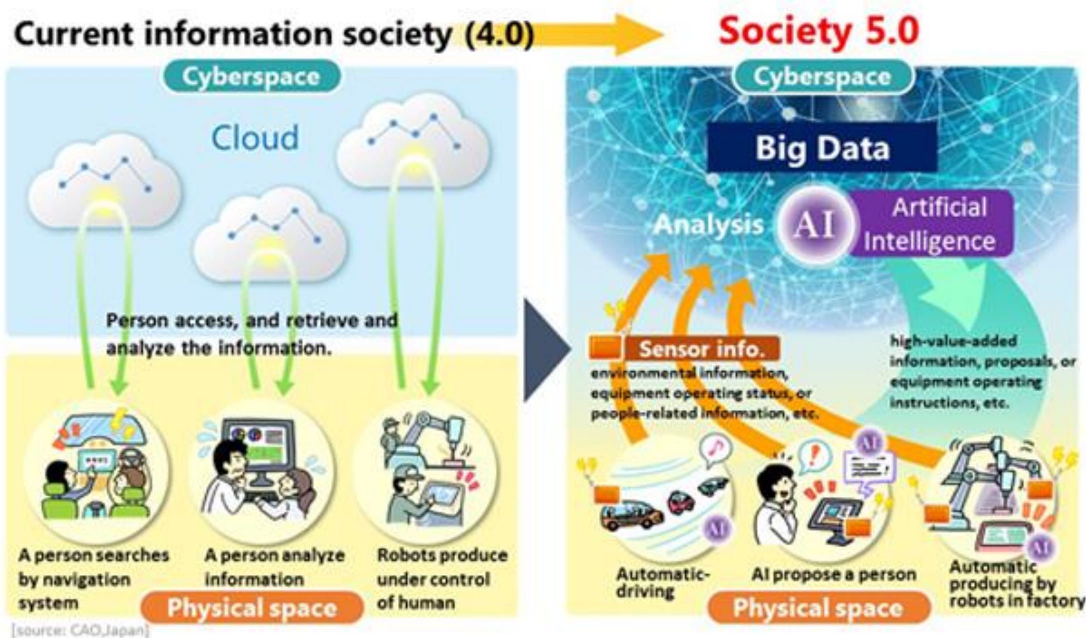

Figure 1.1 Excerpt from the explanatory material for Society 5.0 prepared by the Cabinet Office[1)].

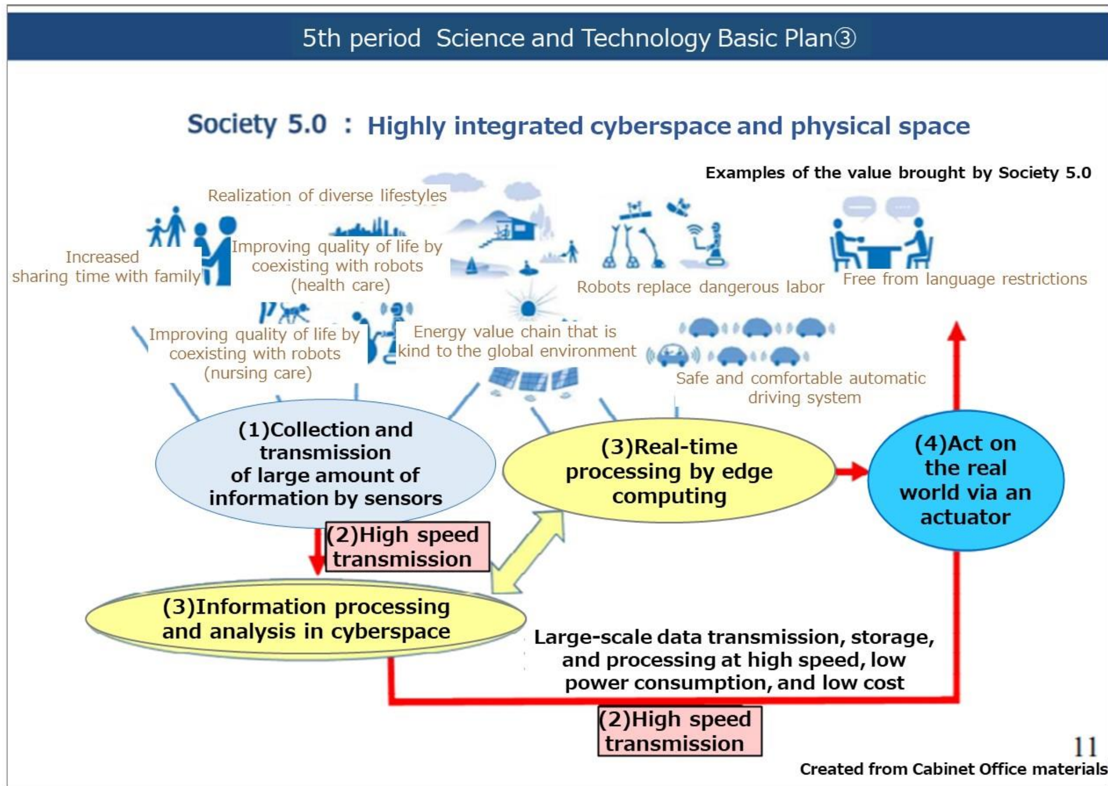

Figure 1.2 Excerpt from the explanatory document of the Science and Technology Basic Plan related to Society 5.0 prepared by the Ministry of Education, Culture, Sports, Science and Technology[2)]. The original is written in Japanese and translated by the author into English.

1.2 Ferroelectric memory

Since ferroelectricity was discovered in 1920[8)], many scientists and engineers have studied many applications in addition to the ferroelectrics themselves. Ferroelectric materials are known for their switchable spontaneous polarizations that are responsive to external stimuli, such as stress, temperature, electric field, and magnetic field. Therefore, ferroelectrics are often called "smart materials" and have found wide applications in sensors and actuators, as well as memory devices (Table 1.1). The applications of ferroelectrics that have been commercialized so far are mainly those using piezoelectricity or pyroelectricity, and those using ferroelectricity are rare. A typical application using ferroelectricity is an application to a non-volatile memory, which has been studied for many years[9),10)]. Ferroelectric Random Access Memory (FeRAM) is similar in construction to DRAM, but using ferroelectric layer instead of dielectric layer to achieve non-volatility. Figure 1.3 shows a typical structure of FeRAM cell and Figure 1.4 shows the crystal structure for perovskite-type ferroelectric $Pb(Zr,Ti)O_3$ (PZT) and the typical hysteresis curve. The ferroelectricity of PZT is caused by the displacement of zirconium atoms or titanium atoms when an external electric field is applied, and the direction of the remanent polarization can be changed by changing the direction of the external electric field by 180 degrees. By setting the remanent polarizations in these different directions to "0" and "1", respectively, the function of the nonvolatile memory is realized. Research on non-volatile memories using ferroelectrics dates back to the 1960s[9)],

but at that time the problem of unstable operation could not be overcome. From the latter half of the 1980s, so-called FeRAM research has been actively conducted[10)-12)]. The background is that progress has been made in oxide thin film deposition technology and the need for new semiconductor nonvolatile memories has increased. Table 1.2 shows a comparison of semiconductor memories at that time[10)]. As shown in Table 1.2, FeRAM was expected to have superior potential in write durability and write speed compared to FLASH memory, which is the same semiconductor nonvolatile memory.

Table 1.1 Characteristics of ferroelectrics and application examples utilizing them.

Properties	Applications
High dielectric constant	Capacitor, Volatile memory
Nonlinear permittivity	Optical modulator, Optical harmonic generator
Piezoelectric	Actuator, Vibrator, Surface acoustic wave filter, Energy harvesting device
Pyroelectric	Heat sensor
Ferroelectric	Non-volatile memory, AI chip
Ferroelectric phase transition	Positive temperature coefficient thermistor
Ferroelectric domain	Quasi phase matching element, Ultra high density recording

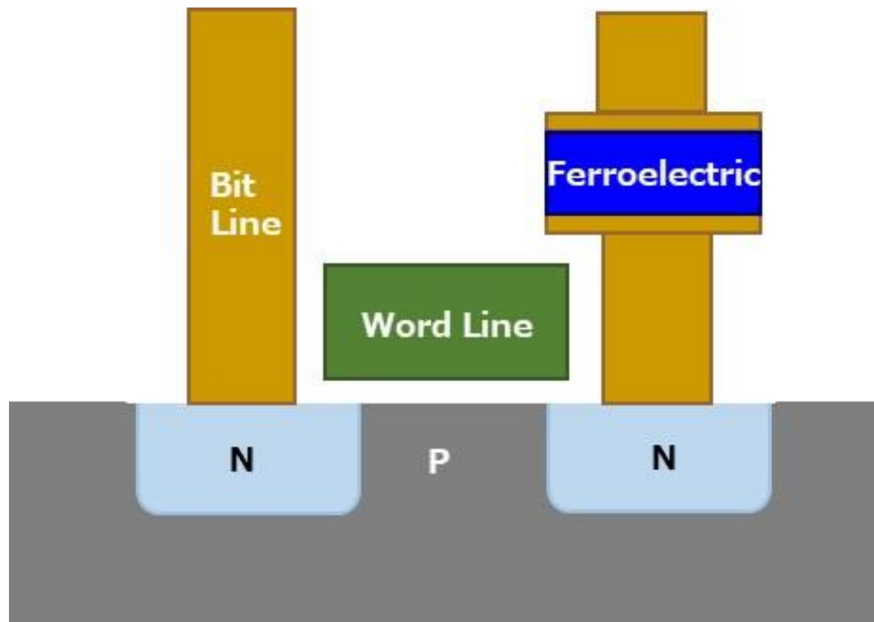

Figure 1.3 Typical structure of Ferroelectric Random Access Memory (FeRAM).

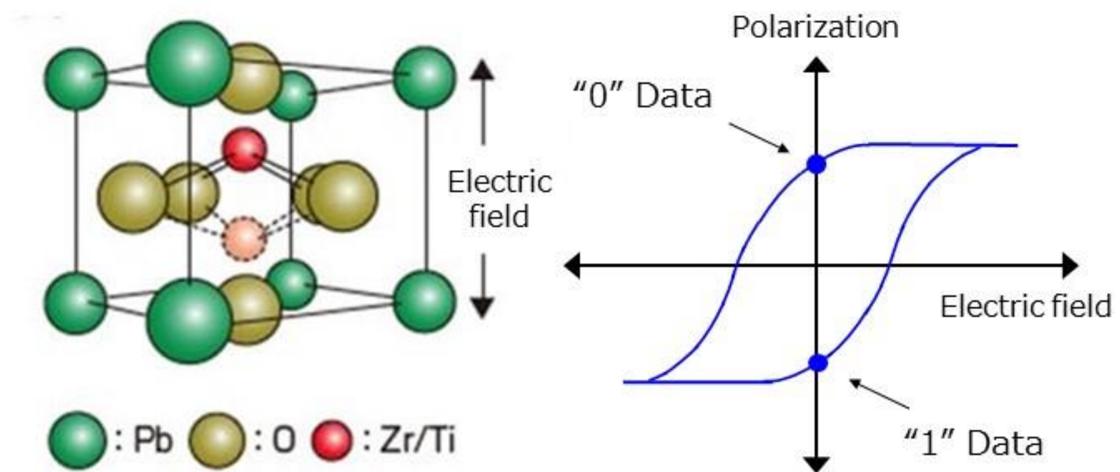

Figure 1.4 Crystal structure for perovskite-type ferroelectric $Pb(Zr,Ti)O_3$ (PZT) (left) and typical hysteresis curve (right).

Table 1.2 Performance comparison between FeRAM and other semiconductor memories created in 2000 with reference to ref. 10.

	FeRAM	DRAM	SRAM	FLASH (NAND)
Nonvolatile	Yes	None	None	Yes
Write durability	10^{6-12}	$> 10^{15}$	$> 10^{15}$	10^{5-6}
Write speed	~100 ns	~50 ns	< 10 ns	~1 ms
Reading durability	10^{6-12}	$> 10^{15}$	$> 10^{15}$	$> 10^{15}$
Standby current	< 1 uA	> 10 uA	> 1 uA	< 1 uA
Cell size	1	1	4	0.8

1.3 Aurivillius- structure-layered bismuth compounds

In the late 1980s, the research on FeRAM using PZT thin film capacitor was preceded, but it had the problem of switching cycle resistance[10),13)]. Capacitors based on Aurivillius-structure layered bismuth compounds[14),15)], such as $SrBi_2Ta_2O_9$ (SBT), with metallic electrode (*e.g.*, Pt), however showed negligible polarization fatigue (Figure 1.5) [12),13)].

Bismuth layered compound is a generic name of a compound in which a Bi_2O_2 layer composed of bismuth and oxygen and a pseudo perovskite layer are connected in a layered manner, and was first synthesized by Aurivillius in 1949[14),15)]. Soon after, the bulk ferroelectric properties were measured by Smolenski[16)] and by Subbarao[17)]. Its crystal structure is a compound having a high crystal anisotropy generally represented by $(Bi_2O_2)^{2+}(A_{m-1}B_mO_{3m+1})^{2-}$. Here, m can take 1 to 8. Figure 1.6 shows a crystal structure when m = 2 ($SrBi_2Ta_2O_9$ (SBT), $SrBi_2Nb_2O_9$ (SBN)). Most of the ferroelectrics of the bismuth layered compound undergo a phase transition from the high temperature side to tetragonal and orthorhombic, and exhibit ferroelectricity in orthorhombic. In the bismuth layered compound, a large spontaneous polarization exists in a plane parallel to the a-axis and the b-axis, that is, in the c-plane. In the case of SBT, rotation occurs in the c-plane in the oxygen octahedron composed of Ta and oxygen, and a dipole moment is generated due to the bias of the charge caused by these displacements[18),19)]. The fatigue of domain inversion in PZT was thought to be caused by oxygen deficiency generated at the

interface between the ferroelectric and the metal electrode[10),13)]. In bismuth layered ferroelectrics, perovskite blocks responsible for ferroelectricity are sandwiched between bismuth oxide layers, so it was recognized as a strong material against oxygen defects. On the other hand, in the perovskite structure or the layered perovskite structure, it is important to control the composition of the multi-component oxides in order to obtain desired electric characteristics and ferroelectric characteristics. Furthermore, when elements having high volatility such as lead (Pb) and bismuth (Bi) are contained, there is a risk that these elements diffuse from the ferroelectric thin film to the electrode and adversely affect the electrical characteristics. There are reports that Pb diffuses into the oxide electrode layer at the interface between the PZT film and the oxide electrode material, forming a reaction layer, and deteriorating the electrical properties[20),21)]. With respect to the SBT film as well, the result of analysis using XPS that Bi was precipitated and existed on the surface was reported[22)] in 1996, and it became necessary to clarify the effect of Bi. Therefore, this research was mainly conducted to clarify the effect of Bi existing on the surface and interface on the electrical properties of the SBT film.

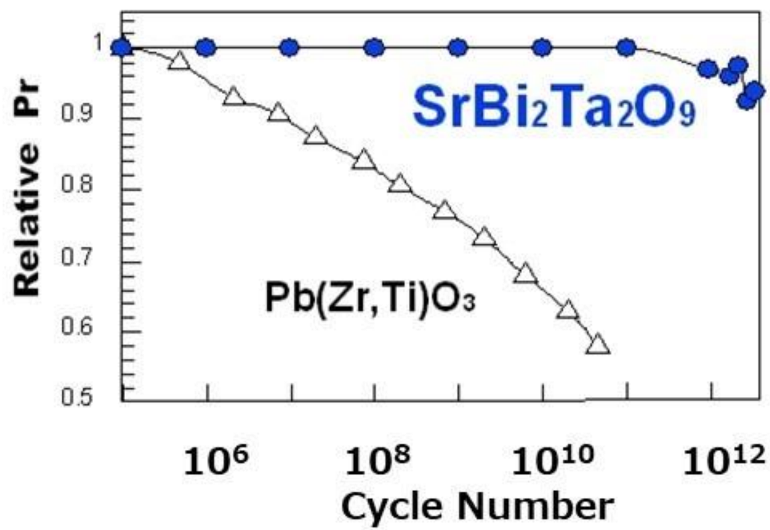

Figure 1.5　Repetition properties of residual polarization (P_r) for Pt/Pb(Zr,Ti)O_3/Pt thin film capacitor and Pt/$SrBi_2Ta_2O_9$/Pt thin film capacitor[13)].

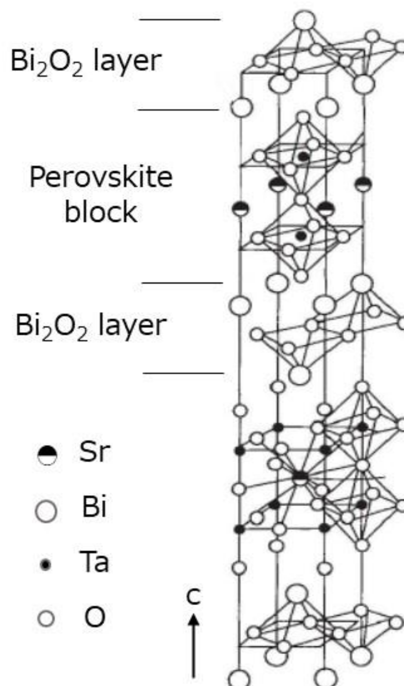

Figure 1.6　Crystal structure of bismuth-layered perovskite. This crystal structure is represented by $(Bi_2O_2)^{2+}(A_{m-1}B_mO_{3m+1})^{2-}$, and this figure is a schematic diagram when m = 2 ($SrBi_2Ta_2O_9$ (SBT), $SrBi_2Nb_2O_9$ (SBN)).

1.4 Structure and approach of this thesis

The author studied SBT thin film capacitors in the late 1990s and applied them to semiconductor nonvolatile memories at the company to which the author belong[23)-27)]. At that time, the technology was not commercialized at that company, but a lot of technical knowledge was obtained.

In this paper, the research results on application of bismuth layered ferroelectrics to FeRAM are introduced. In particular, the electrical and electronic characteristics at the interface between the ferroelectric and the electrode are deeply discussed because contact properties that govern leakage current and breakdown are important for device applications in addition to ferroelectric properties. As mentioned in the previous section, the main purpose was to clarify the influence of Bi existing on the surface and interface. Figure 1.7 shows the structure of this thesis. First, the optimal crystallization process for SBT thin films is discussed. There, an optimal seed layer is selected. The relationship between composition ratio and ferroelectric properties, especially the effect of Bi composition ratio, is also clarified. Next, the electrical properties of Pt/SBT/Pt thin film capacitors are discussed, and then the contact property and the electron conduction mechanism are discussed. Here, the influence of excess Bi is also considered. Subsequently, the surface state and band gap state of SBT will be discussed. And then, the results of the electrical characteristics obtained using the electrical measurement technique and the results of the analysis of the electronic structure

obtained using the surface analysis tool are correlated and the energy band model of the SBT/Pt interface is discussed. Based on these results, discussions are held to clarify the composition ratio of SBT thin films that achieve both high ferroelectric properties and stable contact properties with electrode materials. The control of the Bi composition ratio in the SBT thin film is an important factor. This thesis also discusses how this material technology evolves from recent technological trends. Progress has been made in research on the SBT family of materials, and new ferroelectric materials have also appeared. In addition, areas where future application development is expected are introduced. Although the research results introduced here are a bit old, they relate to basic technologies related to the electrical and electronic properties of ferroelectric thin film capacitors. It is considered useful for current researchers in this field because a ferroelectric thin film capacitor is one of the basic structures when a ferroelectric is applied to a device, and is described here.

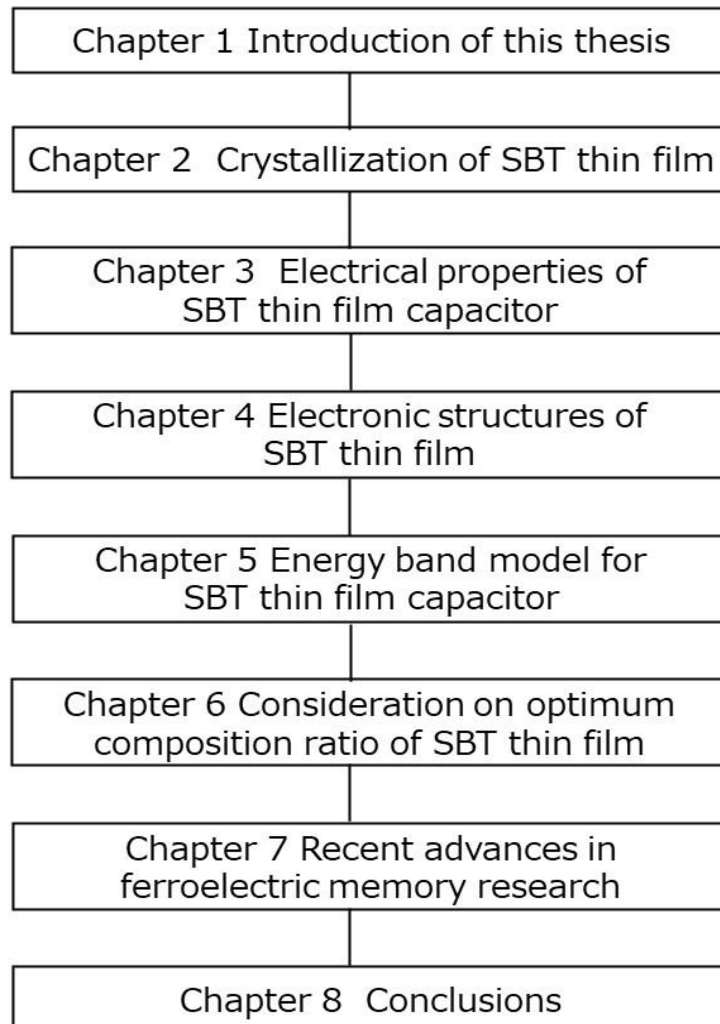

Figure 1.7 Structure of this thesis.

Chapter 2 The effect of Bi contents on the crystallization of SBT thin film

2.1 Introduction

As mentioned in the previous chapter, the SBT showed only negligible polarization fatigue. Therefore, research on the ferroelectric characteristics of SBT thin film capacitors has been actively conducted. However, due to the volatility of bismuth (Bi) in high temperature processing steps, excess Bi fluxes are required to ensure proper phase formation and good electrical properties in SBT thin-film growth. On the other hand, it has been experimentally found that Sr-deficient and Bi-excess SBT thin film has a larger spontaneous polarization value than stoichiometric SBT thin film by Atsuki *et al.*[28)] and by Noguchi *et al*.[29)] They deposited SBT using solution chemistry technology. Although the stoichiometric composition of SBT is Sr/Bi/Ta=1/2/2, they showed that when the starting composition Sr is 0.7 to 0.8 and Bi is 2.2 to 2.4, SBT film exhibits good ferroelectric properties respectively. The reason why the ferroelectric properties of Sr-deficient and/or Bi-excess SBT are excellent was later clarified by Miura, *et al*.[30)] and by Shimakawa *et al*.[31)] The reason is that a part of the Sr site is replaced with Bi, so

that the interaction becomes large and the displacement of the atom becomes large. For these reasons, we want to use Sr-deficient and Bi-excess SBT positively, but as mentioned in the previous chapter, we need to be careful in handling Bi.

SBT films used in this study were prepared using solution chemistry techniques. Although some attempts have been made to form SBT thin films by Metal Organic Chemical Vapor Deposition (MOCVD)[32),33)] or other film forming techniques[34),35)], solution chemistry techniques have been excellent in terms of obtaining stable electrical characteristics. Precursor solutions (Sr/Bi/Ta) used in this study were Sr/Bi/Ta = 0.8/2.4/2.0 and 0.8/2.0/2.0 for the purpose of investigating good ferroelectric properties and the effect of Bi.

2.2 Experiments

The film formation process is shown in Figure 2.1. We used rapid thermal annealing (RTA) for the crystallization process of SBT. The RTA we used is an infrared anneal. In the infrared anneal, the wafer is directly irradiated with light and absorbed, so that high-speed and short-time heating is possible. Figure 2.2 shows a schematic image of the RTA system we used. A wafer placed in the quartz tube is irradiated with infrared rays from a halogen lamp arranged around the quartz tube. The heating rate was 125 °C/second. The RTA process has been widely used in semiconductor processes such as oxidation, doping, and junction formation. In the oxide ferroelectric thin film formation process that we are studying, RTA research has advanced from the viewpoints of shortening the heat treatment, controlling the interface between the substrate and thin film, and realizing a fine microstructure[36)-38)]. And it is a method of obtaining good ferroelectric characteristics. On the other hand, the RTA process has a problem that temperature control is not easy. As shown in Figure 2.2, the quartz tube has a hole just below the wafer, and the pyrometer can detect the radiated light from the back surface of the wafer. Thereby, the radiation temperature from the back surface of the wafer is detected and the temperature is controlled. Here, it should be noted that the radiation temperature detected from the back surface of the wafer largely depends on the state of the back surface of the wafer. We have formed a ferroelectric capacitor on a thermally oxidized silicon (Si) wafer, and the radiation temperature has an error depending on

the presence or absence of silicon dioxide (SiO_2) on the back surface of the wafer. Further, the radiation temperature has an error due to the difference in the SiO_2 film thickness on the back surface. Therefore, in order to remove these uncertainties as much as possible, I used the wafer in which the SiO_2 film on the back surface of the Si wafer after thermal oxidation was removed by etching process. After performing this back surface etching process, titanium (Ti) and Pt, which are the bottom electrode structure of the ferroelectric capacitor, were formed by the sputtering method. The characteristics required for the electrode material of the ferroelectric capacitor include sufficiently low electric resistance, high heat resistance, and low reactivity. For these reasons, I chose Pt as the electrode material. Since Pt has a problem in adhesion with SiO_2, I introduced Ti as an adhesion layer. Next, the solutions of tantalum butoxide, metallic strontium dissolved in 2-ethylhexanoic acid and xylene, and bismuth 2-etylhexanoate were spun onto Pt(200 nm)/Ti(30 nm)/SiO_2/Si substrates. After spin-coating, the films were dried at 250 ℃ and rapid-thermally annealed (RTA) in oxygen ambient for 30 seconds. As will be described later, the temperature of the RTA has an important effect on the crystallinity of the thin film[23)]. In this study, an RTA temperature of 760 ℃ was mainly selected. After this procedure was repeated three times, the films were heated in oxygen ambient at 800 ℃ for 1 hour to promote the crystallization of SBT. The final film thickness was 180 nm. Pt top electrode of 200 nm thickness and 100 μm diameter was deposited by RF sputtering at room temperature with a metal mask. Post-annealing was performed at 800 ℃ for 20 minutes in an oxygen atmosphere to improve the adhesion between the SBT film and the upper Pt

electrode.

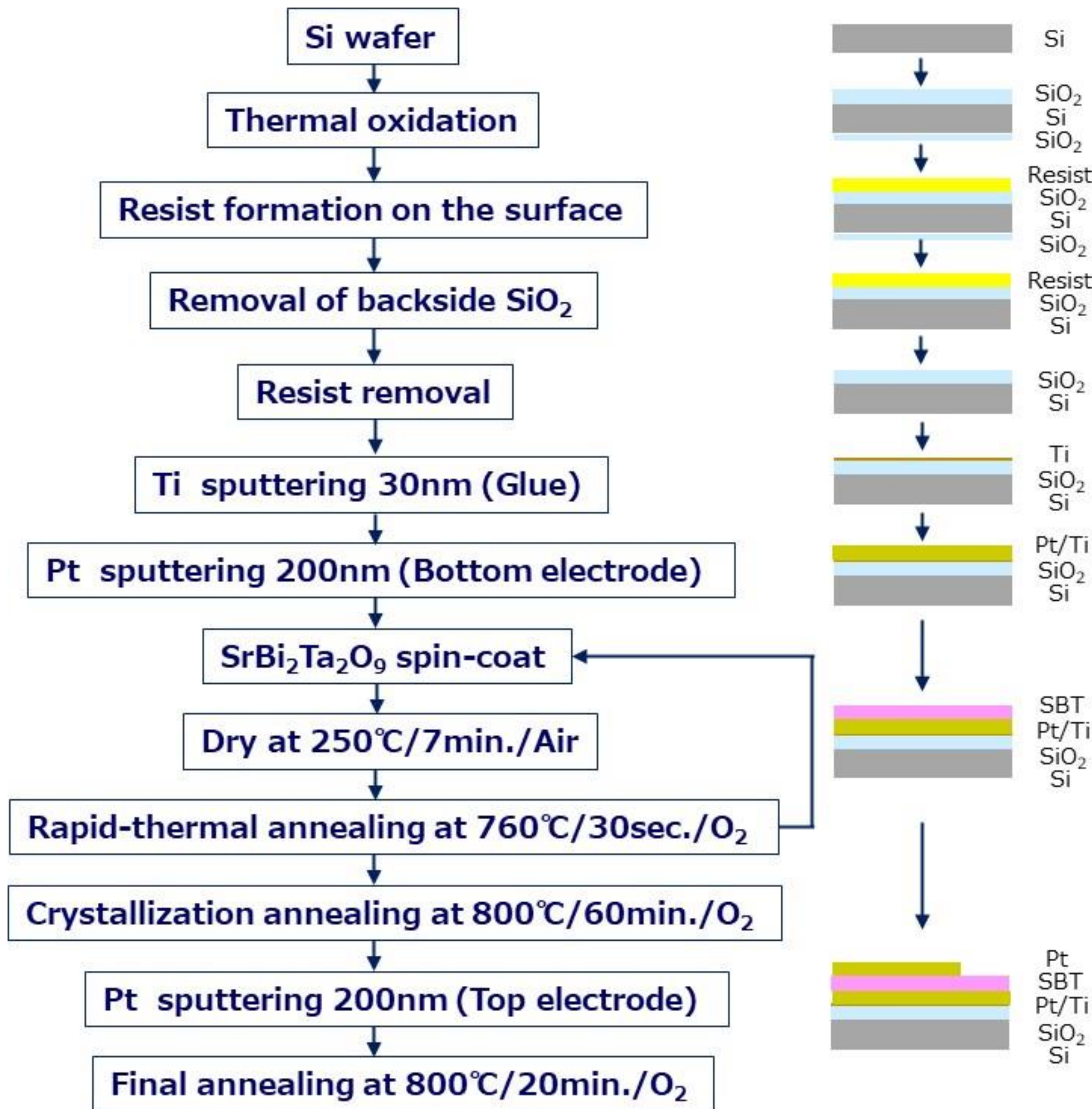

Figure 2.1 Film formation process for SBT film. In this experiment, the process from spin coating to RTA was repeated three times, and a film thickness of 180 nm was obtained.

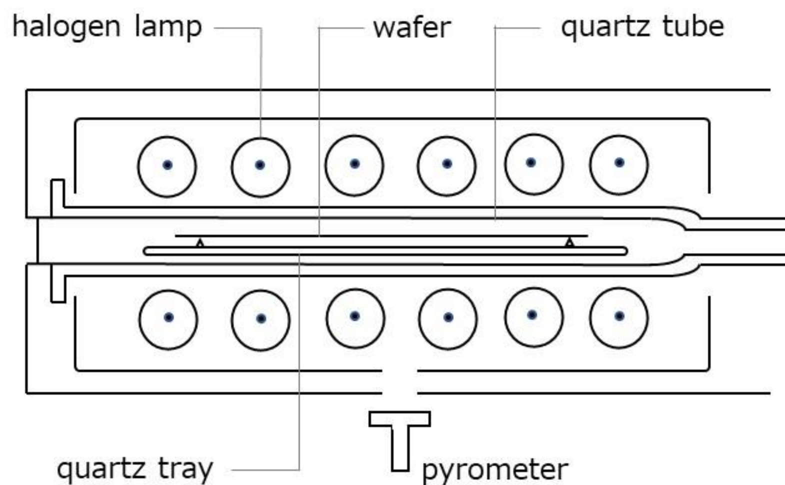

Figure 2.2 Schematic image of the RTA system.

The hysteresis curve was measured by applying a sine wave of 1 kHz at a voltage of 2, 3 and 5 V, and using a Sawyer-Tower circuit (Figure 2.3). The compositions of the precursor solutions were measured using Inductively Coupled Plasma Mass Spectrometry (ICP-MS). Structure analysis of the thin films was performed with X-ray diffraction (XRD) measurements. Cu-Kα radiation using the 2θ scan mode was used. Film compositions were measured by Electron Probe Micro-Analysis (EPMA). The surface morphology and grain structure of films were observed with Scanning Electron Microscope (SEM). X-ray Photoelectron Spectroscopy (XPS) was used to analyze the surface compositions of the films.

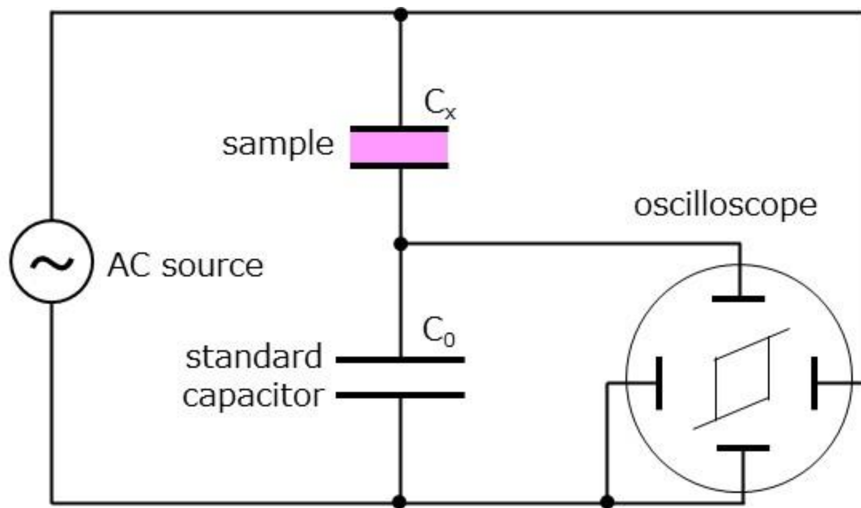

Figure 2.3 Sawyer-Tower circuit for measuring the hysteresis curve of ferroelectrics. If a capacitance C_0 that is sufficiently larger than the capacitance C_x of the sample is inserted in series with the sample, the applied AC voltage is applied to the sample with almost the same magnitude. Since the current flowing through C_x flows into C_0, the change in charge on C_x is equal to the change in charge on C_0, which is C_0 times the change in voltage across C_0. Therefore, the horizontal axis of the oscilloscope shows the voltage applied to C_x, and the vertical axis shows the polarization of C_x.

2.3 The effect of Bi contents for ferroelectric SBT thin film formation

The temperature of the RTA greatly affects the crystallinity of the SBT thin film, and the crystallinity affects the electrical characteristics of the SBT thin film capacitor. Figure 2.4 and 2.5 show the results of XRD measurements and the SEM images of the surface of the SBT films after RTA process. RTA temperature was varied from 690 to 785 ℃. The black circles at the top of Figure 2.4 indicate the positions where the diffraction peaks from the fluorite structure appear, and the open squares indicate the positions where the diffraction peaks from the layered perovskite appear. At lower RTA temperature, fluorite structure which was the precursor structure of SBT was dominant[32),39)]. However, SBT structure became dominant at higher RTA temperatures. Looking at the SEM image in Figure 2.5, when the RTA temperature is 690 ℃, no grain can be seen. And the grains start to appear at RTA temperature of 715 ℃, and the area occupied by grains increases as the RTA temperature rises. Considering this together with the XRD results in Figure 2.4, the grain structure is SBT, which is a layered perovskite structure, and the region where clear grains are not visible, which is dominant in the low temperature region, is considered to be the fluorite structure. For reference, a schematic diagram of the Sr-Bi-Ta-O fluorite structure quoted from ref. 39 is shown in Figure 2.6. The Sr-Bi-Ta-O fluorite structure has a cubic crystal structure and a lattice constant of 5.35 Å[39)]. From these results, when RTA temperature was low, phase transition from

fluorite structure to layered perovskite SBT occurred during the annealing process after RTA. It is considered that it gives a great change to the surface morphology of the SBT thin film. On the other hand, when RTA temperature was 760 ℃ or higher, it is considered that phase transition that significantly changes the surface morphology of the SBT thin film does not occur.

Figure 2.7 shows the SEM images of the surface of the SBT films after the annealing process at 800℃, when RTA temperatures were (a)690 and (b)760 ℃, respectively. The grains in (b) grew uniformly but the grains in (a) were not uniform and pores could be seen. If top Pt electrodes are deposited on the surface with a lot of pores, Pt grains enter pores and may cause electrical shorting. If top Pt electrodes are deposited on the surface with few pores, the insulating property of the capacitor will be maintained. To avoid shorting, high quality surface without pores of the SBT films are required. And it can be understood that the SBT layers are more suitable than the fluorite layers as a seed layer for crystallization of SBT film in order to achieve this high quality surface. Figure 2.8 shows a comparison of main X-ray diffraction peaks around $2\theta=29°$ for SBT films of 0.8/2.4/2.0 precursor with and without the heat treatment at 800 ℃ for 1 h in oxygen atmosphere after RTA. Both films had received the same RTA at 760 ℃, but only the film in bottom trace received the post-RTA annealing at 800 ℃. This shows the benefit of the post-RTA annealing. It can be seen in this figure that the SBT films with 800 ℃ annealing have sharper diffraction peaks of full width at half maximum of 0.23° and hence better crystallinity and those of full width at half maximum of 0.29° in the SBT films without 800 ℃ annealing. Conversely, the SBT films immediately after RTA

processing have been stopped at some midpoint in their growth kinetics. Stated another way, the crystal growth has not saturated. This is also obvious in the SEM images as shown in Figure 2.5 and 2.7.

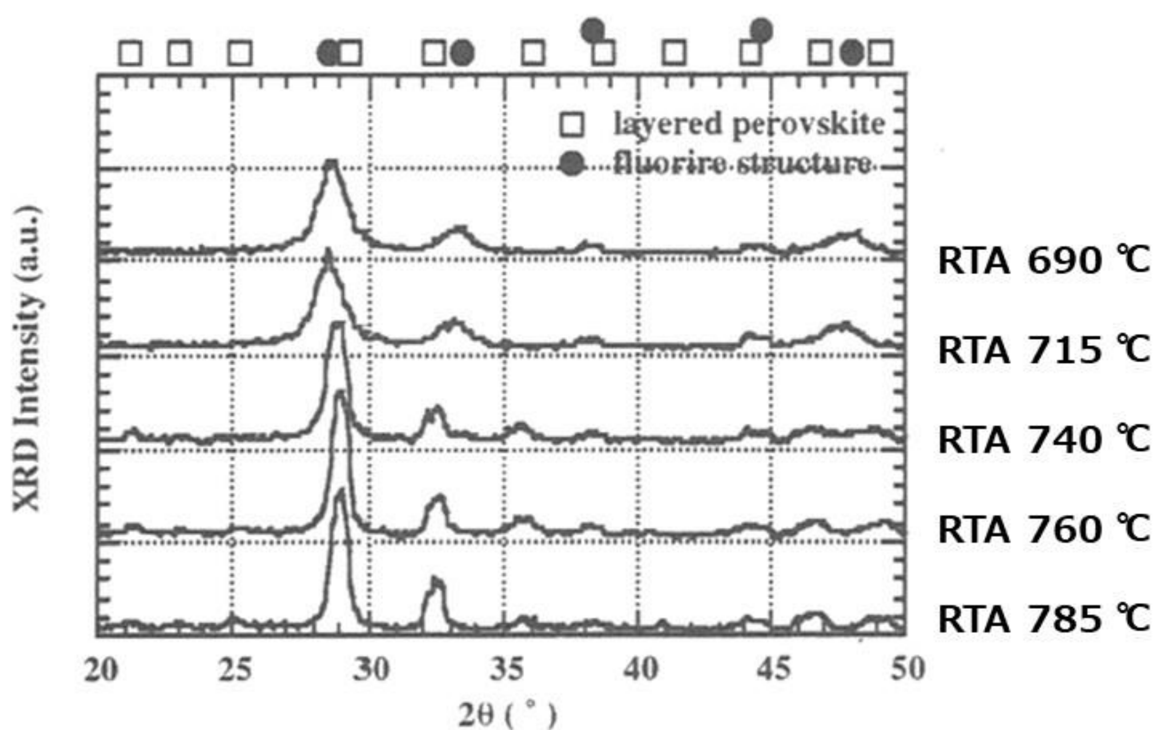

Figure 2.4 XRD patterns for SBT after RTA Process. RTA temperature was varied from 690 to 785 ℃. The black circles at the top of this figure indicate the positions where the diffraction peaks from the fluorite structure appear, and the open squares indicate the positions where the diffraction peaks from the layered perovskite appear.

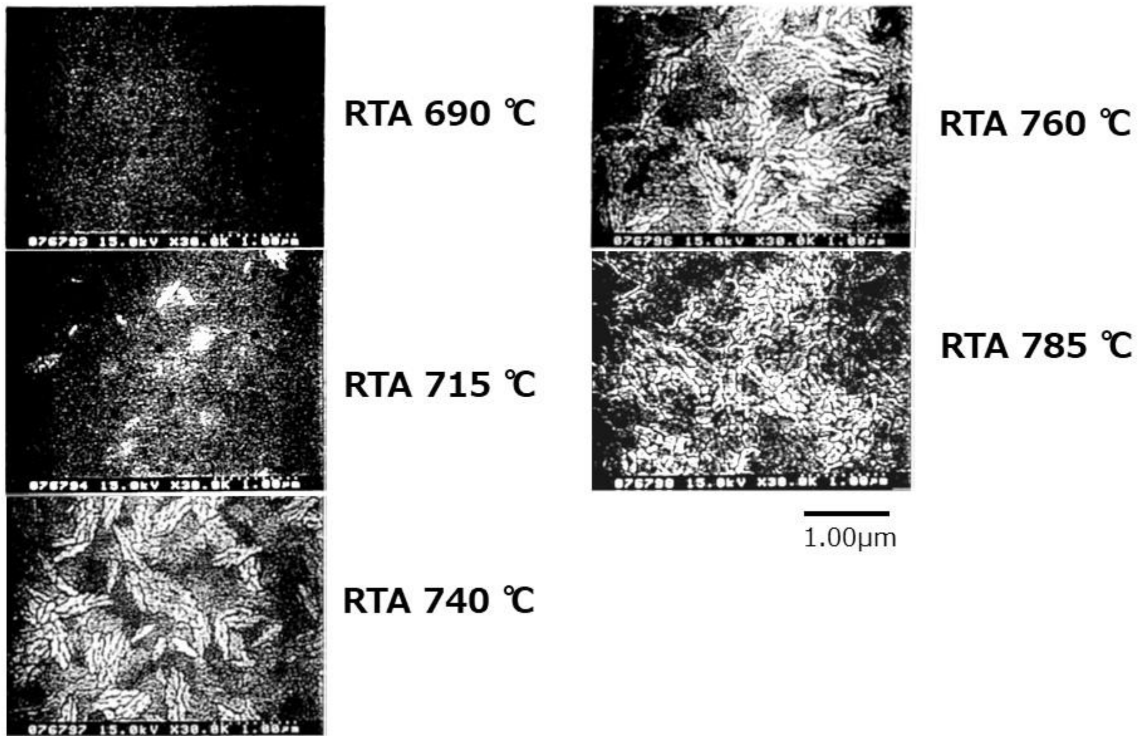

Figure 2.5 SEM images for SBT after RTA Process. RTA temperature was varied from 690 to 785 ℃.

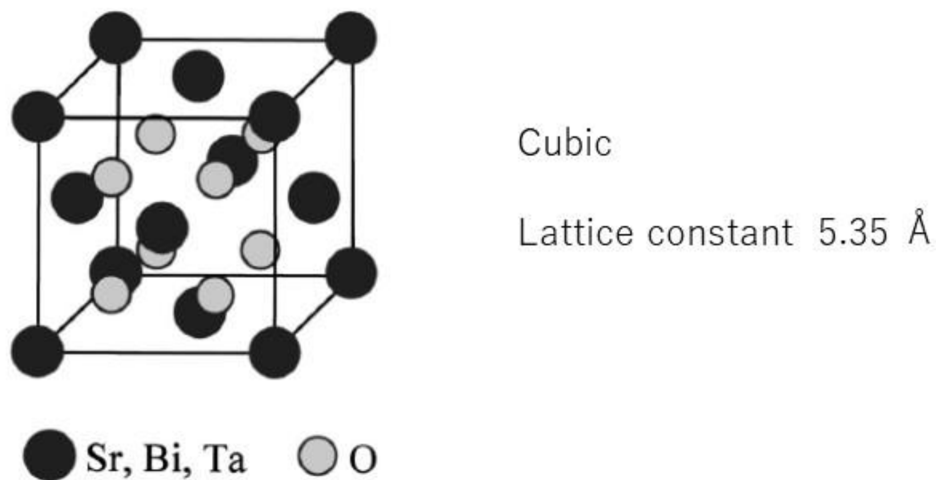

Figure 2.6 Schematic diagram of the Sr-Bi-Ta-O fluorite structure quoted from ref. 39. In this figure the atomic ordering is not considered.

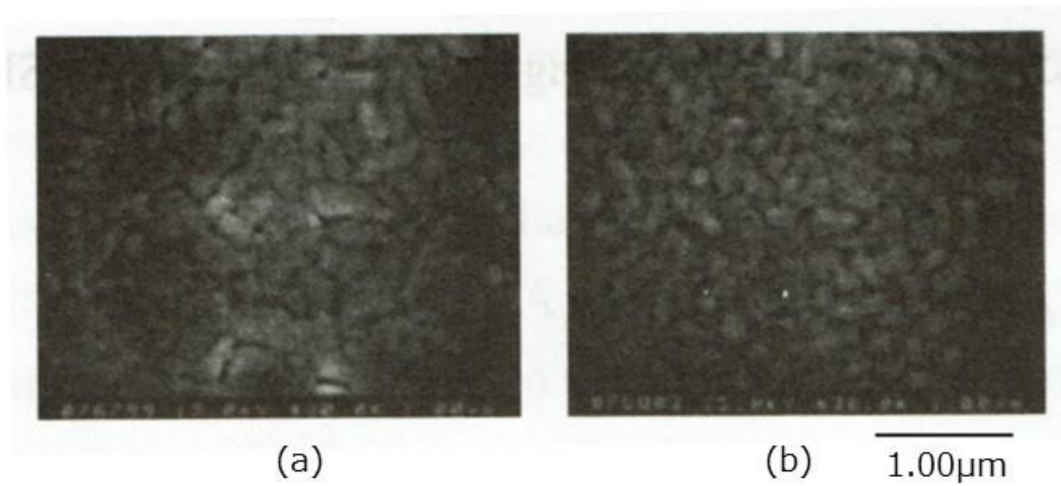

Figure 2.7 SEM images of the surface of the SBT films after the crystallization annealing at 800 ℃ with RTA temperatures at (a)690 and (b)760 ℃, respectively.

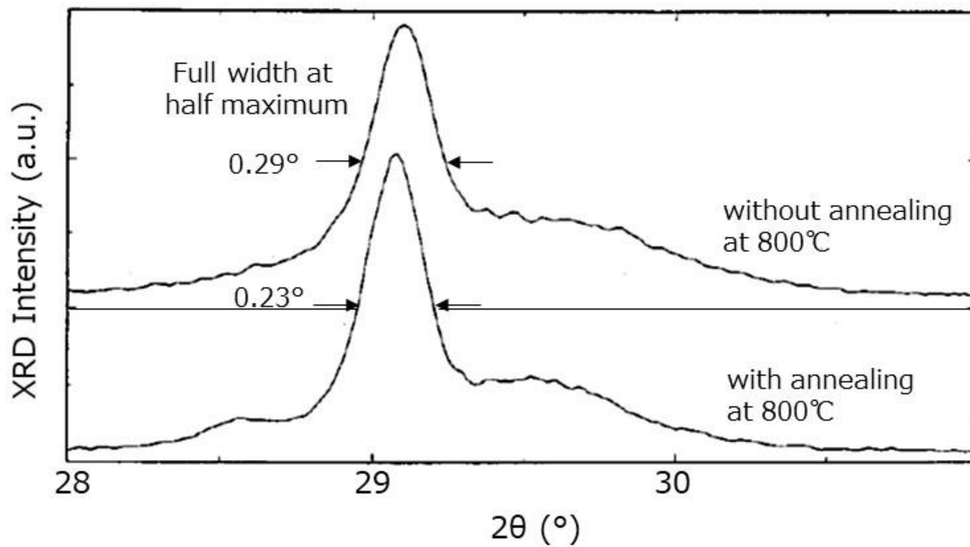

Figure 2.8 Comparison of main X-ray diffraction peaks around 2θ=29° for SBT films of 0.8/2.4/2.0 precursor with and without the heat treatment at 800 ℃ for 1 hour in oxygen atmosphere after RTA.

Figure 2.9 shows the hysteresis curves of the SBT thin film capacitors. The 0.8/2.4/2.0 solution composition was used in these measurements. Each sample was rapid-thermally annealed at 760 ℃ and annealed at 800 ℃ for 1 hour. The hysteresis curves without final-annealing after top Pt electrode deposition are shown in (a), those with final-annealing in O_2 at 450 ℃ for 20 minutes in (b) and those with final-annealing in O_2 at 800 ℃ for 20 minutes in (c). Each sample showed well-shaped hysteresis curves, maintaining high P_r values ($2P_r$ ~20 μC/cm^2 at 3 V). The asymmetry of the hysteresis curves existed without final-annealing but it was modified with final-annealing at 450 ℃ for 20 minutes and good saturation curves were obtained with final-annealing in O_2 at 800 ℃ for 20 minutes. Figure 2.10 shows the applied voltage dependence of the remanent polarization of SBT thin film capacitors with solution compositions of 0.8 / 2.0 / 2.0 and 0.8 / 2.4 / 2.0. Final-annealing in O_2 at 800 ℃ for 20 minutes after top Pt electrode deposition was performed on both samples here. As mentioned at the beginning of this chapter, it is clear that the samples with Sr-deficient and Bi-excess composition have better ferroelectric properties. The reason why SBT with excess Bi exhibits excellent ferroelectric properties was verified using theoretical calculation and crystal structure analysis by other researchers. Miura, *et al*. investigated the possibility of the substitution of Bi ions at the Sr site in the Sr-deficient and Bi-excess SBT using first principle calculations of the electronic structures[30)]. They derived that the Sr ions in SBT do not have covalent interaction with the surrounding O ions, while the substituted Bi ions at the Sr site do. They concluded that due to the covalent interaction, the Bi ions rather than the Sr ions, favour displacement, which is

consistent with the experimental result that the remanet polarization of Sr-deficient and Bi-excess SBT is larger than that of stoichiometric SBT. Shimakawa *et al*. investigated crystal structures of stoichiometric SBT and Sr-deficient and Bi-excess SBT using neutron powder diffraction[31)]. They revealed that both Bi substitution and cation vacancies at the Sr site occurred in Sr-deficient and Bi-excess SBT. And they concluded that those enhanced structural distortion in the TaO_6 octahedra and lead to the larger remanet polarization. These explanations are consistent with our experimental results. These suggest that there are optimum values for Sr deficiency and Bi excess. I will discuss it next section.

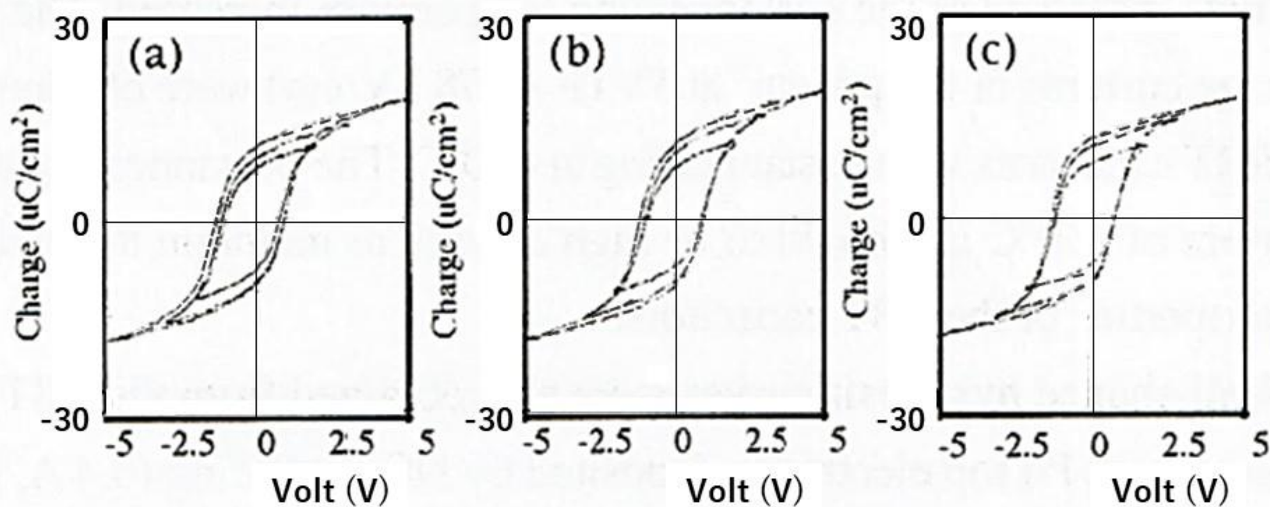

Figure 2.9 Hysteresis curves of the SBT capacitors with 0.8/2.4/2.0 solution composition and RTA at 760 ℃ / annealed at 800 ℃. The hysteresis curves without final-annealing after top Pt electrode deposition are shown in (a), those with final-annealing in O_2 at 450 ℃ for 20 minutes in (b) and those with final-annealing in O_2 at 800 ℃ for 20 minutes in (c).

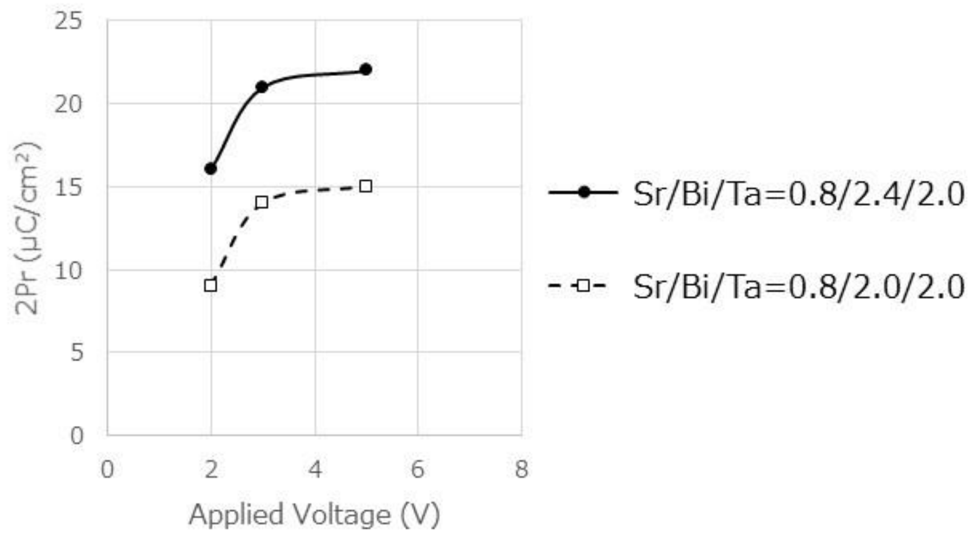

Figure 2.10 Applied voltage dependence of the remanent polarization of SBT thin film capacitors with solution compositions of 0.8 / 2.4 / 2.0 (black circle) and 0.8 / 2.0 / 2.0 (open square). Final-annealing in O_2 at 800 ℃ for 20 minutes after top Pt electrode deposition was performed on both samples.

2.4 Evaluation of Bi contents in SBT film

Figure 2.11 shows the RTA temperature dependence of Bi contents of the SBT films measured by EPMA. The precursor solution of Sr/Bi/Ta = 0.8/2.4/2.0 was used here. The data of the samples taken immediately after the RTA process and those after annealing at 800 ℃ for 1 hour are shown in this figure. It can be seen that a clear jump of Bi content exists between 740 and 760 ℃ in both data. This RTA temperature corresponds to the difference of a main seed layer. When RTA temperature is high, Bi will become more volatile. Moreover, note that 760℃ is the temperature at which the reaction between Bi and Pt can lead to the formation of PtBi and $PtBi_2$[40]. Thus, attention must be paid to the presence of bismuth. In the Sr-deficient and Bi-excess SBT film, it was described in the previous section that Bi enters the Sr site and the remanent polarization value increases[30),31)]. The results of Shimakawa *et al.*[31)] are helpful in considering the optimal values of Sr deficiency and Bi excess. As shown in previous section, both Bi substitution and cation vacancies at the Sr site enhance structural distortion in the TaO_6 octahedra and lead to the larger remanet polarization. Moreover, they showed that powder charged with $Sr_{0.8}Bi_{2.2}Ta_2O_9$ composition does not contain Bi in all vacant Sr sites, but becomes $(Sr_{0.82}Bi_{0.12})Bi_2Ta_2O_9$, leaving empty sites in Sr site. If it is written more accurately,

it will be $(Sr_{0.82}Bi_{0.12}[]_{0.06})Bi_2Ta_2O_9$, where [] represents vacancies. The cation vacancies accompanied by the Bi^{3+} substitution for Sr^{2+} is quite reasonable from ionic considerations of the charge neutrality. These results suggest that in our starting composition $Sr_{0.8}Bi_{2.4}Ta_2O_9$, there is excess Bi that does not enter the both Sr site and Bi site.

The relationship between the compositions of precursor solutions analyzed by ICP-MS, those of the thin films analyzed by EPMA and those of the surface of the films analyzed by XPS for our samples are summarized in Table 2.1. For both samples, RTA was performed at 760°C and crystallization annealing at 800°C. Looking at the composition ratio of the thin film analyzed by EPMA, the precursor composition Sr/Bi/Ta=0.8/2.4/2.0 has a thin film composition of 0.8/2.2/2.0. According to the results of Shimakawa *et al*.[31)], if the composition ratio of Bi is 0.12 in the defect site of the Sr site, the composition ratio of Bi in the SBT crystal is 2.12 together with the original Bi site. Therefore, Bi corresponding to the composition ratio of 0.08 exists without entering the SBT crystal. So where is this surplus Bi? From the surface composition ratio data analyzed by XPS, it can be seen that excess Bi is diffused on the SBT thin film surface. On the other hand, the composition ratio of the SBT film in which the Bi composition ratio of the precursor is close to the stoichiometric composition ratio is Sr/Bi/Ta=0.8/1.8/2.0. This means that Bi is not

supplied to replace the defects at the Sr site, which supports the result of Figure 2.10 that the remanent polarization value is smaller than that of SBT having a large amount of Bi. However, the composition ratio on the surface of this film is 0.9/2.1/2.0, which is close to the stoichiometric composition ratio. These differences in the Bi composition ratio on the surface cannot be distinguished from the surface SEM image. High ferroelectric properties, *ie* high remanent polarization values, are preferred, so Bi-excess SBT film is a preferred option if Bi segregating on the surface has no negative side effects. However, the presence of the metal segregated on the film surface generally affects the contact characteristics with the electrode. The role of excess-Bi in the SBT films on the contact characteristics is examined later.

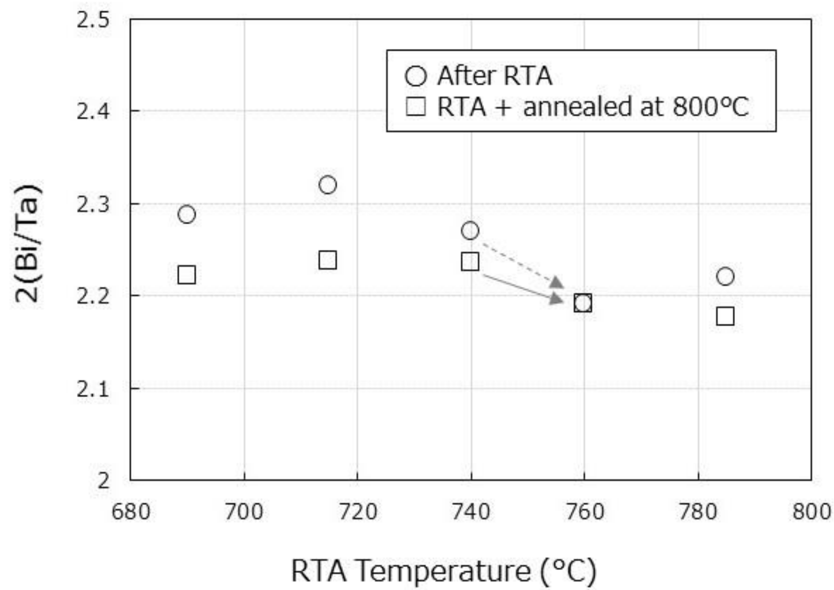

Figure 2.11 RTA temperature dependence of Bi contents of the SBT films measured by EPMA. The precursor solution of Sr/Bi/Ta = 0.8/2.4/2.0 was used here.

Table 2.1 Composition ratios of precursor solutions analyzed by ICP-MS, in the thin films by EPMA and at the surface of the films by XPS. For both samples, RTA was performed at 760 °C and following crystallization annealing at 800 °C.

	Precursor(Sr/Bi/Ta)	Film	Surface
Bi-excess	0.8/2.4/2.0	0.8/2.2/2.0	1.0/3.2/2.0
Bi-Stoichiometric level	0.8/2.0/2.0	0.8/1.8/2.0	0.9/2.1/2.0

2.5 Summary

With RTA processing we established a method to obtain SBT films which showed well-shaped hysteresis curves with or without post-annealing process after top electrode formation, maintaining high $2P_r$ values of 20 μC/cm^2. RTA conditions were optimized for nucleation of SBT. It was understood that fabrication an SBT layer as a seed layer and volatilizing Bi in grain boundaries effectively with RTA process caused good surface morphology. It is expected to have good ferroelectric properties for Sr-deficient and Bi-excess SBT films by replacing Bi with Sr site. On the other hand, it was also clarified from the results of composition analysis that surplus Bi was present on the surface. This is the result with the same tendency as the report of Gutleben *et al.*[22)] Good ferroelectric properties are preferred, so Bi-excess SBT film is a preferred option if Bi segregating on the surface has no negative side effects. However, the presence of the metal segregated on the film surface generally affects the contact characteristics with the electrode. These will be confirmed in the next chapter.

Chapter 3 The effect of Bi contents on current-voltage characteristics of SBT thin film capacitor

3.1 Introduction

Knowledge of the electrical properties of the material, particularly the current–voltage dependence, is essential to assessment of future device performance. The current–voltage dependence in ferroelectric thin films may be complex due to interdiffusion layers and surface traps generally. The previous chapter mentioned that excess Bi contained in the SBT film may affect the contact characteristics with the electrode. In this chapter, the effects of excess Bi are studied through a comparison of the electrical characteristics of Pt/SBT/Pt thin-film capacitors using Bi-stoichiometric SBT film and those using Bi-excess SBT film.

3.2 Experiments

The evaluated samples were Pt/SBT/Pt thin film capacitors using the two types of the SBT shown in Table 2.1. The RTA temperature used was 760 ℃ at which good morphology was obtained. Leakage current density was measured with a parametric analyzer and/or a pico-ammeter. The depth profiling was carried out using XPS. Figure 3.1 shows an image of the sequence for leak current measurement (current-voltage dependence). A positive voltage was applied to the top electrode. To remove the effect of the polarization reversal current, a poling voltage of 5 V was first applied. The poling voltage of 5 V may be considered to be valid by looking at the results of the applied voltage dependence of the remanent polarization value shown in Figure 2.8. The current-voltage dependence characteristics were measured while applying a voltage stepwise as shown in Figure 3.1. The voltage was changed in steps of 0.05 V (ΔV = 0.05 V). At each voltage step, the measurement was started after 1 second (t_{delay} = 1 second), and the measurement time was 0.1 second ($t_{measure}$ = 0.1 second).

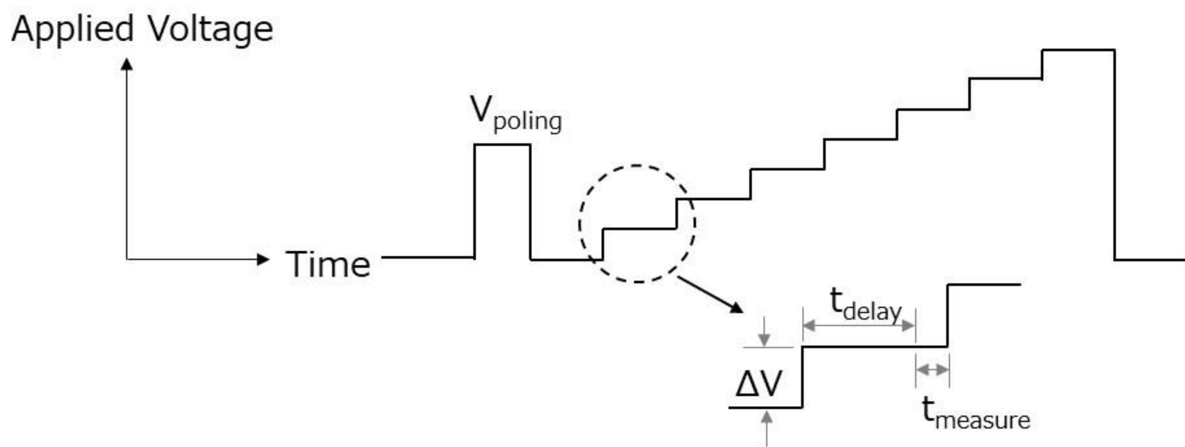

Figure 3.1 Image of voltage application sequence for leak current (current-voltage dependence) measurement.

3.3 Current-voltage characteristics dependence of Bi contents

Figure 3.2 shows the variation of the leakage current density, J, of (a) the Bi-stoichiometric sample and (b) the Bi-excess sample shown in Table 2.1 as a function of square root of the applied voltage ($V^{0.5}$) at 30 °C. SBT has a wide band gap of 4.2 eV[41),42)] and an electron affinity χ=3.5 eV[41),42)], these are detailed in Chapters 4 and 5, such that the SBT/Pt junction has the Schottky characteristics. However, the data displayed in Figure 3.2 indicate that the contact properties and the electronic conduction mechanisms for the Bi-stoichiometric and Bi-excess specimens are somewhat different. The former shows a slight kink near 1.2 eV, whereas the latter exhibits a real negative differential resistivity. The curves for both capacitor (a) and (b) increase linearly with applied voltage up to 1.0–1.2 V. In curve (b) a dip appears at 3.2 V and the conduction characteristics are different for higher voltages. Next, the difference between these two types of current-voltage characteristics will be discussed.

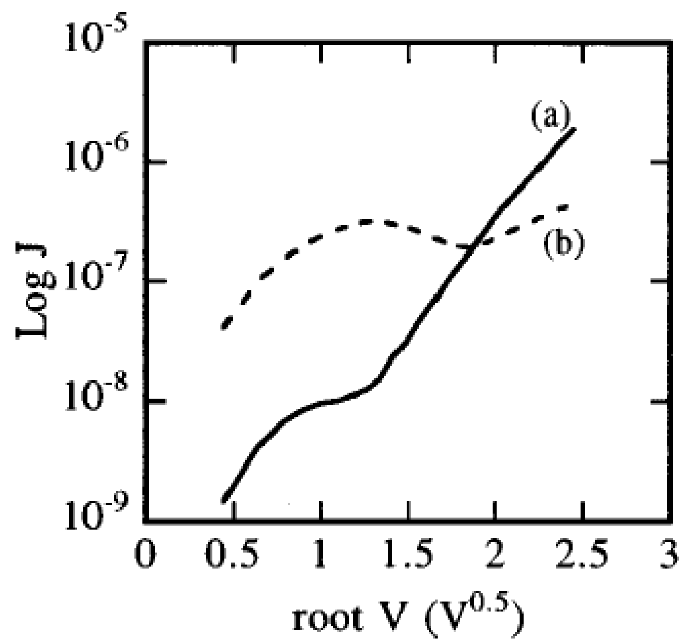

Figure 3.2 Variation of the leakage current density, *J*, of (a) the Bi-stoichiometric and (b) the Bi-excess samples.

3.4 Evaluation of contact in Pt/SBT/Pt capacitor

To understand the observed current-voltage behavior, analogue measurements have been performed at high temperatures. The leakage current governed by the Schottky emission is given by[43)]

$$\ln (J/T^2) = (-q\Phi_b + q\sqrt{(qV / 4\pi d\varepsilon_0\varepsilon_r)}) / kT + \ln (A^*) \qquad (1)$$

where Φ_b is the potential height at the interface, d the film thickness, ε_0 the dielectric permittivity of vacuum, ε_r the dielectric constant of the SBT and A^* the effective Richardson's constant. If the current obeys the Schottky emission model, the fitted curves in the semi-log plot of (J/T^2) versus $V^{0.5}$ should be straight because $\ln (J/T^2)$ is proportional to the square root of the applied voltage. Figure 3.3 shows the variation of $\log(J/T^2)$ as a function of the square root of the applied voltage (V) in the 1.8–3.0 V range at different measuring temperatures in the Bi-stoichiometric Pt/SBT/Pt capacitor (a) shown in Figure 3.2. The data are clearly linear in the 1.8–3.0 V range. Figure 3.4 shows a Schottky plot using the extrapolated value of J/T^2 at V=0 from Eq. (1). The barrier height was estimated to be about 0.9 eV from the slope of the fitting line in this figure. Regarding the validity of this Schottky barrier height, there are independent experimental results by Seong *et al*. [44)] They derived the Schottky barrier of 1.0 eV from the current-voltage characteristics of SBT film on platinum deposited by plasma-enhanced MOCVD, which supports our result.

This is also considered to be an appropriate range in view of the Schottky barrier height at the interface between various ferroelectrics and Pt estimated so far[42)]. This

is because there are many reports of the Schottky barrier height around 1 eV.

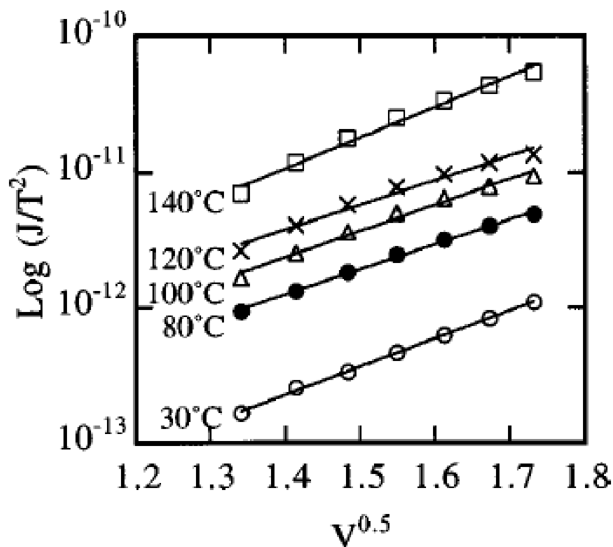

Figure 3.3 Variation of *log(J/T²)* as a function of the square root of the applied voltage (V) in the 1.8–3.0 V range at different measuring temperatures in the Bi-stoichiometric Pt/SBT/Pt capacitor (a) shown in figure 3.2.

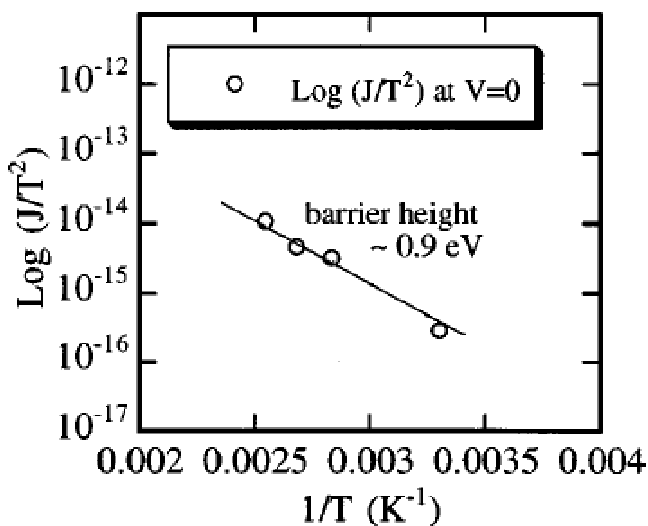

Figure 3.4 The Schottky plot of the Bi-stoichiometric Pt/SBT/Pt capacitor. The slope gives the barrier height.

An analogous procedure was performed in the Bi-excess SBT film capacitor. Figure 3.5 shows the *log* (J/T^2) versus $\sqrt{V}$ plot for this Bi-excess SBT film capacitor in the same temperature range. The current above 3 V was linear, but it was found that the slope of the fitting line increased steeply with measuring temperature. A Schottky plot based on extrapolation of this high-V region back to V=0 would result in a negative number for the barrier height (see Figure 3.6). It can therefore be concluded that the Schottky emission is not the dominant characteristic of the contact studied here.

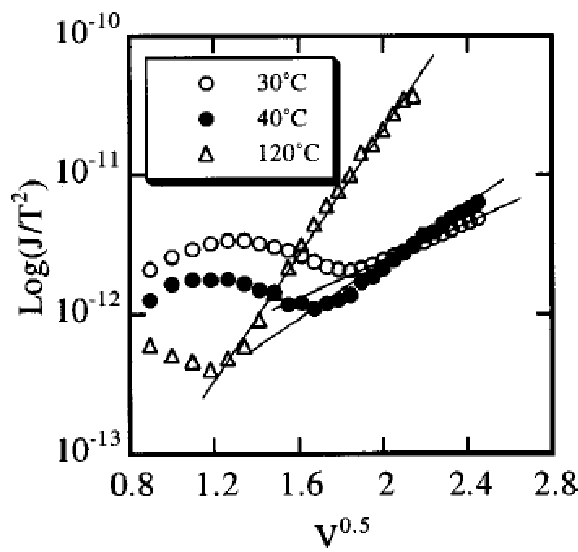

Figure 3.5 Variation of $log(J/T^2)$ as a function of the square root of the applied voltage (V) at different measuring temperatures in the Bi-excess Pt/SBT/Pt capacitor (b) shown in Figure 3.2.

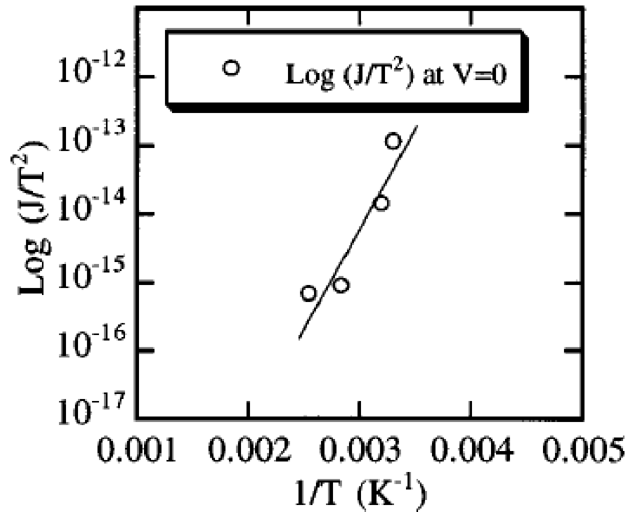

Figure 3.6 The Schottky plot of the Bi-excess Pt/SBT/Pt capacitor. The plot gives an unphysical negative barrier height.

To understand this contact property and electron conduction mechanism, a different analysis needs to be carried out. Figure 3.7 shows the linear plot of J-V curves for these data. These data are separated into three regions. The data at low voltages (up to 1.0–1.1 V) are linear in their J(V) characteristics. A dip appears at higher voltages. This dip would be described as negative differential resistivity. Negative differential resistivity in ferroelectric thin films was first reported by Scott *et al.* [45)] It was suggested that it occurred as a result of double injection of both electrons and holes into a ferroelectric from the electrodes attached to it. Chen *et al*. reported negative differential resistivity in ferroelectric $Pb(Zr,Ti)O_3$ thick films, which was suggested to arise from a trap filling process[46)]. Above this transition region, the voltage dependency of the current is quadratic. This suggests that the associated conduction mechanism is described as space charge-limited currents

(SCLC) under an Ohmic or nearly Ohmic contact[47]. The predicted dependence for space-charge limited currents[48] is

$$J(V) = AV + B(V - V_0)^2 \qquad (2)$$

where V_0 is the trapping potential for the principal impurities in the ferroelectric film. Coefficient A is a bulk property related to Ohmic conduction whereas B depends upon the nature of electrode–ferroelectric interface such as trap densities[47]. For this SBT film V_0, the intersection between the linear line and the quadratic curve of

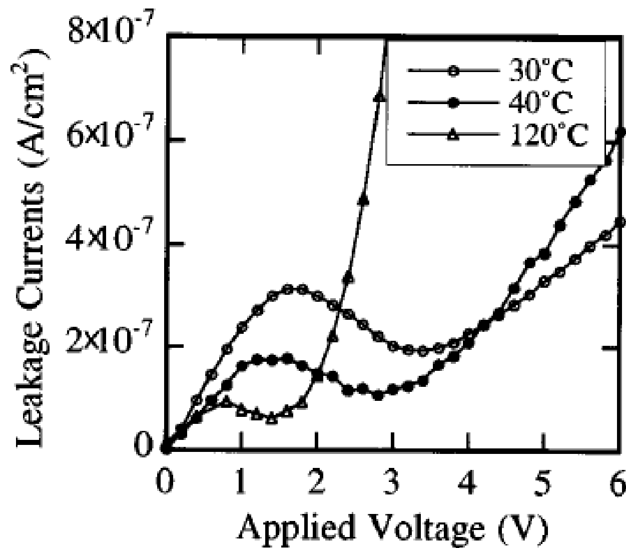

Figure 3.7 Linear plot of J-V curves in the Bi-excess Pt/SBT/Pt capacitor.

the $J(V)$ curve, is estimated to be 1.0–1.1 V when the negative differential resistivity region is ignored and the quadratic curve is extrapolated. Under the environment where the trap exists, current-temperature dependence of SCLC for the capacitor

with Bi-excess SBT film can be described by the Rose's theory[49),50)]

$$J = N e \mu [\varepsilon /(e K T^* A'))]^{T^*/T} d^{-[2(T^*/T)+1]} V^{(T^*/T)+1} \quad (3)$$

where *N* is the trap concentration; *ε*, dielectric constant; *k*, Boltzmann's constant; *T**, a parameter related to average trap energy; *A'*, the pre-exponential factor in the trap distribution function. In the Rose's model the current density *J* decreases with increasing temperature whereas *J* in the ferroelectric film always increases with increasing temperature. The temperature dependence of the dielectric constant should therefore be included in Eq. (3). The temperature dependence for dielectric constant of the SBT thin film following a Curie-Weiss behavior is described as Eq. (4)[51)].

$$\varepsilon = 2 \times 10^5 / (463 - T[K]) \quad (4)$$

The current-temperature dependence of the quadratic regime at the different applied voltages are plotted in Figure 3.8. The solid lines are calculated from Eq. (3) and Eq. (4) and provide the corresponding T^* values 314 K (0.027 eV) at 3 V and 290 K (0.025 eV) at 4 V respectively. These values are considered to be valid since they generate a quadratic current-voltage dependence in Eq. (3), $T^*/T \sim 1$ (Child's Law). The SCLC in Bi-excess SBT capacitor can be well explained using the Rose's model.

Previous XPS studies by other researchers, revealed that elemental Bi may diffuse into the Pt electrode[22),52),53)]. As the work function of Bi is 1.1 eV less than that of Pt[54)], I thought that this would influence the electrical properties of the junction significantly. In order to analyze the film compositions near the ferroelectric–metal interface, I performed XPS depth profiles of the both Bi-

stoichiometric SBT capacitor and Bi-excess SBT capacitor as shown in Figure 3.9. A significant amount of Bi diffused into the Pt electrode was detected for the Bi-excess SBT interface but the amount of diffusion decreased with decrease in the Bi content of the SBT film. The work function of Bi is 1.1 eV less than that of Pt as mentioned above and therefore this would influence the electronic properties of the junction. In the next section, I will try to explain this phenomenon from the electronic structure of the interface.

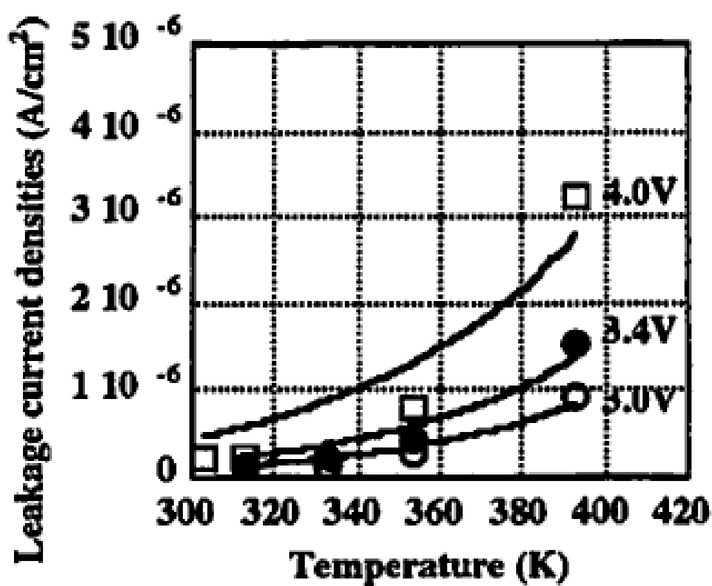

Figure 3.8 Current-temperature dependence of the quadratic regime at the different applied voltages in the Bi-excess Pt/SBT/Pt capacitor. Solid lines are calculated from Eqs. (3) and (4).

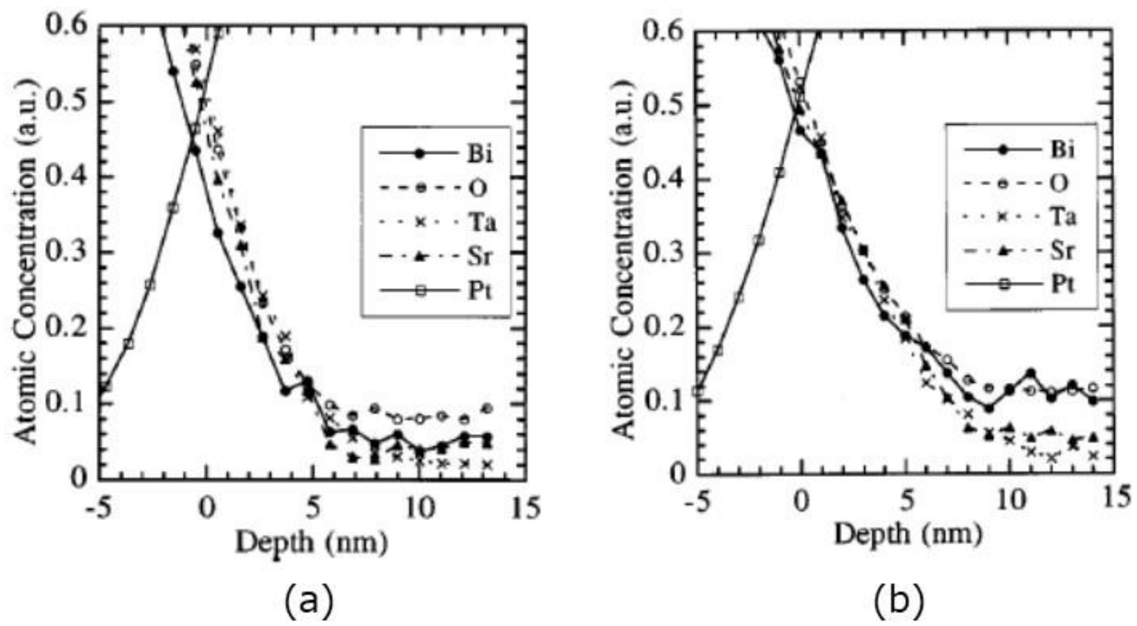

Figure 3.9 XPS depth profiles of the both (a) Bi-stoichiometry and (b) Bi-excess SBT capacitors.

3.5 Summary

In this study, I have found from leakage current data that simple Schottky behavior is characteristic of Bi-stoichiometric SBT films on Pt, with a barrier height of 0.9 eV, but that Ohmic or quasi-Ohmic contact can be dominant in the Pt/SBT/Pt specimens with the Bi-excess SBT film. The current–temperature dependence of Pt/Bi-excess SBT/Pt can be explained quantitatively via Rose's theory. This is the first attempt to apply the Rose's theory to ferroelectric thin films. XPS depth profiling data show that significant Bi diffusion into the Pt electrode occurs in the Bi-excess SBT film. This Bi diffusion seems to make the ferroelectric-Pt contact unstable, perhaps by forming PtBi and $PtBi_2$ which does not result in a Schottky contact but instead an Ohmic one. This Ohmic high conductivity junction produces space-charge-limited currents above 2 V. This work therefore suggests that for the device applications stable SBT-Pt Schottky contacts will require control of Bi in SBT thin film.

Chapter 4 Electronic Structures dependence on Bi contents of SBT thin film

4.1 Introduction

I have discussed the significant influence of the Bi diffusion on the electrical properties in the previous chapter. Since SBT has a bandgap energy of 4.2 eV and an electron affinity of 3.5 eV , those are described in detail later, and the Pt has a work function of 5.3 eV, it is expected that the Pt/SBT contact has the Schottky properties. The Bi-excess-SBT/Pt contact, however, has Ohmic or nearly Ohmic properties and only the nearly Bi-stoichiometric-SBT/Pt contact has the Schottky properties as introduces in the previous chapter. These results indicate that the excess Bi influences the density of states (DOS) near the bandgap of SBT and therefore the electrical properties of the SBT/Pt junction significantly. In this chapter, I discuss the bandgap state of SBT.

4.2 Experiments

One method for the investigation of occupied DOS near the bandgap is photoelectron spectroscopy. I have investigated the electronic structure of Bi-stoichiometric SBT film in the surface region and Bi-excess SBT film in the surface region shown in Table 2.1 using X-ray photoelectron spectroscopy (XPS) and ultraviolet photoelectron spectroscopy (UPS). The data for Bi-excess SBT film in Table 2.1 indicate that significant amounts of Bi diffused to the surface. X-ray diffraction and scanning electron microscopy indicated that the thin-film material almost entirely composed the desired layered Bi compound phase, and that the Bi concentration difference did not cause a significant strange state in crystallinity or grain structures (Figures 2.2 and 2.3).

For XPS measurements, a monochromatic Al Kα_1 source (1486.6 eV) was used and the instrumental resolution was 0.28 eV. For the UPS experiments He I ($h\nu$ = 21.2 eV) radiation was used with the resolution of the instrument being 0.03 eV. Prior to photoelectron spectroscopy analyses, the samples were annealed at 350 ℃ for 5 minutes in vacuum (10^{-8} mbar) in order to clean the surface. No residual carbon 1*s* peak was detectable using XPS after this heat treatment. Since all measurements were performed using the samples without top electrodes, the detected signals were thought to originate from the SBT surface. For these measurements, the top of the valence band has been determined to be as follows: An undoped Si(111) wafer was etched by Ar^+-ion with energy of 3 keV and

subsequently annealed in UHV for 1 hour (temperature 900 ℃). The XPS binding energy of the resolved $Si_{2p3/2}$ peak was 99.1 eV. The valence band of the 'clean' silicon sample was detected using UPS and XPS and the top of the silicon valence band was estimated by subtracting half the bandgap from the Fermi level position (the bandgap of silicon is 1.12 eV). Silicon and SBT valence-band measurements have been normalized (the UPS spectra with respect to the He I satellite intensity and the XPS spectra with respect to an energy range well below the valence band) and the initial rise of valence-band intensity of the SBT spectra has been aligned with that of the silicon spectra.

4.3 Electronic structures evaluated by XPS and UPS

Figure 4.1 shows XPS valence-band spectra for Bi-stoichiometric and Bi-excess SBT thin films. Figure 4.2 shows the DOS obtained from ref. 55, which was calculated using the tight-binding method. The O(1) and O(2) indicate that the DOS is related to the oxygen ions bonded to two Ta ions, while the O(3) is bonded to one Ta ion. The O(4) ions are the oxygen ions in the Bi–O layers of SBT. According to these calculations, the small peak near 9 eV following the valence band is related to Bi *s* states and its intensity reveals the difference between the bismuth concentrations in the surfaces of the two samples in Figure 4.1. The width of the valence band in Figure 4.1 is approximately 6 eV which is close to the calculated value of 5.5 eV.

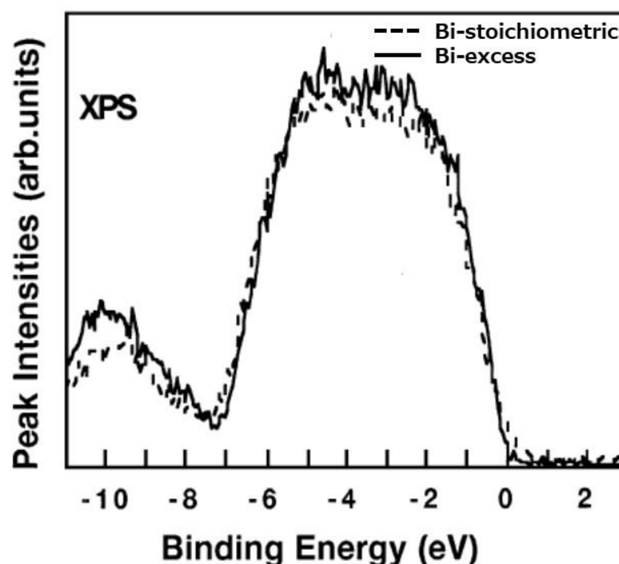

Figure 4.1 XPS valence-band spectra for Bi-stoichiometric (dotted line) and Bi-excess (solid line) SBT thin films.

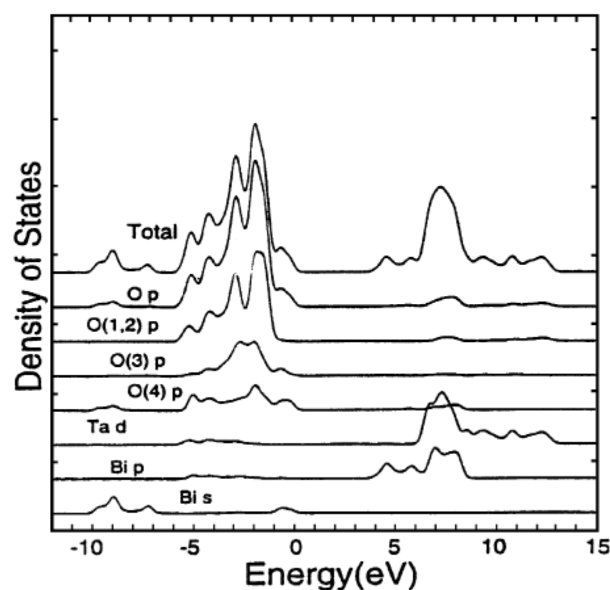

Figure 4.2 Total and partial density of state of SBT film taken from ref. 55. The O(1) and O(2) indicate that the DOS is related to the oxygen ions bonded to two Ta ions, while the O(3) is bonded to one Ta ion. The O(4) ions are the oxygen ions in the Bi–O layers of SBT.

In order to investigate the bandgap state in more detail, analysis using a UPS was performed. Figures 4.3 and 4.4 show spectra of the valence band and valence-band edge of the SBT films, respectively, which were measured using He I (21.2 eV)-UPS. The shapes of these SBT valence band spectra are different from those of the XPS measurements which is related to differences between the cross sections for excitation with X-rays (XPS) and ultraviolet photons (UPS). XPS cross sections have high sensitivity for metals, while UPS cross sections have high sensitivity for light atoms such as oxygen[56]. According to the calculation (Figure 4.2), the valence band of the SBT consists mainly of oxygen 2*p* states which are mostly reproduced by the UPS measurements.

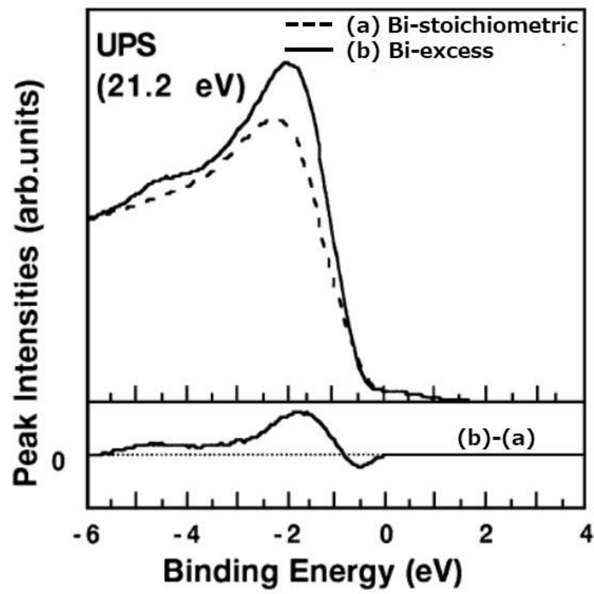

Figure 4.3　He I (21.2 eV)-UPS valence-band spectra for Bi-stoichiometric (dotted line) and Bi-excess (solid line) SBT thin films.

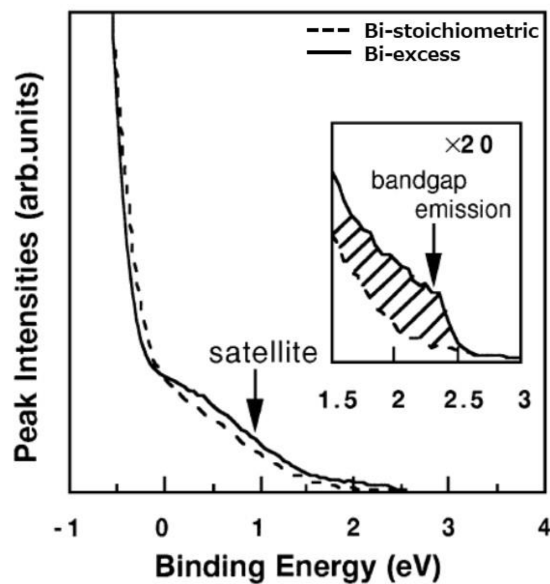

Figure 4.4　Valence-band edge of the SBT thin film measured by He I (21.2 eV)-UPS.

4.4 Evaluation of bandgap states

The spectrum for Bi-excess SBT film shown in Figure 4.3 has additional intensity at approximately 1.3 eV and above 4 eV which is not significantly different than the energy of the O(4) *p* states in the Bi–O planes (compare to Figure 4.2; the peak at 1.3 eV in Figure 4.3 could be related to the intensity between 1 and 2 eV in Figure 4.2). This intensity is possibly related to O in additional oxidized Bi (it is assumed that the DOS of O in oxidized Bi is similar to that of O(4) ions in the Bi–O planes). The He I spectra shown in Figure 4.4 demonstrate the DOS in the bandgap region. The He I (21.2 eV) line is accompanied by a 23.1 eV satellite and part of the intensity in these spectra is related to the satellite. The additional intensity up to approximately 2.7 eV in the spectrum for Bi-excess SBT film, however, cannot be explained in terms of the satellite and indicates additional occupied DOS in the bandgap. Since the Bi-excess SBT film contains more Bi or Bi–O on the surface than the Bi-stoichiometric SBT film (see Table 2.1), these bandgap states are expected to be related to Bi or Bi–O. My collaborator, Hartmann did a supplemental experiment. Figure 4.5 shows a Bi *4f*-XPS measurement for Bi-stoichiometric SBT thin film being executed by Hartmann[57)]. The main peaks are centered at 158.9 and 164.2 eV and are from Bi^{3+} (Bi_2O_3). The smaller peaks at 156.6 and 162.0 eV are associated with metallic Bi. For Figure 4.5 (b) the sample was tilted 60° with respect to the photoelectron analyzer, which doubles the surface sensitivity compared to Figure 4.5 (a). The relative intensity of Bi is concentrated in a surface layer. This

result is considered to suggest that the states in the band gap shown in Figure 4.4 is due to Bi. Since Bi is oxidized to Bi_2O_3 in the presence of oxygen at around 300 °C[58)], it is a surprising result that Bi that does not become Bi_2O_3 exists in the SBT sample that has been heat-treated in a high temperature oxygen atmosphere. It is possible that a part of Bi_2O_3 was destroyed during XPS measurement. It has been reported that if sputter etching with Ar^+ is performed in the pretreatment before XPS measurement, a part of Bi_2O_3 is destroyed and becomes Bi[59),60)]. However, in my experiment, the pretreatment was only heat treatment at 350 ℃ for 5 minutes in vacuum (10^{-8} mbar) as described in Section 4.2. There is a possibility that Bi_2O_3 will be reduced by heat treatment under vacuum, but there are no reported cases and further investigation is not possible at this time. In addition to my experimental results, there are several reports that metal Bi exists on the surface of SBT, and they all say that the reason is unknown[22),61)]. Anyway, these impurity states would significantly influence the Pt/SBT contact properties and would explain the observed differences between the electrical properties of Bi-stoichiometric and Bi-excess SBT films. It is possible that these Bi-impurity states result in the Ohmic contact properties of the Pt/SBT junction. Bi-excess SBT film, however, is widely used for device applications (due to its higher remanent polarization value than Bi-stoichiometric SBT film) and consequently, the electrical properties of these devices are not ideal (*i.e.*, they have high leakage currents).

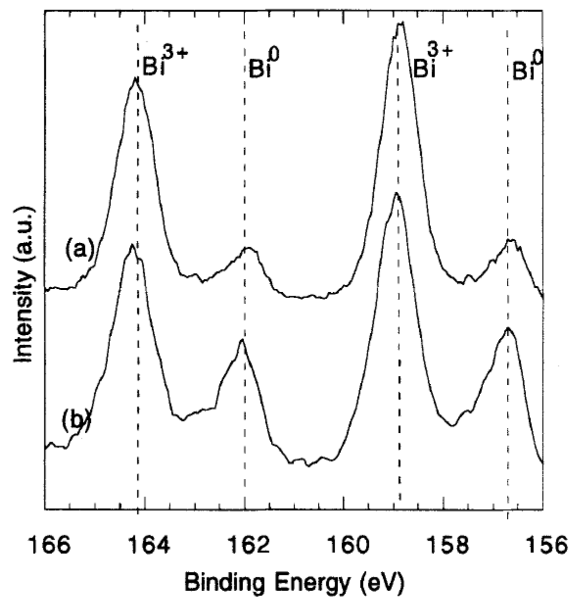

Figure 4.5 Bi *4f*-XPS spectra for Bi-stoichiometric SBT thin film at (a) normal incidence emission; (b) 60 degree sample tilt. This figure is taken from ref. 57.

4.5 Summary

The occupied density of states near the bandgap of SBT has been investigated using XPS and UPS and the measured results for Bi-stoichiometric SBT film are comparable with theoretical results. For Bi-excess SBT film, the UPS measurements revealed the presence of states in the bandgap. These additional occupied states are extended up to approximately 2.7 eV above the top of the valence band, and the effective surface bandgap is therefore significantly smaller than the bulk bandgap (4.2 eV) shown later. It was also found that these band gap states are likely due to Bi segregated on the surface by XPS measurement results that emphasized information from the surface. The bandgap states influence the Pt/SBT contact properties, particularly current-voltage dependence, and are responsible for the Ohmic contact properties of the Bi-excess SBT/Pt junction. Bi-excess SBT film is, however, used for device applications as it has ferroelectric advantages (remanent polarization). Further investigations are required to obtain device-quality Pt/SBT/Pt sandwich structures with both high remanent polarization and the Schottky contacts and therefore low leakage currents.

Chapter 5 Energy band model for SBT thin film capacitor

5.1 Introduction

By the previous chapter, I have discussed electrical properties of the SBT thin film capacitor and electronic structure of the SBT thin film. In the development of new devices such as FeRAM mentioned here, the development of integration may precede, and the priority of verification of mechanisms and models may be lowered. However, in order to improve the device characteristics, I think that understanding the mechanism-based energy band model is important. Integrating the electrical characteristics and electronic structure introduced in this thesis, I discuss an energy band model mainly for the interface between the ferroelectric and the electrode.

5.2 Energy band model

From the results of detailed electrical property measurements in Chapter 3, I have found from leakage current data that the simple Schottky behavior is characteristic of Bi-stoichiometric SBT films on Pt, with a barrier height of 0.9 eV, but that the Ohmic or quasi-Ohmic contact can be dominant at the interface of Bi-excess SBT film and Pt. The current–temperature dependence of Bi-excess SBT film can be explained quantitatively via the Rose's theory. This is the first attempt to apply Rose's theory to ferroelectric thin films. XPS depth profiling data show that significant Bi diffusion into the Pt electrode occurs in the Bi-excess SBT film. This Bi diffusion seems to make the ferroelectric-Pt contact unstable.

In order to clarify the influence of Bi, detailed analysis of the surface structure and band gap state using XPS and UPS was performed shown in Chapter 4. The measured results for Bi-stoichiometric SBT film are comparable with theoretical results. For Bi-excess SBT film, the UPS measurements revealed the presence of states in the bandgap. These additional occupied states are extended up to approximately 2.7 eV above the top of the valence band, and the effective surface bandgap is therefore significantly smaller than the bulk bandgap (4.2 eV) shown later.

To understand the band models for SBT/Pt interface, it is important to know SBT band gap, valence band edge and electron affinity information. My collaborators, Hartmann and Scott experimentally obtained these physical property values. SBT

bandgap was measured using UV-visible absorbance technique[41]. Figure 5.1 shows the UV-visible absorbance data of SBT thin film on a platinum coated substrate. The thick line in Figure 5.1 is the data for SBT film on platinum, and the thin line is the data for the sample in which only platinum was coated on the substrate. Below 4.2 eV the intensity of the SBT thin film measurement is determined by interference which would indicate that the film is transparent for the low energy range. Above 4.2 eV no interference is visible and the band gap of the SBT thin film is thought to be about 4.2 eV. The valence band edge and electron affinity are discussed in ref. 57. Figure 5.2 shows the XPS measurement results near the Fermi level. From the

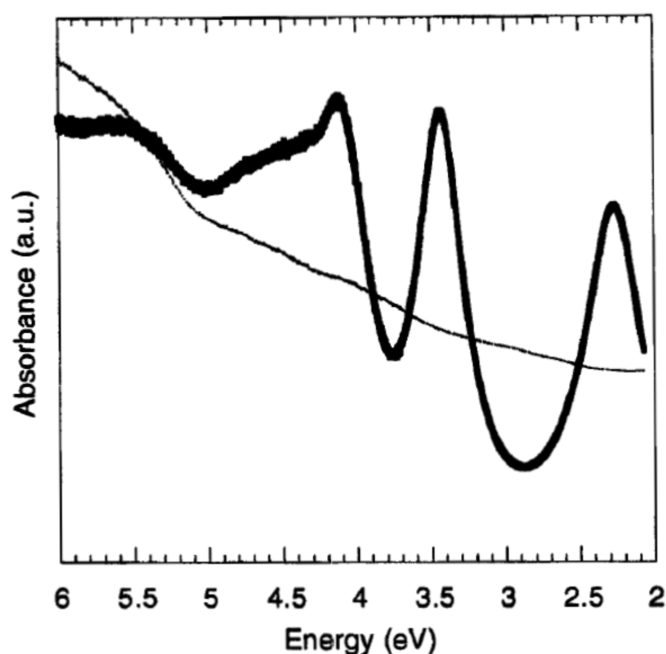

Figure 5.1 UV-visible absorption measurement for SBT thin film on platinum coated substrate (thick line) and platinum coated substrate only (thin line). This figure is taken from ref. 41.

results in Figure 5.2, it can be seen that there is approximately 2.4 eV[57)] between the Fermi level of platinum and the valence band edge of SBT film. This number is considered reasonable. Because my other collaborator, Gutleben, independently measured the band alignment at the SBT/Pt interface using XPS and concluded that the energy difference between the Fermi level of platinum and the valence band edge of SBT film was between 2.2 and 2.8 eV depending on the platinum film thickness[53)]. Considering that the work function of platinum (Φ_{Pt}) is 5.3 eV and the band gap of SBT film is 4.2 eV, the electron affinity of SBT film is required to be 3.5

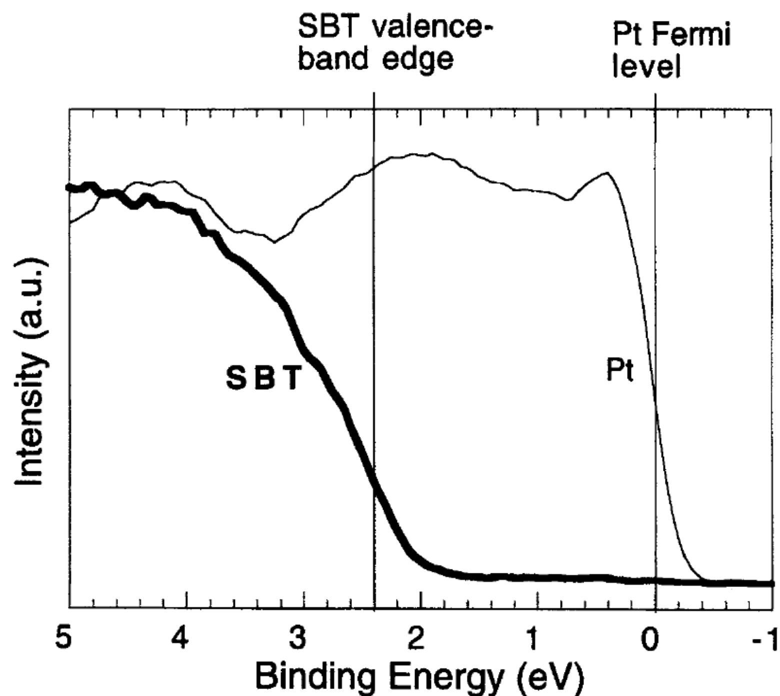

Figure 5.2 XPS measurement data showing the region near the Fermi level of SBT and Pt. This figure is taken from ref. 57.

eV[57]. Therefore the zero-voltage Schottky barrier height should be Φ_{Pt} - 3.5 eV = 1.8 eV. Assuming the Fermi level of SBT film is near the band gap center[51], the band structure at SBT/Pt interface should be shown in Figure 5.3. The concrete picture of the interface between the ferroelectric and the metal electrode is always controversial and difficult to understand completely. The discussion about the interfacial layer between PZT and Pt in the late 1990s, during which the author was doing this research, is particularly known. According to Scott *et al.*, there is a damaged layer with a thickness of 15 nm to 20 nm on the surface of the PZT thin film, which forms an n-type inversion layer at the interface with Pt[42),62)]. From these results, an interface model in which an n-type damage layer exists on the surface of an oxide ferroelectric thin film represented by perovskite has come to be considered. On the other hand, Scott *et al.* also reported that SBT has few damage

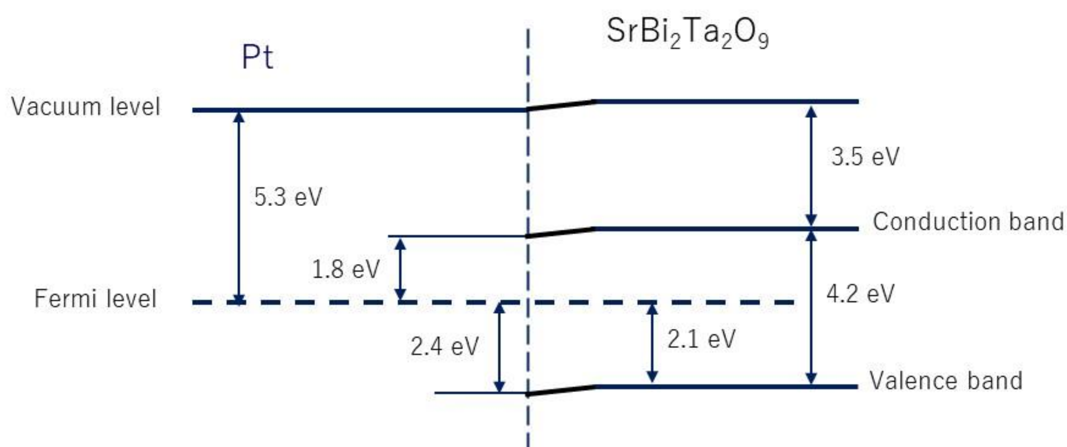

Figure 5.3 Energy-band match-up at the SBT/Pt interface obtained from XPS data and band gap estimated from UV absorption data. The Fermi level of SBT is assumed to be near the center of the band gap.

layers on the surface and is probably about 2 nm thick[42]. In any case, since it is difficult to completely identify the interface layer, the possible interface states will be inferred below.

Next, let me consider the effect of excessive Bi. As mentioned above, excessive Bi exists on the surface of SBT film or diffuses into the Pt electrode. It was also stated that Pt and Bi can form an alloy in the region of crystallization temperature of SBT. Therefore, the Pt electrode in contact with the Bi-excess SBT film may have a Pt-Bi alloy at a part of the interface. Since the work function of $PtBi_2$ is reported around 4.8 eV[63], which is smaller than the work function of Pt by 0.5 eV. Therefore, the band structures at the SBT/$PtBi_2$ interface are different. Unfortunately, we do not have data on the energy difference between the valence band edge of SBT film and the Fermi level of $PtBi_2$, and none of the data of other researchers have determined it. Therefore, I again assume that the SBT Fermi level is near the center of the bandgap and is pinned to the $PtBi_2$ Fermi level. The SBT/$PtBi_2$ interface would be represented as shown in Figure 5.4. Based on the assumption in Figure 5.4, the Schottky barriers are estimated to be about 1.3 eV, and which are smaller than the value for the Schottky barrier height at the SBT/Pt interface. Note that the energy band model presented here is premised on the inclusion of errors, as there is no data on the contact characteristics of $PtBi_2$ and SBT. However, since there is a difference in work function between Pt and $PtBi_2$, there is no doubt that the Schottky barrier height at the interface with SBT film is lower in PtB_{i2} than in Pt.

Next, let me consider Bi and Bi_2O_3. As mentioned in the previous chapter,

whether or not metal Bi exists on the surface of the SBT film is an unclear point of discussion. In the surface SEM image shown in Figure 2.7, Bi metal crystals and grains thought to be Bi_2O_3 were not observed. Therefore, it is suggested that Bi or Bi_2O_3 may be very thinly coated on the grain boundary of SBT. If Bi exists in the form of metal on the SBT film surface, it may behave like an electrode. The interface

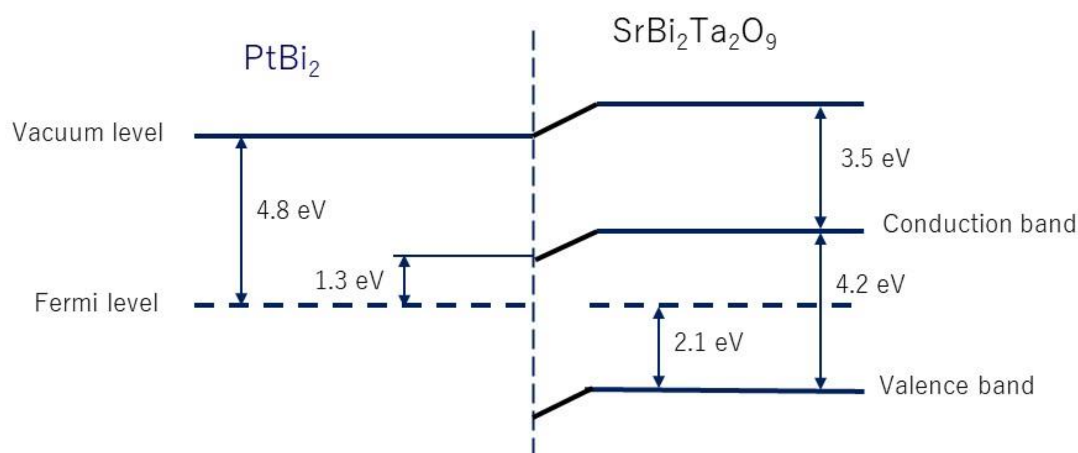

Figure 5.4 Expected energy-band match-up at the SBT/$PtBi_2$ interface. At the interface with the Bi-excess SBT film, an alloy of Pt and Bi may be formed at a part of the interface during the high temperature heat treatment for crystallization of SBT.

between SBT film and Bi is expressed in the same way as $PtBi_2$, as shown in Figure 5.5. The work function of Bi is 4.2 eV, so the estimated Schottky barrier height for SBT/Bi contacts is small. It is also consistent with the fact that the intra-band gap level of Bi-excess SBT film, which is considered to be due to Bi, is located near the middle of the band gap of SBT film, as shown in Figure 4.4. This will result in quasi-Ohmic contact properties. It is also necessary to consider the case where Bi_2O_3

exists on the SBT film surface. Bi_2O_3 is reported in the literature to be a semiconductor with a bandgap of about 2.8 eV[58),64)]. However, we do not have any data on the contact properties between Bi_2O_3 and metals, and we cannot find any reference work. It is certain that the band gap of Bi_2O_3 is much smaller than that of SBT. Further, the current-voltage characteristics of the capacitor using the Bi-excess

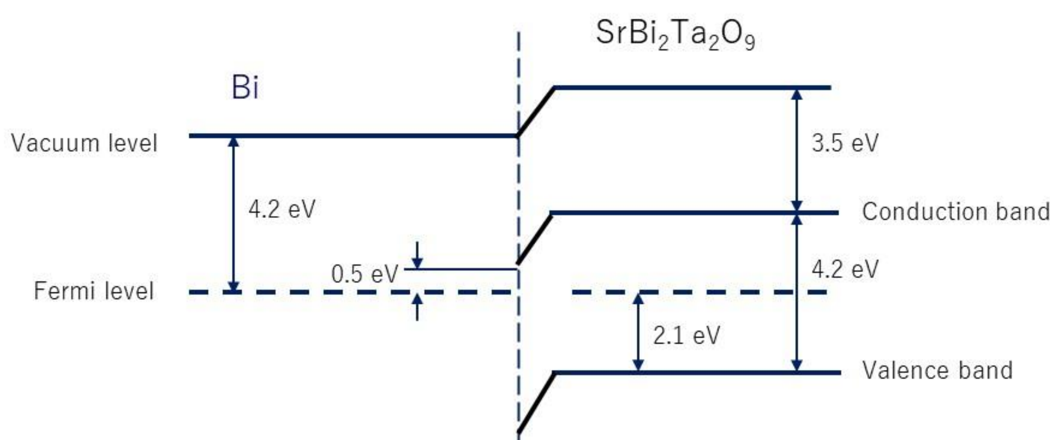

Figure 5.5 Expected energy-band match-up at the SBT/Bi interface. In contrast to the case in Figure 5.4, if Bi that did not form an alloy with Pt remains at the interface, the band structure shown in this figure may occur.

SBT thin film have a current density higher than that of the SBT film having a Bi-stoichiometric composition ratio by one digit or more. Therefore, if Bi_2O_3 is present at the interface between the Pt electrode and SBT film, it should have the function of facilitating the transfer of charges. Therefore, although it may not be accurate, it is safe to think that Bi_2O_3 will be positioned like the intra-band gap level of SBT film. Based on that assumption, the energy bands of Pt, Bi_2O_3, and SBT film are shown

in Figure 5.6. Here, I assume that the Fermi level of Bi_2O_3 is near the center of the band gap. Please note that the position of the energy level of Bi_2O_3 is not accurate. However, there is no doubt that Bi_2O_3 plays a role in facilitating charge transfer to SBT film.

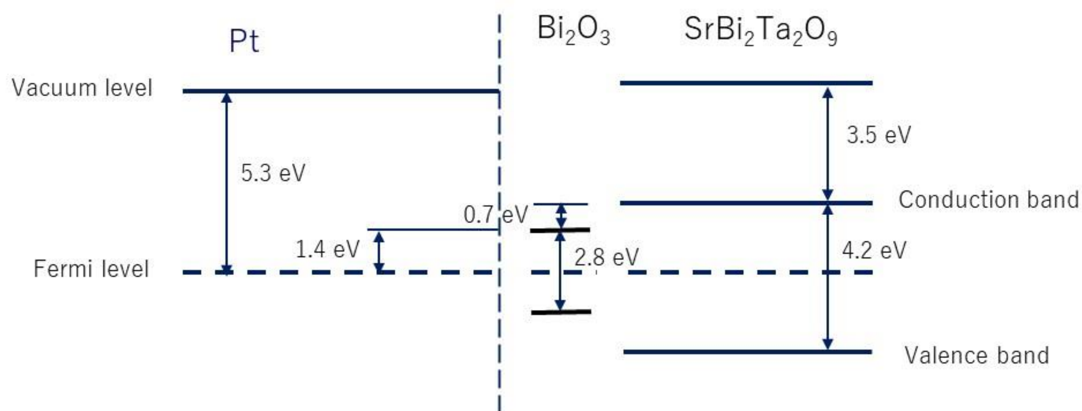

Figure 5.6 Expected energy-band match-up at the SBT/Bi_2O_3/Pt interface. Please note that the position of the energy level of Bi_2O_3 is not accurate.

So far, I have discussed the Schottky barrier height at 0 V. Next, let me consider the Schottky barrier height when an external electric field is applied to correlate with current-voltage characteristics in Bi-stoichiometric SBT film. There, it is necessary to take the Schottky effect into consideration. The Schottky effect is an effect of reducing the energy required for electrons to cross the electric field barrier by image field correction, and occurs when an external electric field is applied. The

reduction amount $\Delta\Phi$ of the electron barrier is represented by the following formula[43).

$$\Delta\Phi = (eE/4\pi\varepsilon)^{1/2} \qquad (5)$$

Here, attention must be paid to E and ε. According to Sze[43)], this E is the maximum value of the electric field at the junction, not the so-called average value V/d. It is difficult to determine this E, but it is considered to be a value that is an order of magnitude larger than the average value $E=V/d$. Here, it is set to 10 to 100 times the measured electric field. Furthermore, according to Sze[43)], the time for electrons to pass through the potential barrier at the metal-semiconductor interface is shorter than the time for dielectric relaxation, so the semiconductor does not have enough time to be polarized. Therefore, ε has a value smaller than the static dielectric constant. Therefore, the optical permittivity ε_{op} is considered reasonable here, which is equal to the square of the refractive index. It has been reported that the refractive index of SBT film in the visible region shifts to 2.0 on the long wavelength side and increases to 2.2 on the shorter wavelength side[65)], so here I set ε_{op} = 4.4 with n = 2.1. From these values, $\Delta\Phi$ is calculated to be in the range of approximately 0.2 to 0.7 eV in the range of E described above. Joshi *et al.* reported[66)] that $\Delta\Phi$ was 0.7 eV for the contact between the ferroelectric $Ba_{0.7}Sr_{0.3}TiO_3$ film and Pt. This is a numerical value close to our estimation result for the SBT/Pt interface this time, and it is considered to give validity to our estimation result. Based on the band lineup diagram shown in Figure 5.3, consider the effective barrier height considering this reduction in barrier height. The effective barrier

height at the Pt/SBT interface is estimated to be *2.1 eV-ΔΦ*, which is between 1.4 and 1.9 eV. It can be seen that when the amount of reduction in the electron barrier due to the image electric field correction is the maximum, the barrier height is close to 0.9 eV derived from our current-voltage characteristics and 1.0 eV derived from Seong *et al*. [44)] However, there is still a difference of 0.4 to 0.5 eV. There are two possible causes for this difference. One is that it is unclear what is the correct numerical value of the electric field and the dielectric constant when estimating the Schottky effect. Another point is the effect of the surplus of Bi existing on the surface, even if the surface is close to the stoichiometric composition ratio as shown in Figure 4.5. In particular, the author would like to mention the latter factor here. The Schottky barrier height of 0.9 eV was derived from the current-voltage characteristics for the SBT thin film with the starting composition ratio Bi of 2.0 and the Bi-stoichiometric composition ratio. However, it is known that Bi easily volatilizes and diffuses, and that the amount of Bi that can enter the defect site of Sr is limited as described in Chapter 2. Considering these, it can be said that excess Bi may exist on the surface of this SBT thin film. Therefore, it is considered that there are some factors that reduce the barrier height at the interface with Pt as shown in Figures 5.4, 5.5 and 5.6 even in the SBT thin film having a starting composition ratio Bi of 2.0. The work function of $PtBi_2$ is 0.5 eV smaller than that of Pt[63)]. When Bi_2O_3 is present at the interface, the bandgap is smaller than that of SBT by 1.4 eV[58),64)], and it is considered that the barrier height between Pt and SBT is reduced. Therefore, it is considered that the combined effect of these effects results in a Schottky barrier height of 0.9 eV derived from the current-voltage characteristics.

5.3 Summary

An attempt was made to construct an energy band model by integrating the results of the current-voltage characteristics described in Chapter 3 and the results of the electronic structure described in Chapter 4. From the results of current-voltage characteristics, it was shown that the Bi-stoichiometric SBT/Pt interface has the Schottky contact and the Bi-excess SBT/Pt interface has the Ohmic contact or Ohmic-like contact. From the results of electronic structure analysis using XPS and UPS, it was shown that more Bi exists on the surface of Bi-excess SBT film than on the surface of Bi-stoichiometric SBT film. And it was found that they caused Bi-excess SBT film to form bandgap states. From optical measurements and XPS analysis results, the band gap and electron affinity of SBT film were required to be 4.2 and 3.5 eV, respectively. Using these values and considering that the work function of Pt is 5.3 eV, the Schottky barrier height at the SBT/Pt interface at 0 V is estimated to be 1.8 eV. When excessive Bi exists at the interface between the SBT and the Pt electrode, a part of the platinum electrode may form an alloy with Bi at the interface with the SBT film, or Bi that does not form an alloy may exist. In addition to these, a model in which the semiconductor Bi_2O_3 exists between Pt and SBT film was also considered. In that case, the Schottky barrier height at the interface with SBT film will be low, and it will be possible to become quasi-Ohmic especially at the contact between Bi and SBT film. In the presence of an external electric field, it is necessary to consider the electron barrier lowering due to image

field effect correction. It is difficult to accurately estimate this effect, and some assumptions regarding the interfacial electric field and dielectric constant are necessary. If the interface electric field is assumed to be 10 to 100 times the average *V/d* and the permittivity is assumed to be the optical one, it is estimated that the maximum amount of reduction is 0.7 eV. The Schottky barrier height is estimated to be 1.4 eV when the reduction effect is maximum. It is close to the Schottky barrier height obtained from the current-voltage characteristics of SBT film near the Bi-stoichiometric composition ratio, but there are still differences. There are two possible causes for this difference. One is that it is unclear what is the correct numerical value of the electric field and the dielectric constant when estimating the Schottky effect. Another point is the effect of the surplus of Bi existing on the surface, even if the surface is close to the stoichiometric composition ratio. The author thinks that the complex factor due to the presence of Bi on the surface affects the reduction of the effective barrier height.

Comprehensively judging the results described so far, it is understood that the stoichiometric composition ratio as SBT near the surface is preferable for realizing stable contact with the electrode. On the other hand, in order to obtain a large remanent polarization value, Sr-deficient and Bi-excess SBT are preferable, but it is necessary to perform delicate control of the Bi composition ratio in consideration of the upper limit of the amount of Bi substituted in the Sr site[31)]. It is considered that this makes it possible to suppress the excessive Bi that diffuses to the surface and achieve both stable contact characteristics with the electrode and a large remanent polarization value. In the next chapter, the optimum composition

ratio of SBT thin film will be considered.

Chapter 6 Consideration on optimum composition ratio of SBT thin film

6.1 Introduction

From the discussion so far, it was experimentally shown that the ferroelectric properties of Sr-deficient and Bi-excess SBT film are superior to those of SBT film with a stoichiometric composition ratio. It was also introduced using the results of other researchers that the principle is that the strain of TaO_6 octahedron becomes large by substituting Bi for a part of vacancy of Sr site. On the other hand, it was also clarified that the presence of Bi, which is not incorporated in the crystal structure of SBT, diffuses to the surface of SBT film and adversely affects the contact characteristics with the electrode material. From these facts, in order to achieve both high ferroelectric properties and stable contact properties, it is necessary to finely control the composition of Bi, and this creates a kind of contradictory situation.

In this chapter, I discuss the optimum composition ratio of SBT thin film to achieve both high ferroelectric properties and stable contact properties.

6.2 Consideration on optimum composition ratio of SBT thin film

There are two points about what is important in considering the optimum composition ratio of the SBT thin film. The first point is how much Bi substitutes into the vacancy of the Sr site. The second point is how much Bi can diffuse, or how to suppress the diffusion of Bi. First, consider the substitution amount of Bi for the Sr site. As discussed in Chapter 2, the results of Shimakawa *et al*. [31)] are very helpful in this regard. According to it, it is found that the occupied state of the Sr site of SBT aimed at $Sr_{0.8}Bi_{2.2}Ta_2O_9$ is $Sr_{0.82}Bi_{0.12}[]_{0.06}$, where [] represents vacancies. This is also reasonable from the viewpoint of charge neutrality. Because the charge of Sr site is +2 when the substituted Bi and vacancies are combined. The optimal composition ratio of Bi in this case is considered to be 2.12 together with the original Bi site 2.0. In the same way as this, possible cases of Sr site occupancy in Sr-deficient state are given. For example, $Sr_{0.85}Bi_{0.10}[]_{0.05}$, $Sr_{0.88}Bi_{0.08}[]_{0.04}$ and $Sr_{0.91}Bi_{0.06}[]_{0.03}$ may be considered. The Bi composition ratios in these cases are considered to be 2.10, 2.08, and 2.06 together with the original Bi site 2.0, respectively.

On the other hand, it is necessary to know the composition range in which high ferroelectric properties are actually obtained. So far, we have selected the starting compositions Sr/Bi/Ta=0.8/2.4/2.0 and 0.8/2.0/2.0 for detailed discussion. Here, author would like to mention the results of examining the composition ratios

in the vicinity of these. Figure 6.1 shows the voltage dependence of the remanent polarization value obtained by adding the results of the composition ratio of the periphery to Figure 2.10. Table 6.1 is a comparison of the composition ratio of the precursor solution (starting composition ratio), the film composition ratio, and the surface composition ratio obtained by adding the results of the composition ratio of the periphery to Table 2.1. Looking at Figure 6.1, it can be seen that in addition to the starting composition ratio of 0.8/2.4/2.0, the ferroelectric properties of 0.9/2.4/2.0 and 0.9/2.2/2.0 are excellent. On the other hand, it is again recognized that when the starting composition ratio Bi becomes 2.0, the ferroelectric properties deteriorate. In order to discuss the final film composition, Figure 6.2 shows the index of composition ratio in the graph of Figure 6.1 described in Table 6.1 as the film composition ratio by EPMA. Further, in Figure 6.3, the relationship between the composition ratio of Sr and the composition ratio of Bi by EPMA and the residual polarization value 2Pr at 5 V of the film shown in Figure 6.2 is represented in three dimensions. Looking at Figures 6.2 and 6.3, it seems good that the Sr composition ratio is close to 0.9 and the Bi composition ratio is around 2.1 from the viewpoint of ferroelectric properties. Referring to the results of Shimakawa *et al.*[31)], it can be said that the Sr sites are $Sr_{0.88}Bi_{0.08}[]_{0.04}$ and $Sr_{0.91}Bi_{0.06}[]_{0.03}$, and the total Bi composition ratio is preferably around 2.1. This means around 0.9/2.3/2.0 in terms of the starting composition of the precursor solution.

Next, let me consider the diffusion of Bi. Looking at Table 6.1, the surface composition ratios of the films having the starting composition ratios of 0.9/2.2/2.0 and 0.9/2.4/2.0 are 1.5/3.1/2.0 and 1.4/3.6/2.0, respectively. Therefore, it can be

seen that Bi is excessively present on the surface. It can be said that the surface composition ratio of 1.5/3.1/2.0 of the film having the starting composition ratio of 0.9/2.2/2.0 is close to an appropriate state when focusing on the ratio of Sr and Bi. If the ratio of Sr and Bi is proper on the surface, Ta is insufficient. It is not known here what structure it forms. However, considering the results of the surface composition ratios of other samples, it can be said that Bi easily diffuses to the surface. In particular, in film formation by spin coating, it is considered that Bi, which is in an easily movable state, may diffuse before being incorporated into the crystal structure during RTA or heat treatment. In order to avoid this, it is considered preferable to form the film while heating the substrate by a method such as sputtering so that Bi is firmly incorporated into the film immediately after the film formation. From this viewpoint, it can be said that it is more preferable if a film forming method such as Atomic Layer Deposition (ALD) is developed.

From the above discussion, the composition ratio of SBT film is preferably Sr/Bi/Ta=0.9/2.1/2.0 in order to achieve both high ferroelectric properties and stable contact properties with electrode materials. Then, as a film forming method, it is better to avoid a spin coating method in which Bi easily moves. A sputtering method or the like, which is expected to incorporate Bi into its crystal structure during film formation by heating the substrate, is preferable. Even so, there is a risk that Bi will spread and surplus Bi will exist on the surface. Finally, assuming that Bi diffuses to some extent, the author would like to propose to intentionally create a Bi composition distribution in the film thickness direction. The image is shown in Figure 6.4. An initial layer near the lower electrode and a final layer near the upper

electrode are formed aiming at the film composition ratio of $Sr_{0.9}Bi_{2.0}Ta_2O_9$. Then, the layer sandwiched between them is made a little Bi-rich film composition to be $Sr_{0.9}Bi_{2.1}Ta_2O_9$. By this measure, it is considered that both high ferroelectric property and stable contact property with the electrode can be achieved. In particular, if film formation by ALD that enables precise composition control is established, it will be easy to realize this ideal composition ratio structure.

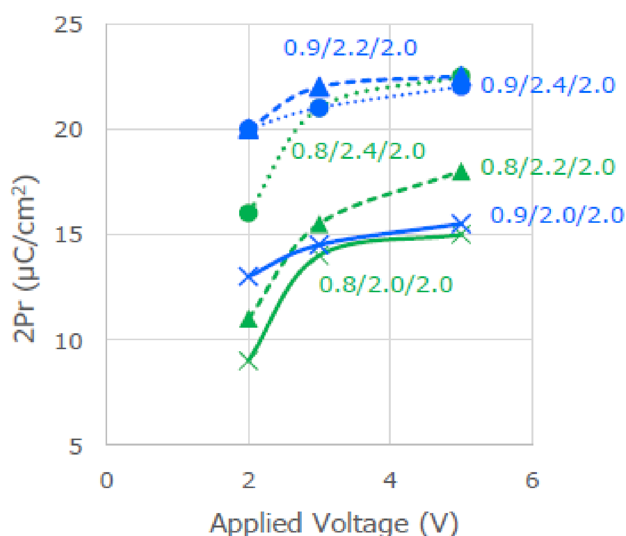

Figure 6.1 Voltage dependence of the remanent polarization value obtained by adding the results of the composition ratio of the periphery to Figure 2.10.

Table 6.1 Comparison of the composition ratio of the precursor solution (starting composition ratio) measure by ICP, the film composition ratio measured by EPMA, and the surface composition ratio measured by XPS obtained by adding the results of the composition ratio of the periphery to Table 2.1.

Precursor(Sr/Bi/Ta)	Film	Surface
0.8/2.4/2.0	0.8/2.2/2.0	1.0/3.2/2.0
0.8/2.2/2.0	0.8/2.0/2.0	1.1/2.9/2.0
0.8/2.0/2.0	0.8/1.8/2.0	0.9/2.1/2.0
0.9/2.4/2.0	0.9/2.2/2.0	1.4/3.6/2.0
0.9/2.2/2.0	0.9/2.0/2.0	1.5/3.1/2.0
0.9/2.0/2.0	0.9/1.8/2.0	1.2/2.3/2.0

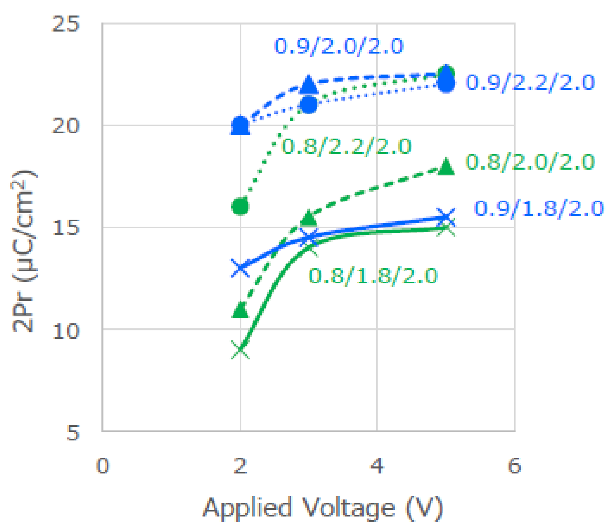

Figure 6.2 The same data as in Figure 6.1, but the voltage dependence of the remanent polarization value when the composition ratio was expressed by the film composition measured by EPMA.

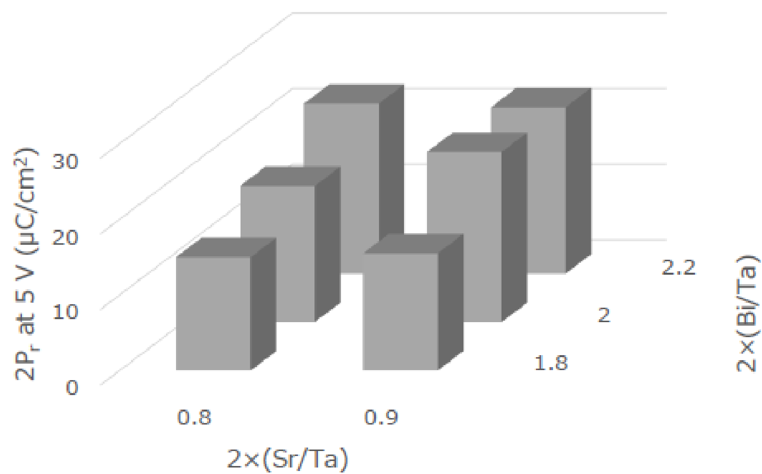

Figure 6.3 Relationship between the composition ratio of Sr and the composition ratio of Bi by EPMA and the residual polarization value 2Pr at 5 V of the film shown in Figure 6.2

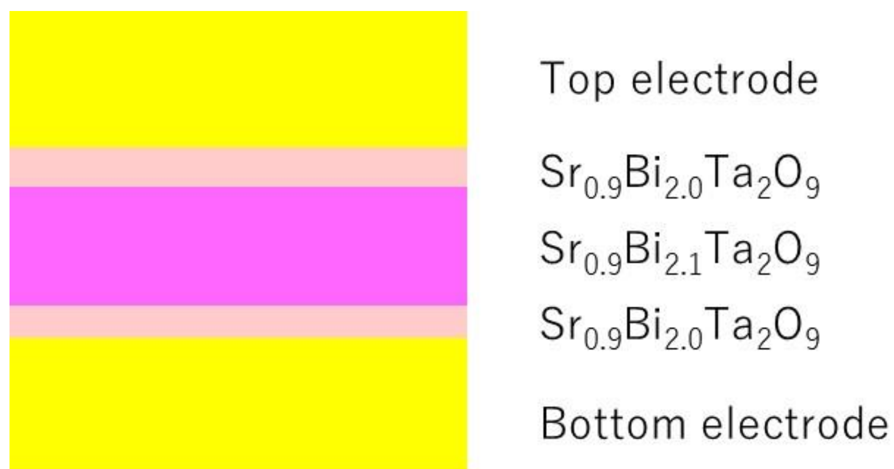

Figure 6.4 A schematic diagram of a film structure proposed by the author as an optimal SBT thin film composition for changing the Bi composition ratio in the film thickness direction.

6.3 Summary

In this chapter, the optimal SBT thin film composition was considered. In order to achieve both high ferroelectric characteristics and stable contact characteristics with electrodes, it is necessary to precisely control the Bi composition ratio while keeping the Sr deficiency and Bi excess composition ratios as the basis. The amount of Bi that can be substituted for vacancy on the Sr site was estimated with reference to the results reported by Shimakawa *et al*. [31)] Considering together with the experimental results of changing the composition ratio of Sr and Bi, the optimum composition ratio of the film was Sr/Bi/Ta=0.9/2.1/2.0. In film formation by spin coating, Bi, which is originally in an easily movable state, easily moves during the heat treatment. Therefore, a method of forming a film while heating the substrate, such as sputtering, is preferable. This is because it becomes possible to incorporate Bi into the film structure at the time of film formation. Furthermore, it was proposed to intentionally create a Bi composition distribution in the film thickness direction, assuming that Bi will diffuse to some extent. By this measure, it is considered that high ferroelectric characteristics and stable contact characteristics with electrodes can be achieved at the same time. It would be even better if ALD film formation was developed, which enables precise composition control to realize this ideal composition ratio structure.

Chapter 7 Recent advances in ferroelectric materials for ferroelectric memory research

7.1 Introduction

The research written in this thesis was mainly conducted about 20 years ago. During the last 20 years, research on ferroelectric materials and applications for ferroelectric memories have been progressing steadily but not quickly. The structure of the ferroelectric memory that was mainly studied 20 years ago was a memory cell structure similar to the DRAM introduced in Chapter 1. It was a 1T1C type which constituted a memory cell with one cell selection transistor and one ferroelectric capacitor. This is a structure called FeRAM. Much research has been done on this structure, including my own work, and many things have become clear regarding device characteristics. On the other hand, in recent years, research on a memory cell in which a ferroelectric material is used for a gate insulating film of a transistor, such as metal-oxide-semiconductor field-effect transistor (MOS FET) has been activated. The gate structure usually has an MFIS structure of a gate metal (M), a ferroelectric thin film (F), a protective insulating film (I), and a silicon substrate (S) from the top[67)]. This structure is also called FeFET (Ferroelectric FET) memory. It is also called the 1T type as compared with the 1T1C type described above. Compared with the 1T1C type, the 1T type is advantageous for high integration, so research has been actively conducted while evolving ferroelectric material technology.

Furthermore, a new ferroelectric material that has affinity for semiconductor processes, such as Complementary MOSFET (CMOS) integration processes has also appeared. In this chapter, I will consider the recent technological trends and basic ideas such as the electrical conduction mechanism.

7.2 Research progress of SBT

Since SBT film has a fatigue-free and low leakage current[12)], research on applying SBT film to a ferroelectric memory is being continued in several research groups[68)-70)]. Among them, the research of Sakai *et al.* [68),71),72)] at the National Institute of Advanced Industrial Science and Technology is worthy of attention. They are conducting research to apply SBT film to 1T type FeFET. A feature of their technology is that they use a material that is difficult to be polycrystallized even by heat treatment at 800 ℃ for the insulating film between SBT film and Si. It is HfO_2 or HAO in which HfO_2 is doped with aluminum (Al)[68),71)]. This maintains a good SBT/insulator interface even after high-temperature heat treatment at 800 ℃. Pt and iridium (Ir) are used for the electrodes on the SBT. Since the work function of Ir is 5.27 eV[54)], which is almost the same as that of Pt, it is considered to be a selection assuming a stable Schottky contact. It is considered that they do not use Bi-excess SBT film but use SBT film which is close to stoichiometric composition ratio. To improve the ferroelectric properties of SBT, a structure in which a part of the Sr site was replaced with calcium (Ca) was adopted. They used $Ca_{1-x}Sr_xBi_2Ta_2O_9$ (CSBT) film. Both remanent polarization and coercive field are improved in CSBT compared with SBT. For example, when Ca is 0.2 and Sr is 0.8, it is reported that the remanent polarization value P_r is 23 μC/cm^2 and the coercive field E_c is 134 kV/cm[73)], and both values are 2 times or more of the typical value of SBT. It is an important point of the experimental result on CSBT film that high remanent

polarization value can be obtained without excess Bi. It is therefore considered that this can stabilize the contact with Pt and Ir. And it can be considered that the structure of the SBT/Ir interface when Ir is used as an electrode is equivalent to that in Figure 5.6 because the work function is equal to Pt. Figure 7.1 shows the typical device structure which they employ[72)]. The composition ratio of CSBT film used here is $Ca_{0.2}Sr_{0.8}\ Bi_2Ta_2O_9$. They demonstrated 10^9 cycle endurance and 10^5 s retention of FeFETs by 3.3 V writing with this structure. Their combination of Bi-stoichiometric SBT (CSBT) film with Pt and Ir electrodes is expected to have stable contact characteristics. On the other hand, the electronic structure of CSBT in which a part of the Sr site of SBT is replaced with Ca has not been clarified yet. It is expected that the analysis described in this thesis will be conducted in the future in order to understand in detail the effect of the substitution of Sr sites by Ca on the electrical and electronic properties.

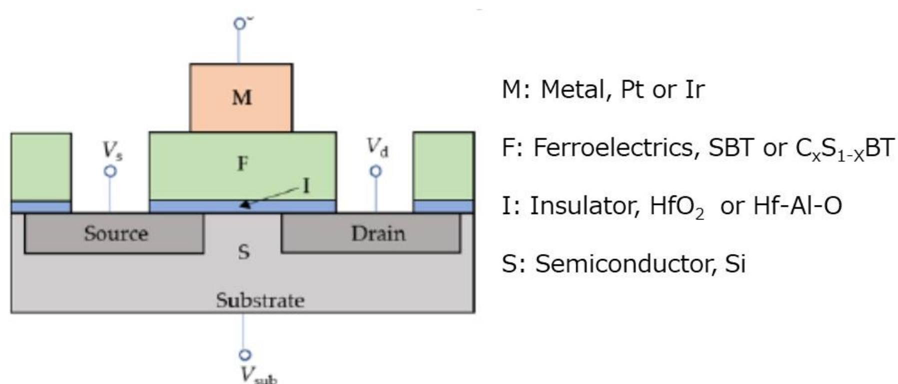

Figure 7.1 Schematic figure of the FeFET with MIFS stack take from ref. 72.

7.3 New ferroelectric material

As mentioned above, research on FeFET using SBT film is progressing. On the other hand, it has been found experimentally that thin films of ferroelectric materials such as SBT and PZT have a serious weakness that the amount of polarization rapidly decreases when the film thickness is reduced. This property is called "size effect", and the thickness limit is said to be approximately 100 nm. This film thickness means that the 130 nm rule is the lower limit in the generation of the CMOS process. In fact, it has been reported that when the PZT thin film has a thickness of 276 nm as a reference, the residual polarization value decreases by 55% at a thickness of 90 nm[74]. It has been reported that, when the SBT thin film has a thickness of 240 nm as a reference, the remanent polarization value decreases by 16% at a thickness of 90 nm[74]. This is because the perovskite structure or the layered perovskite structure requires heat treatment at a high temperature and complicated composition ratio control, and thus a transition layer is easily formed near the interface with the electrode. This size effect reduces the attractiveness of ferroelectric memories. Because the minimum feature size of 28 nm/20 nm is used as standard in CMOS logic, 130 nm is still large. Therefore, it will be necessary to consider use cases that do not require large memory capacity. Since this is a problem based on the experimental results, it can be considered that the problem includes both the essential problem of the ferroelectric material and the problem of the manufacturing process of the ferroelectric thin film. To overcome this limitation,

improvements in ferroelectric materials and/or processes are required.

Against the background described above, it is very significant that the German research group reported the development of ferroelectricity in a thin film of hafnium oxide (HfO_2) having a fluorite structure as a basic composition in 2011[75]. HfO_2 obtained by oxidizing metal hafnium has been used in semiconductor devices as a paraelectric insulating film having a high dielectric constant. Specifically, it is a gate insulating film of a metal gate or a dielectric film of a DRAM capacitor. In terms of the HfO_2 process, film forming techniques such as the ALD method for producing a three-dimensional structure have been established, and microfabrication technology has also been established. Therefore, it can be said that HfO_2 is a material that is compatible with advanced CMOS processes. It was shown that when HfO_2 was added with trace elements and heat-treated, it exhibited ferroelectricity. Moreover, it has been found that there is little deterioration of the ferroelectric characteristics in the treatment under a reducing atmosphere[76], and that even if the film thickness is reduced to 2.5 nm, the deterioration of the ferroelectric characteristics is small[77]. Therefore, it can be said that HfO_2 is a material that can overcome the size effect, which has been a problem with existing materials.

The origin of ferroelectricity of HfO_2-based thin films has been well understood. Figure 7.2 shows the crystal structures of HfO_2 based ferroelectrics and perovskite-based ferroelectrics taken from ref. 78. It has been shown that the ferroelectricity of HfO_2-based thin films appears in the orthorhombic phase[79)-81]. It is considered that the composition of the HfO_2 ferroelectric is easier to control than that of the perovskite ferroelectric or the layered perovskite ferroelectric because

the HfO_2 ferroelectric has few constituent elements even if an additive element is added. Further, perovskite ferroelectrics and layered perovskite ferroelectrics require heat treatment at a high temperature of 550 °C to 800 °C, but HfO_2 ferroelectrics have different optimum heat treatment temperatures depending on the type of dopant added and it is also a feature. For example, when doping Si or Al, a high temperature treatment of 800 °C or the like is performed[82)], but when doping Zr, a low temperature process of 400 °C or lower is possible[83)]. The former is suitable for the FEOL (Front-end of line) process, and the latter is suitable for the BEOL (Back-end of line) process. These offer the advantage of process flexibility.

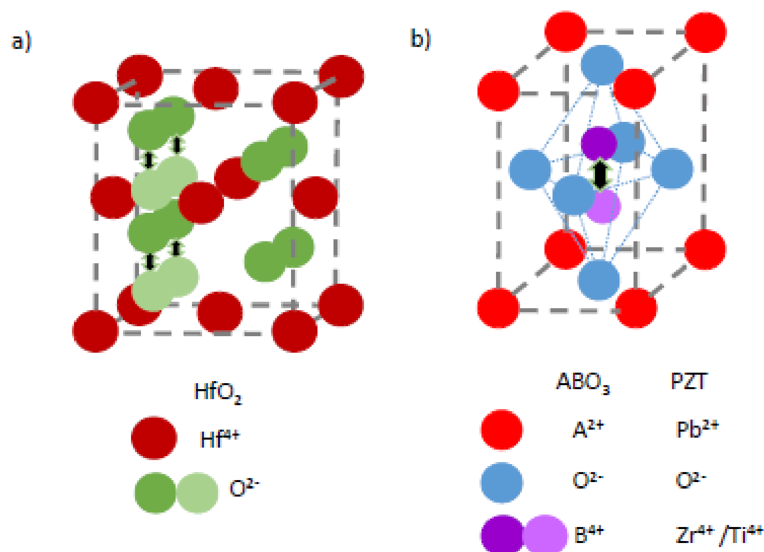

Figure 7.2 Crystal structures of HfO_2 based ferroelectrics and perovskite-based ferroelectrics taken from ref. 78. The arrows indicate the movement of the ions during ferroelectrics switching.

7.4 Benchmark of various ferroelectric thin films and memory devices using them

Table 7.1 shows a comparison table of characteristics of ferroelectric materials and characteristics of recent ferroelectric memory devices using them. In preparing this table, regarding the material properties of SBT and CSBT films, the literatures with reference numbers 44, 73, 74 and 84 were referred to in addition to the research results of this thesis. Regarding the material properties of PZT film, those of 74, 85, 86 and 87 were referred to. Regarding the material properties of HfO_2 film, those of 77, 79 and 88 were referred to. Regarding the memory properties of each material, those of 71, 89, 90, 91 and 92 were referred to.

The HfO_2 ferroelectric has a high remanent polarization value of 15 μC/cm^2 even in a thin film of 10 nm. On the other hand, SBT and PZT, which are representatives of perovskite ferroelectrics and layered perovskite ferroelectrics, have been mainly used for films thicker than 100 nm. The thickness dependence of the ferroelectric properties is as described in the previous section. For SBT and PZT films, the lower grain size limits at which ferroelectricity appears have been calculated and reported to be 2.6 nm[84)] and 5.6 nm[85)], respectively. Similar reports on HfO_2 are not yet available. The coercive electric field of HfO_2 ferroelectrics is also characteristic. The coercive electric fields of PZT and SBT are both around 50 kV/cm, whereas that of HfO_2 ferroelectrics is 1 MV/cm. The very high coercive electric field of HfO_2 ferroelectrics poses a problem with the device driving voltage when the film

Table 7.1 Comparison of characteristics of ferroelectric materials and characteristics of recent ferroelectric memory devices using them. The data marked with * is the data of this thesis. The following web information is partially used as reference.
https://pc.watch.impress.co.jp/docs/column/semicon/1226051.html

	Ferroelectric material	SBT	CSBT	PZT	HfO_2	
Material properties	Remanent polarization value P_r ($\mu C/cm^2$)	10 * (180 nm thickness)	23 [73] (350 nm thickness)	25 [86] (276 nm thickness)	15 [79] (10 nm thickness)	
	Coercive electric field E_c	50 kV/cm *	134 kV/cm [73]	47 kV/cm [86]	1 MV/cm [79]	
	Reduction of Pr value in thin film	-16 % [74] (240 nm -> 90 nm)	unknown	-55 % [74] (276 nm -> 90 nm)	No reduction to 10 nm or less	
	Lower grain size limit for ferroelectricity (calculation)	2.6 nm [84]	unknown	5.6 nm [85]	unknown	
	Proven thin film deposition method	Spin-coating, Sputtering, CVD	Laser-deposition, Sputtering, CVD	Spin-coating, Sputtering, CVD	ALD, Sputtering, CVD	
	Electron affinity (eV)	3.5 *	unknown	3.5	3.0 [88]	
	Bandgap (eV)	4.2 *	unknown	3.4 [87]	5.0 – 5.9 [77],[88]	
	Schottky barrier height at the interface with electrode at 0V from XPS/UPS (eV)	1.8 on Pt *	unknown	1.8 on Pt [87]	1.7 on TiN [77]	
	Schottky barrier height at the interface with electrode under voltage application from I-V data (eV)	0.9–1.0 *,[44] on Pt at 3 V	unknown	1.5 [87] on Pt at 3 V	Unknown	
	Reactivity with electrode material	Bi easily reacts	unknown	Pb easily reacts	Small risk	
	References	44, 74, 84	73	74, 85, 86, 87	77, 79, 88	
Recent memory device properties	Example of prototype device type	FeFET (1T)	FeFET (1T)	FeRAM (1T/1C or 2T/2C)	FeFET (1T)	FeRAM (1T/1C)
	Structure sandwiching a ferroelectric	Pt/SBT/Hf-Al-O/Si	$Ir/Ca_{0.2}Sr_{0.8}Bi_2Ta_2O_9$ $/HfO_2/Si$	$TiAlN/Ir/PZT/IrO_2$	TiN/HfO_2 (Si doped)/SiON/Si	$TiN/Hf_{0.5}Zr_{0.5}O_2$ /TiN
	Production technology	Gate length 5 μm Gate width 5 μm	Gate length 10 μm Gate width 20 μm	130 nm CMOS	28 nm High-k metal gate	130 nm CMOS
	Area of ferroelectric	25 μm^2 (Gate area)	200 μm^2 (Gate area)	0.4 μm^2	0.045 μm^2 (Cell area)	0.27~0.12 μm^2
	Write time	1 ms	10 μs	110 ns	500 ns	100 ns
	Write cycle	10^8	10^8	10^{15}	10^5	10^{11}
	Retention time	unknown	10 y (120 ℃)	10 y (125 ℃)	10 y (105 ℃)	10 y (125 ℃)
	References	89	71	90	91	92

thickness is large. However, when the film thickness becomes thin due to advanced thickness scaling, the advantage is that a memory window can be secured even under an ultrathin film. This feature is also the reason why the HfO_2 ferroelectric is suitable for high integration. As in the case of SBT and PZT films, the Schottky contact is expected to be the basic contact property between the HfO_2 ferroelectric and the electrode material. However, this technical area is in the developing stage, and there are not many reports. Chernikova *et al*. analyzed the electronic structure of the $Hf_{0.5}Zr_{0.5}O_2$ ferroelectric thin film using XPS and estimated the Schottky barrier height at the interface with the TiN electrode to be 1.7 eV[77)]. However, no comparison has been made with electrical characteristics such as current-voltage characteristics. Since HfO_2-based thin films have long been used as gate insulating films for metal gates and dielectric films for DRAM capacitors, research on electronic structures as high dielectric thin films is progressing. For example, Kumar *et al*. have clarified the electronic structure and electron conduction mechanism of the $Al/HfO_2/Si$ structure using the same method as our method of using current-voltage characteristics and UPS analysis together[88)]. They showed that the Schottky barrier height at the interface between Al and HfO_2 was 1.12 eV for the amorphous phase HfO_2 thin film with the thickness of 39 nm formed by using the solution technique. Together, they show that the electron conduction mechanism is dominated by the Schottky emission in the low voltage region and by space charge limited current in the high voltage region. As for the reactivity with the electrode material, as described in this thesis, Bi is liable to cause diffusion and reaction in SBT film. Similarly, the presence of Pb is a risk in PZT film. On the other hand, HfO_2 has a

lower risk of reaction with the electrode material than SBT and PZT. For SBT and PZT, composition control and interface engineering are also important issues.

In order to consider the application of the memory using each ferroelectric material, a graph of the key parameters was made from the material data of upper half of Table 7.1 and the reference literature that became the source. Figure 7.3 shows the relationship between the film thickness of the ferroelectric and its remanent polarization value P_r. And Figure 7.4 shows the relationship between the remanent polarization value P_r of the ferroelectric and its coercive electric field E_c. As can be seen from these figures, and as will be repeatedly stated, the ferroelectric

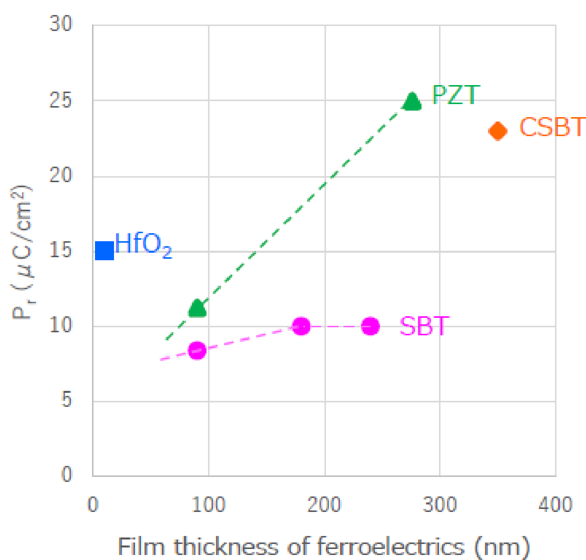

Figure 7.3 Relationship between the film thickness of the ferroelectric and its remanent polarization value P_r.

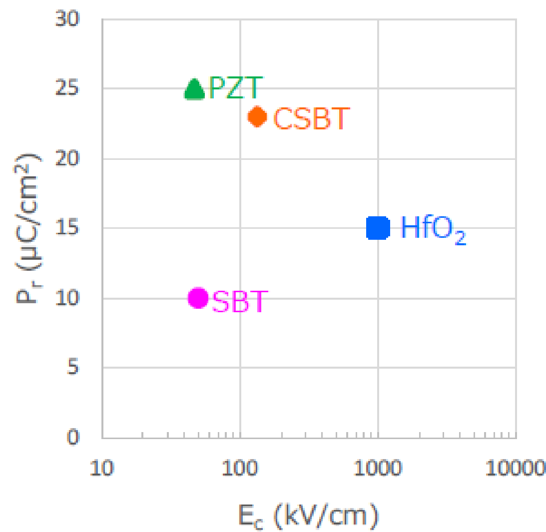

Figure 7.4 Relationship between the remanent polarization value P_r of the ferroelectric and its coercive electric field E_c.

characteristics and high coercive electric field of HfO_2 in the ultra-thin film region are suitable for miniaturization/advanced integration. On the other hand, it is expected that it will be difficult to reduce the thickness of SBT and PZT films to the same level as HfO_2 film, because the deterioration of the ferroelectric properties is noticeable when the thickness is reduced at the current level of technology. Among them, CSBT is interesting. By replacing part of the Sr site of SBT with Ca, both P_r and E_c become large as described in the previous section. And CSBT is valuable in that it does not require excess Bi to obtain high P_r. This may be suitable for higher integration than SBT film. However, since only sporadic data exists in CSBT film, it is expected to acquire detailed physical property data of CSBT film.

Regarding the characteristics of recent memory devices, progress has been made in PZT 1T1C/2T2C types[90)] and CSBT 1T type[71)]. The device characteristics using CSBT and PZT are good. The write cycles have reached over 10^8 cycles for CSBT and 10^{15} cycles for PZT. And the retention characteristic can secure a data retention period of 10 years in both. Figure 7.5 shows the relationship between the area and film thickness of the ferroelectric used in the prototype memory device shown in the lower part of Table 7.1. As described in this figure, the problem that

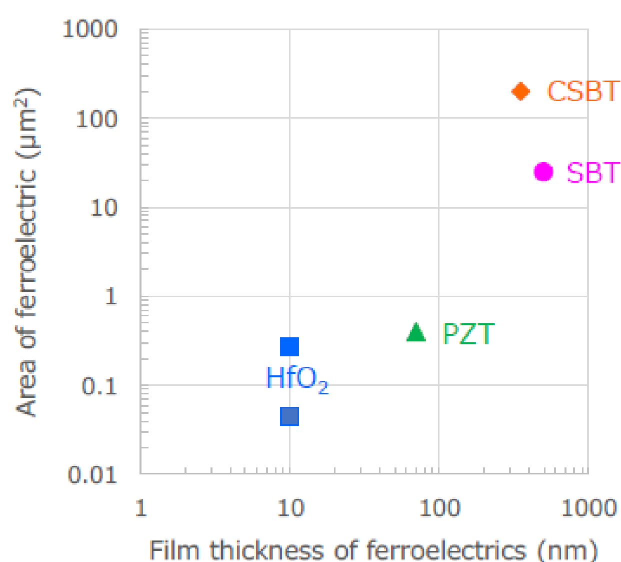

Figure 7.5 Relationship between the area and film thickness of the ferroelectric used in the prototype memory device shown in the lower part of Table 7.1.

the minimum processing size remains large can be seen for SBT, CSBT and PZT films. Especially in SBT and CSBT films, it seems that the current focus is on

obtaining a proof of concept with a loose design. In the PZT memory device evaluation using the 130 nm CMOS process described here, the PZT film thickness reaches 70 nm. On the other hand, looking at Figure 7.3, it can be seen that the PZT film thickness of 70 nm is in a region where the ferroelectric characteristics are considerably low. From this, it is considered that the current PZT thin film is approaching the miniaturization limit. Regarding the SBT (CSBT), there are only verification results for low-capacity memory elements, but the potential of the SBT film is equivalent to PZT near a film thickness of 100 nm or less, as shown in Figure 7.3. Therefore, the SBT film is considered to be compatible with 130 nm CMOS process like the PZT film. Therefore, the device using SBT or PZT film has reached a level where the basic characteristics can be satisfied, so the use case for low capacity is suitable. Paradoxically, using low-cost processes such as the 130nm CMOS process is also meaningful as a corporate strategy. By the way, it is considered that the deterioration of the ferroelectric properties of the SBT-based and PZT-based thin films is caused by the remarkable surface effect of grains. Specifically, the space charge due to the grain surface defects and the domain pinning due to the surface layer of the grains are considered to be the factors[86]. It is expected that further miniaturization will be expected when ALD that can form a dense and high-quality film can be used for film formation with respect to SBT and PZT films. What is the potential for SBT and PZT to be refined? As shown in the upper half of Table 7.1, the calculation result on the minimum grain size where ferroelectricity of SBT and PZT appears has been reported. SBT is reported to be 2.6 nm[84] and PZT to be 5.6 nm[85]. Assuming that a film thickness 10 times the minimum size is required to

obtain stable ferroelectric properties, it is estimated that a film thickness of 26 nm or more is required for SBT and 56 nm or more is required for PZT. Further, it is assumed that 100 times the minimum size is necessary for one side of the capacitor area in consideration of the effect on the variation of the element characteristics. Under this assumption, an area of 260 nm × 260 nm or larger for SBT and that of 560 nm × 560 nm or larger for PZT are required. Figure 7.6 shows these estimation lines added to Figure 7.5. In this figure, it can be seen that the PZT film has reached the trial manufacture evaluation in the region near the lower limit value on the estimation. On the other hand, regarding the SBT film, it can be seen that there is still a lot of room for miniaturization as a potential of the material. Although there is no report on the lower limit size of CSBT, since CSBT is an SBT family, a size close

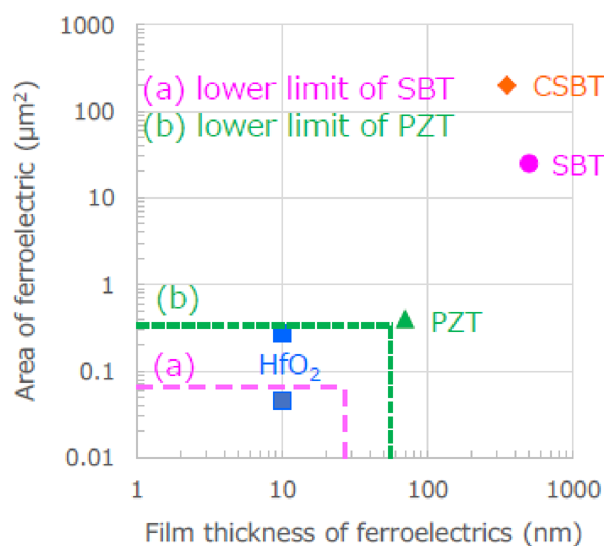

Figure 7.6 Estimated lower limit of film thickness and area for SBT and PZT. The lower limit lines have been added to Figure 7.5.

to SBT is expected. In order to prove this hypothesis on SBT and CSBT, it will be necessary to develop the process technology as well as the film formation technology, and to expand the basic data with the miniaturization in mind.

Next, let me consider the possibility of miniaturization from the viewpoint of the coercive electric field of each material. In Figure 7.7, the lines of the necessary coercive electric field derived under certain preconditions are included in Figure 7.4, and the relationship between P_r and E_c is shown again. These show the necessary coercive electric field, assuming that 1/3 of the rewriting voltage of the memory element is an appropriate coercive voltage of ferroelectric films. The line (a) is the necessary coercive electric field when rewriting voltage is 1.5 V, coercive voltage is 0.5 V, and ferroelectric film thickness is 10 nm. This area will be the exclusive venue for HfO_2 film. The line (b) shows the necessary coercive electric field assuming a rewriting voltage of 3.0 V, a coercive voltage of 1.0 V, and a ferroelectric film thickness of 50 nm. From this figure, it can be seen that CSBT film has potential in this area. Therefore, there seems to be room for further study on CSBT film from this perspective, too. There is a possibility that P_r and E_c can be further optimized by optimizing the Ca content and examining the Ca gradient composition in the film thickness direction. Again, it is expected that the basic data of CSBT film will be further expanded to expand its application.

On the other hand, HfO_2 film has already been tested and verified in the 28 nm process generation[91)], and it is clear that it has a great advantage in miniaturization. However, there is a problem in write cycle, and it remains at 10^5 cycles as shown in Table 7.1. Interestingly, with the 1T1C type using $Hf_{0.5}Zr_{0.5}O_2$

film, the write cycle is 10^{11} cycles[92], and good performance has been obtained. The reason that the write cycle characteristics of 1T type devices using HfO_2 ferroelectrics is low is thought to be due to the behavior of the charge near the interface between the gate metal and the ferroelectric and its interface state, and the behavior of the charge near the interface between the protective insulating film and the silicon substrate and its interface state[93]. In order to solve this problem, it is effective to deeply pursue the interface characteristics while comparing with the 1T1C type using $Hf_{0.5}Zr_{0.5}O_2$ film. In addition, since the film thickness of HfO_2-based

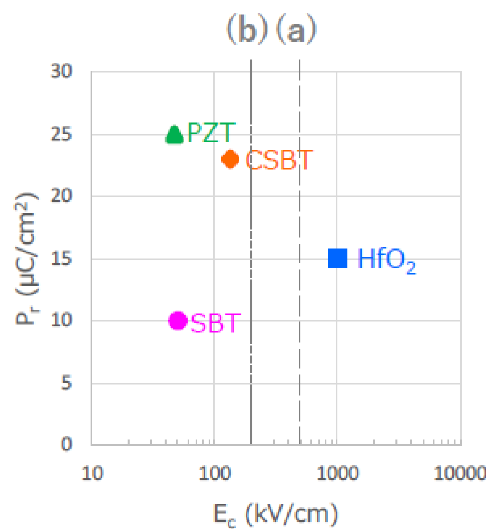

Figure 7.7 Relationship between the remanent polarization value P_r of the ferroelectric and its coercive electric field E_c including the lines of the necessary coercive electric field derived under certain preconditions. The line (a) is the necessary coercive electric field when rewriting voltage is 1.5 V, coercive voltage is 0.5 V, and ferroelectric film thickness is 10 nm. The line (b) shows the necessary coercive electric field assuming a rewriting voltage of 3.0 V, a coercive voltage of 1.0 V, and a ferroelectric film thickness of 50 nm.

ferroelectric film becomes thinner than 50 nm with the miniaturization, understanding of the electron conduction mechanism and interface engineering become more important.

As mentioned above, the electronic structure and interface characteristics centered on the interface between the ferroelectric phase HfO_2 thin film and the electrode are still under study. With respect to HfO_2 thin films, research and development of device integration are ahead, and verification is often limited to the scope of the research and development. The research for the detailed understanding of the interface characteristics due to the difference in the composition of HfO_2-based thin films, the difference in the elements to be doped, and the difference in the electrode material types to be combined will be enhanced in the future. In order to solve the problems toward the realization of devices using HfO_2-based ferroelectric thin films, it is essential to deepen the understanding of the interface characteristics represented by the ferroelectric/electrode interface. It is expected that research on ferroelectric/electrode interface characteristics based on our method will become more active. In addition to the pursuit of interface characteristics, it may be meaningful to consider using high-k HfO_2 film for the buffer layer as a structural optimization proposal for the purpose of suppressing interface defects and the interface engineering is important there, too.

7.5 Future application development

As introduced in Chapter 1, non-volatile memory with high speed and low power consumption is essential to realize the world of Society 5.0. With Society 5.0, edge devices will become more important and will require non-volatile memory for edge device use cases. Figure 7.8 is a figure in which the author added the use cases assumed in Figure 1.2. The cloud side requires a large capacity. On the other hand, on the edge side, the required capacity is expected to change depending on the use case. For example, not only a normal data memory but also a buffer memory, a non-volatile SRAM, *etc*. can be considered as a use case. The memory using SBT film and PZT film can be a strong candidate there. Moreover, it should be reiterated that utilizing low-cost processes such as the 130nm CMOS process is also meaningful as a corporate strategy. There are some notable points regarding future edge computing. The neuromorphic device is an essential element of the neural network which is the basic configuration of machine learning. In-memory computing in edge device has been attracting attention for efficient processing of neural networks. The ideal form from the viewpoint of energy efficiency is an analog AI chip[3)]. Studies have been proposed for using FeFET as a non-volatile memory arranged at a cross point in an analog AI chip[4)-7)]. There are studies of both HfO_2-FeFET applications[4)-6)] and CSBT-FeFET applications[7)]. Sakai's team at AIST and Morie's team at Kyushu Institute of Technology are verifying the principles of analog neuromorphic devices with FeFET using CSBT film[7)]. They applied FeFET to a

weighted sum calculation circuits, and reported that the calculation accuracy met the necessary accuracy to realize inference operations and could be 100 times more energy efficient than a digital AI processor. For reference, Table 7.2 shows a simple performance comparison of semiconductor nonvolatile memories recently summarized by Schenk *et al*.[94] Each method has advantages and disadvantages. What we would like to pay attention to is the low energy consumption of FeFET using ferroelectrics. This is the reason why FeFET is expected to be applied to analog AI chips. In this way, it is expected that the application of FeFET to in-memory computing technology will be activated.

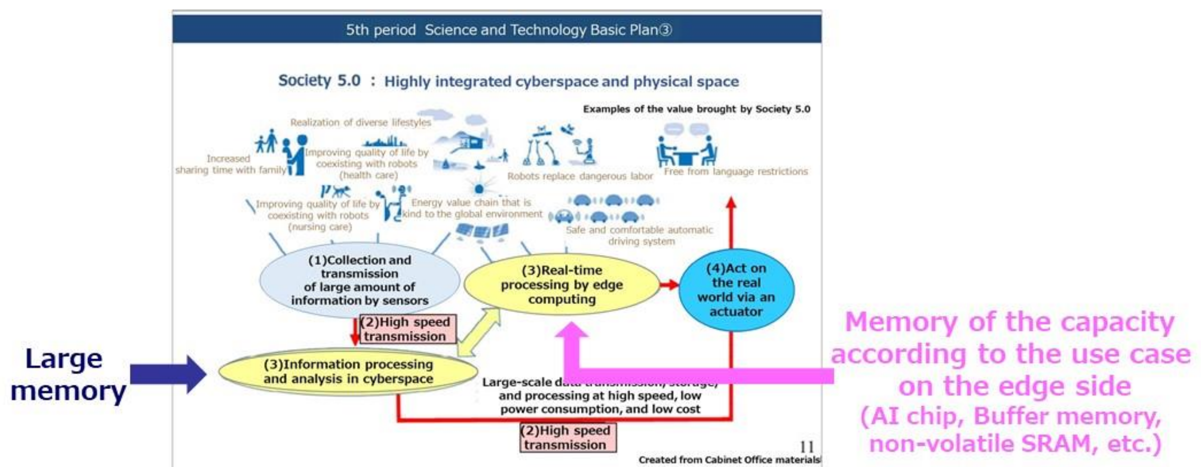

Figure 7.8 Diagram in which the author adds the use cases to Figure 1.2. Figure 1.2 is taken from the website of Ministry of Education, Culture, Sports, Science and Technology[2].

Table7.2 Simple comparison table of semiconductor nonvolatile memory extracted from ref. 94. (Only the comparison of non-volatile memory is excerpted from the original.)

Parameter/NVM	FeRAM	FeFET	MRAM	PCM	RRAM	NAND flash	NOR flash
R/W speed	10 ns	100 ns	<10 ns	>100 ns	<10 ns	100 μs	1μs to 1 s
Endurance	1×10^{15}	1×10^{5}	1×10^{15}	$>1 \times 10^{8}$	1×10^{9}	1×10^{4}	1×10^{6}
Retention	10 years	10 years	10 years	10 years	10 years	10 years	10 years
Energy	50 fJ bit^{-1}	<1 fJ bit^{-1}	2 pJ bit^{-1}	3 pJ bit^{-1}	50 pJ bit^{-1}	1 nJ bit^{-1}	10 nJ bit^{-1}
Cell size	$6F^2$	6-10F^2	$20F^2$	$5.5F^2$	$4F^2$	$4F^2$	$10F^2$

7.6 Summary

In this chapter, the progress of research on ferroelectric devices and materials with application to ferroelectric memories is introduced, and the research status of the ferroelectric/electrode interface in the latest material composition is also introduced. As for research on SBT film, research on the FeFET type, which is advantageous for high integration, is progressing compared to the FeRAM type. As for the device characteristics, the write cycle has reached 10^8 cycles or more, and the retention characteristic has a data retention period of 10 years, which is sufficiently good. It is considered that this is due to the accumulation of many technical knowledges regarding SBT film. For the application to FeFET, CSBT film is used in which a part of Sr site is replaced with Ca for the purpose of optimizing the coercive electric field of the ferroelectric thin film. The electronic structure of this CSBT has not yet been clarified. In order to understand in detail the effect of Ca substitution of Sr sites on electrical and electronic properties, it is expected that the analysis described in this thesis will be conducted in the future. As mentioned above, the basic characteristics of FeFETs using SBT thin films are good, but SBT have a weak point that the ferroelectric characteristics deteriorate when the film thickness is reduced due to the size effect. The thickness limit is said to be approximately 100 nm with conventional technology, and the 130 nm generation of the CMOS process is considered to be suitable. On the other hand, when the possibility of miniaturization was estimated from the theoretical lower limit of the

size of the ferroelectricity development of SBT, it became clear that there was room for further miniaturization. For SBT and CSBT films, it is expected that the basic data collection will be enhanced with the miniaturization in mind.

The HfO_2-based thin film, whose ferroelectricity was discovered by a German research group in 2011, has the property of compensating for the weakness of existing materials such as SBT-based materials, that is, the ferroelectric property does not deteriorate even if the film thickness is thin. Moreover, since it is a material that has been used in the CMOS process, it has good compatibility with the CMOS process and microfabrication. Here, a comprehensive comparison of the physical properties and device properties of conventional materials and HfO_2 was performed. HfO_2-FeFET has a result in 28nm generation process, and is leading in miniaturization and advanced integration. However, there is a problem in the write cycle, and detailed understanding of the electronic structure at the interface is essential for solving the problem. With regard to HfO_2-based ferroelectric thin films, development of device integration has been preceded, and basic research in areas such as the electronic structure of interfaces is in progress at the same time. Research using a method similar to the analysis method described in this thesis will become active.

In order to anticipate the future of non-volatile memories using ferroelectrics, detailed comparisons were made using some literature data on some of these promising ferroelectric materials. From the data of P_r, E_c, and film thickness, it was reconfirmed that HfO_2 system is suitable for miniaturization and advanced integration. On the other hand, the CSBT in which a part of Sr site of SBT is replaced

with Ca has high P_r and high E_c without excessive Bi. Therefore, the CSBT film may be able to be smaller and more highly integrated than SBT film. However, since CSBT film mainly has point data with a loose design, it is desirable to enrich the basic data including verification of miniaturization.

With regard to the application and development of FeRAM and FeFET, non-volatile semiconductor memory is indispensable as a technology for realizing Society 5.0, so there are expectations for future development. Edge computing is a new feature in Society 5.0. There is a need for energy efficient AI chips, and analog AI chips are expected. Studies have been proposed for using FeFET as a non-volatile memory arranged at a cross point in an analog AI chip. It is expected that the application of FeFET to in-memory computing technology will be activated.

Chapter 8 Conclusions

8.1 Summary of this thesis

Ferroelectrics are smart materials that are expected to be applied to various devices. One of the typical forms when a ferroelectric is applied to a device is a ferroelectric thin film capacitor, such as that used for FeRAM. $SrBi_2Ta_2O_9$ (SBT), which is a bismuth layered ferroelectric, has a fatigue-free and low leakage current, which make it an attractive material for FeRAM applications. However, since it contains a highly volatile element called bismuth (Bi), it is necessary to understand the effect of Bi on the electrical properties and electronic structure. The purpose of this study was to clarify the interfacial properties between SBT film and platinum (Pt) electrodes for the Pt/SBT/Pt capacitor, especially the effect of Bi, by making full use of the measurement of electrical properties and surface analysis. Another purpose is to clarify the composition ratio of the SBT thin film that achieves both high ferroelectric properties and stable contact properties with electrode materials.

Using the RTA process, the optimal crystallization process of SBT thin film by spin coating was derived. The high $2P_r$ values of 20 $\mu C/cm^2$ were obtained. It was understood that fabrication an SBT layer as a seed layer and volatilizing Bi in grain boundaries effectively with RTA process caused good surface morphology. It is expected to have good ferroelectric properties for Sr-deficient and Bi-excess SBT by replacing Bi with Sr site. On the other hand, it was also clarified from the results of

composition analysis that surplus Bi was present on the surface. Bi present on the surface may affect the electrical characteristics, especially the contact characteristics with the electrode.

I have found from leakage current data that simple Schottky behavior is characteristic of nearly stoichiometric SBT film on Pt, with a barrier height of 0.9 eV, but that Ohmic or quasi-Ohmic contact can be dominant in the Pt/SBT/Pt specimens with Bi-excess SBT film. The current–temperature dependence of Pt/Bi-excess SBT/Pt can be explained quantitatively via the Rose's theory based on the existence of traps. This is the first attempt to apply the Rose's theory to ferroelectric thin films. XPS depth profiling data show that significant Bi diffusion into the Pt electrode occurs in the Bi-excess SBT film. This Bi diffusion seems to make the ferroelectric-Pt contact unstable, perhaps by forming $PtBi_2$ which does not result in the Schottky contact but instead the Ohmic one. This Ohmic high conductivity junction produces space-charge-limited currents above 2 V. This work therefore suggests that for the device applications stable SBT-Pt Schottky contacts will require control of Bi in SBT thin film.

The occupied density of states near the bandgap of SBT has been investigated using XPS and UPS and the measured results for Bi-stoichiometric SBT film are comparable with theoretical results. For Bi-excess SBT film, the UPS measurements revealed the presence of states in the bandgap. These additional occupied states are extended up to approximately 2.7 eV above the top of the valence band, and the effective surface bandgap is therefore significantly smaller than the bulk bandgap 4.2 eV. It was also found that these band gap states are

likely due to Bi segregated on the surface by XPS measurement results that emphasized information from the surface. The bandgap states influence the Pt/SBT contact properties, particularly current-voltage dependence, and it is considered that they can cause the Ohmic contact properties of the Bi-excess SBT/Pt junction.

An attempt was made to construct a device model by integrating the results of the current-voltage characteristics and the results of the electronic structure. From optical measurements and XPS analysis results, the band gap and electron affinity of SBT were required to be 4.2 eV and 3.5 eV, respectively. Using these values and considering that the work function of Pt is 5.3 eV, the Schottky barrier height at the SBT/Pt interface at 0 V is estimated to be 1.8 eV. When excessive Bi exists at the interface between the SBT film and the Pt electrode, a part of the platinum electrode may form an alloy with Bi at the interface with the SBT film, or Bi that does not form an alloy may exist. In addition to these, a model in which the semiconductor Bi_2O_3 exists between Pt and SBT film was also considered. In that case, the Schottky barrier height at the interface with SBT film will be low, and it will be possible to become quasi-Ohmic especially at the contact between Bi and SBT film. In the presence of an external electric field, it is necessary to consider the electron barrier lowering due to image field effect correction for the Schottky contact. It is difficult to accurately estimate this effect, but it is estimated that the maximum amount of reduction is 0.7 eV. The Schottky barrier height is estimated to be 1.4 eV when the reduction effect is maximum. Although there are still some differences, it is close to the Schottky barrier height derived from the current-voltage characteristics of 0.9 - 1.0 eV.

The optimal SBT thin film composition to achieve both high ferroelectric characteristics and stable contact characteristics with electrodes was considered. The precise control of the Bi composition ratio while keeping the Sr deficiency and Bi excess composition ratio is the key issue. The amount of Bi that can be substituted for vacancy on the Sr site was estimated with reference to the results reported by Shimakawa *et al*.[31)] Considering together with the experimental results of changing the composition ratio of Sr and Bi, the optimum composition ratio of the film was Sr/Bi/Ta=0.9/2.1/2.0. In film formation by spin coating, Bi, which is originally in an easily movable state, easily moves during the heat treatment. Therefore, a method of forming a film while heating the substrate, such as sputtering or ALD, is preferable. This is because it becomes possible to incorporate Bi into the film structure at the time of film formation. Furthermore, it was proposed to intentionally create a Bi composition distribution in the film thickness direction, assuming that Bi will diffuse to some extent. By this measure, it is expected that high ferroelectric characteristics and stable contact characteristics with electrodes can be achieved at the same time.

The progress of research on ferroelectric memories and ferroelectric materials with application to ferroelectric memories is introduced, and the research status of the ferroelectric/electrode interface in the latest material composition is also introduced. As for research on SBT family, it was found that the CSBT film in which a part of Sr site was replaced with Ca exhibited higher remanent polarization value and higher coercive electric field than the SBT film. Furthermore, the CSBT film has a high remanent polarization value without excessive Bi, and has the potential to solve our problems concerning Bi by the material itself. There is

progress in research on FeFET using this CSBT film. Although it was verified with a size that was not miniaturized, the write cycle has reached 10^8 cycles or more, and the retention characteristic has a data retention period of 10 years, which are sufficiently good. It is considered that these are the characteristics of the SBT film that are strong against fatigue. On the other hand, the SBT and CSBT films still have issues regarding miniaturization.

From the viewpoint of miniaturization, the fact that ferroelectric properties have been found in HfO_2-based thin films in recent years is significant. Since it is a material that has been used in the CMOS process, it has good compatibility with the CMOS process and microfabrication. HfO_2-FeFET has a result in 28 nm generation process, and is leading in advanced integration. However, there is a problem in the write cycle, and detailed understanding of the electronic structure at the interface is essential for solving the problem.

On the other hand, for the SBT film, which has not been studied for miniaturization, the possibility of miniaturization was estimated from the theoretical lower limit of the grain size that exhibits ferroelectricity. As a result, it was found that the potential for miniaturization was higher than that of the PZT film. Verification of miniaturization of the SBT family is expected, including CSBT, which has high ferroelectric properties.

As a future application destination of non-volatile memory using ferroelectrics, efforts toward realizing Society 5.0 are promising. Edge computing is a new feature there. There is a need for energy efficient AI chips, and analog AI chips are expected. Studies have been proposed for using FeFET as a non-volatile

memory arranged at a cross point in an analog AI chip. It is expected that the application of FeFET to in-memory computing technology will be activated.

8.2 Conclusions of this thesis

In this thesis, the science and engineering of the interface regarding the capacitor structure in which a complex oxide ferroelectric thin film is sandwiched between metal thin films is pursued with the motif of the ferroelectric material called SBT, which is characterized by the ferroelectric properties of fatigue free. The existence of Bi, which is highly volatile and easily diffused at the interface, adversely affects the characteristics of the interface between the SBT film and the electrode, which was derived from the results of several verifications presented this time. On the other hand, SBT film exhibits high ferroelectric properties by substituting Bi for part of the Sr site. It was also shown that it is necessary to target the Bi-rich composition rather than the stoichiometric composition ratio. It is necessary to solve the trade-off between these Bi composition ratios. The author has proposed a structure in which a film with a basic composition of Sr/Bi/Ta=0.9/2.1/2.0 is sandwiched from the top and bottom with 0.9/2.0/2/0 composition with slightly reduced Bi as the optimum composition. This is exactly the proposal made by the deep digging of interface science and engineering from the viewpoint of both macroscopic physical properties, mainly current-voltage characteristics, and microscopic physical properties such as the level in the band gap. And the author believes that the composition ratio structure proposed here will be easily realized if the film formation by ALD that enables precise composition control is developed for SBT film.

The author worked on this research about 20 years ago. At that time, research on FeRAM type ferroelectric memory was actively conducted in the world. Although a part of the developed FeRAM has been commercialized, it has not yet made a big movement in the market as a product. The reason for this is that the complex oxide material formation process lacks compatibility with the CMOS process, and the instability of the characteristics of the ferroelectric substance that plays a leading role. This is partly due to the problems related to interfaces as dealt in this thesis. Recently, however, expectations for using FeFET for AI chips used in neural networks have increased. This is because FeFET type ferroelectric memory, which consumes an extremely little energy, is considered suitable for multiply-accumulate operations of analog AI chips with excellent energy efficiency. Attention in this application area has a great impact. In that context, it seems meaningful to issue this thesis at this timing, which discusses the basic aspects of science and engineering of the interface between the ferroelectric and the electrode. This is because the interface engineering will become more important in the research of miniaturization for practical use in the future. Therefore, such a method of exploring both macro and micro approaches should be modeled for research aimed at improving the characteristics of ferroelectric memories and putting them to practical use.

8.3 Future direction

The author has been studying SBT film. On the other hand, in recent years, it has been found that ferroelectricity is exhibited in HfO_2 film, and the miniaturization verification of the ferroelectric memory has been rapidly advanced. This is because HfO_2 film has long been used as a high-k film in the CMOS process and has high compatibility with the CMOS process. We are pleased to see progress in miniaturization verification of ferroelectric memories using HfO_2 film as a motif. On the other hand, since HfO_2 ferroelectric films are characterized by a high coercive electric field of 1 MV/cm, they must be operated under a high electric field of several MV/cm. The reliability under this high electric field will need to be verified in the future. On the other hand, SBT film has the potential to be miniaturized one step or two steps ahead of PZT film, according to my estimation. Therefore, SBT film featuring fatigue free is considered to have less concern about reliability, and its value can be expected to increase. We hope that further research on SBT film will proceed using the optimum composition proposed by the author in this thesis. Furthermore, recent studies have shown that by substituting a part of the Sr site of SBT with Ca, a higher remanent polarization value and a higher coercive electric field than SBT can be obtained without excessive Bi. If excessive Bi is unnecessary in CSBT, the risk of delicate Bi in SBT film is reduced. However, regarding the CSBT film, there are still few data on the interface characteristics with the electrode, and the behavior of Bi has not yet been clarified. The author would like to expect CSBT

film from the collection of basic physical property data. Moreover, since verification of miniaturization has not progressed for both SBT and CSBT films, the author hopes that the technological development and miniaturization verification required for miniaturization will proceed in the future. For example, if ALD, *etc*., capable of forming a film with precise composition control is developed, miniaturization verification of SBT and CSBT films will proceed. And at that time, interface engineering using both macro and micro approaches discussed in this thesis will become even more important.

References

1) From the website of the Cabinet Office, Japanese Government. <https://www8.cao.go.jp/cstp/english/society5_0/index.html>

2) From the website of the Ministry of Education, Culture, Sports, Science and Technology, Japan. <https://www.mext.go.jp/b_menu/shingi/gijyutu/gijyutu2/015-8/shiryo/_icsFiles/afieldfile/2017/08/16/1393681_4_1.pdf>

3) K. Hosokawa, "AI computing hardware," OYO BUTURI, 88, 5, p.357 (2019), in Japanese.

4) M. Jerry, P. Y. Chen, J. Zhang, P. Sharma, K. Ni, S. Yu and S. Datta, "Ferroelectric FET Analog Synapse for Acceleration of Deep Neural Network Training," IEDM Technical Digest, 6.2.1-4 (2017).

5) Y. Long, D. Kim, E. Lee, P. Saha, B. A. Mudassar, X. She, A. I. Khan and S. Mukhopadhyay, "A Ferroelectric FET-Based Processing-in-Memory Architecture for DNN Acceleration," IEEE Journal on Exploratory Solid-State Computational Devices and Circuits, 5, 113 (2019).

6) Y. Luo, P. Wang, X. Peng, X. Sun and S. Yu, "Benchmark of Ferroelectric Transistor-Based Hybrid Precision Synapse for Neural Network Accelerator," IEEE Journal on Exploratory Solid-State Computational Devices and Circuits, 5, 142 (2019).

7) M. Harada, M. Takahashi, S. Sakai and T. Morie, "A time-domain analog

weighted-sum calculation circuit using ferroelectric-gate field-effect transistors for artificial intelligence processors," Japanese Journal of Applied Physics, 59, 040604 (2020).

8) J. Valasek, "Piezoelectric and Allied Phenomena in Rochelle Salt," Physical Review, 15, 537 (1920).

9) J. L. Moll and Y. Tarui, "A new solid state memory resistor," IEEE Transactions on Electron Devices, ED-10, 333 (1963).

10) J. F. Scott, "Ferroelectric Memories," (Springer, Berlin, 2000).

11) J. F. Scott and C. A. Araujo, "Ferroelectric Memories," Science, 246, 1400 (1989).

12) C. A. Paz de Araujo, J. D. Cuchiaro, L. D. McMillan, M. C. Scott, and J. F. Scott, "Fatigue-free ferroelectric capacitors with platinum electrodes," Nature, 374, 627 (1995).

13) T. Kawai, "Kienai IC memory," (Kougyochosakai, Tokyo, 1996), in Japanese.

14) B. Aurivillius, "Mixed bismuth oxides with layer lattices: I. Structure type of $CaBi_2B_2O_9$," Arkiv Kemi, 1, 463 (1949).

15) B. Aurivillius, "Mixed bismuth oxides with layer lattices II. Structure of $Bi_4Ti_3O_{12}$," Arkiv Kemi, 1, 499 (1949).

16) G. A. Smolenski, V. A. Isupov and A. I. Agranovskaya, "Ferroelectrics of the Oxygen-Octahedral Type with Layered Structure," Soviet Physics, Solid State, 3, 651 (1961).

17) E. C. Subbarao, "A family of ferroelectric bismuth compounds," Journal of

Physics and Chemistry of Solids, 23, 665 (1962).

18) R. E. Newnham, R. W. Wolfe and J. F. Dorrian, “Structural basis of ferroelectricity in the bismuth titanate family,” Materials Research Bulletin, 6, 1029 (1971).

19) M. Kimura, “Study on orientation control of bismuth layered compound and its piezoelectric properties,” (Dissertation, Nara Institute of Science and Technology, 2008).

20) D. P. Vijai and S. B. Desu, “Electrodes for $PbZr_xTi_{1-x}O_3$ Ferroelectric Thin Films,” Journal of The Electrochemical Society, 140, 2640 (1993).

21) K. Watanabe, J. F. Tressler, M. Sadamoto, C. Isobe and M. Tanaka, “Characterization of Solution Derived RuO_2 Electrodes for $Pb(Zr,Ti)O_3$ Microcapacitors,” Journal of The Electrochemical Society, 143, 3008 (1996).

22) C. D. Gutleben, Y. Ikeda, C. Isobe, A. Machida, T. Ami, K. Hironaka, and E. Morita, “The Microstructure of $SrBi_2Ta_2O_9$ Films,” Materials Research Society Symposium Proceedings, 415, 201 (1996).

23) K. Watanabe, M. Tanaka, N. Nagel, K. Katori, M. Sugiyama, H. Yamoto, and H. Yagi, “Development of a New Annealing Process to Allow New Top Electrode Materials for $SrBi_2Ta_2O_9$ Capacitors,” Integrated Ferroelectrics, 17, 451 (1997).

24) K. Watanabe, A. J. Hartmann, R. N. Lamb and J. F. Scott, “A Comparison of Schottky-Limited and Space-Charge-Limited Currents in $SrBi_2Ta_2O_9$ Thin Films,” Integrated Ferroelectrics, 21, 241 (1998).

25) K. Watanabe, A. J. Hartmann, R. N. Lamb and J. F. Scott, “Electronic

Characteristics of the $SrBi_2Ta_2O_9$-Pt Junction," Journal of Applied Physics, 84, 2170 (1998).

26) K. Watanabe, A. J. Hartmann, R. N. Lamb, R. P. Craig, S. M. Thurgate, and J. F. Scott, "Valence Band and Bandgap States of Ferroelectric $SrBi_2Ta_2O_9$ Thin Films," Japanese Journal of Applied Physics, 39, L309 (2000).

27) K. Watanabe, A. J. Hartmann, and J. F. Scott, "A novel fabrication method for stoichiometric strontium bismuth tantalate thin films for memory devices," Applied Physics A, 70, 243 (2000).

28) T. Atsuki, N. Soyama, T. Yonezawa, and K. Ogi, "Preparation of Bi-Based Ferroelectric Thin Films by Sol-Gel Method," Japanese Journal of Applied Physics Part 1, 34, 5096 (1995).

29) T. Noguchi, T. Hase and Y. Miyasaka, "Analysis of the Dependence of Ferroelectric Properties of Strontium Bismuth Tantalate (SBT) Thin Films on the Composition and Process Temperature," Japanese Journal of Applied Physics Part 1, 35, 4900 (1996).

30) K. Miura, and M. Tanaka, "The Effect of Bi Ions Substituting at the Sr Site in $SrBi_2Ta_2O_9$," Japanese Journal of Applied Physics, 37, 2554 (1998).

31) Y. Shimakawa, Y. Kudo, Y. Nakagawa, T. Kamiyama, H. Asano, and F. Izumi, "Crystal structures and ferroelectric properties of $SrBi_2Ta_2O_9$ and $Sr_{0.8}Bi_{2.2}Ta_2O_9$," Applied Physics Letters, 74, 1904 (1999).

32) T. Ami, K. Hironaka, C. Isobe, N. Nagel, M. Sugiyama, Y. Ikeda, K. Watanabe, A. Machida, K. Miura, and M. Tanaka, "Preparation and Properties of ferroelectric $Bi_2SrTa_2O_9$ thin films for FeRAM using Flash-MOCVD," Materials

Research Society Symposium Proceedings, 415, 195 (1996).

33) T. Jimbo, H. Sano, Y. Takahashi, H. Funakubo, E. Tokumitsu and H. Ishiwara, "Preparation of $SrBi_2Ta_2O_9$ Thin Films by Liquid-Delivery Metalorganic Chemical Vapor Deposition using a Double Alcoholate Source," Japanese Journal of Applied Physics 38, 6456 (1999).

34) K. Suu, T. Masuda, Y. Nishioka and N. Tani, "Preparation of $SrBi_2Ta_2O_9$ ferroelectric thin film by rf magnetron sputtering," Integrated Ferroelectrics, 21, 407 (1998).

35) C. Bae, J. K. Lee, S. H. Lee, Y. B. Park and H. J. Jung, "Role of abnormal grain growth on the ferroelectric properties of $SrBi_2Ta_2O_9$ thin films fabricated by R.F. Magnetron sputtering," Integrated Ferroelectrics, 21, 419 (1998).

36) H. J. Cho, W. Jo, and T. W. Noh, "Leakage current behaviors in rapid thermal annealed $Bi_4Ti_3O_{12}$ thin films," Applied Physics Letters, 65, 1225 (1994).

37) H. Watanabe, T. Mihara, H. Yoshimori, and C. A. Paz de Araujo, "Preparation of Ferroelectric Thin Films of Bismuth Layer Structured Compounds," Japanese Journal of Applied Physics Part 1 34, 5240 (1995).

38) T. Nakamura, Y. Nakao, A. Kamisawa, and H. Takasu, "Preparation of $Pb(Zr,Ti)O_3$ thin films on electrodes including IrO_2," Applied Physics Letters, 65, 1522 (1994).

39) J. S. Lee, H. J. Kwon, Y. W. Jeong, H. H. Kim, S. J. Hyun and T. W. Noh, "Structural characterization of the low-temperature phase in Sr–Bi–Ta–O films," Applied Physics Letters, 74, 2690 (1999).

40) H. Okamoto, "The Bi-Pt (Bismuth-Platinum) system," Journal of Phase

Equilibria, 12, 2, 207 (1991)

41) A. J. Hartmann, R. N. Lamb, J. F. Scott, and C. D. Gutleben, “The bandgap of $SrBi_2Ta_2O_9$,” Integrated Ferroelectrics, 18, 101 (1997).

42) J. F. Scott, “The Physics of Ferroelectric Ceramic Thin Films for Memory Applications,” Ferroelectrics Review, 1, 1 (1998).

43) S. M. Sze, “Physics of Semiconductor Devices,” (Wiley, New York, 1981).

44) N. J. Seong and S. G. Yoon, “Effect of second phase on the electrical properties of $SrBi_2Ta_2O_9$ (SBT) thin films deposited at 550°C by PEMOCVD,” Integrated Ferroelectrics, 21, 207 (1998).

45) J. F. Scott, B. M. Melnick, J. D. Cuchiaro, R. Zuleeg, C. A. Paz de Araujo, L. D. McMillan, and M. C. Scott, “Negative differential resistivity in ferroelectric thin-film current-voltage relationships,” Integrated Ferroelectrics, 4, 85 (1994).

46) H. D. Chen, K. R. Udayakumar, K. K. Li, C. J. Gaskey, and L. E. Cross, “Dielectric breakdown strength in sol-gel derived PZT thick films,” Integrated Ferroelectrics, 15, 89 (1997).

47) J. F. Scott, C. A. Paz de Araujo, B. M. Melnick, L. D. McMillan, and R. Zuleeg, “Quantitative measurement of space-charge effects in lead zirconate-titanate memories,” Journal of Applied Physics, 70, 382 (1991).

48) C. Hamann, B. Burghardt, and T. Frauenheim, “Electrical Conduction Mechanism in Solids,” (VEB, Berlin, 1988).

49) A. Rose, “Space-Charge-Limited Currents in Solids,” Physical Review 97, 1538 (1955).

50) A. Rose, “Concepts in Photoconductivity and Allied Problems,” (Krieger, New York, 1978).

51) J. F. Scott, “Prospects for Gigabit ferroelectric nonvolatile memories using strontium bismuth tantalate thin films,” AIP Conference Proceedings, 436, 294 (1998).

52) A. J. Hartmann, C. D. Gutleben, G. Foran, C. Whitby, C. Isobe, K. Watanabe, R. N. Lamb, and J. F. Scott, “Atomic environment of tantalum in the intermediate fluorite phase of $SrBi_2Ta_2O_9$ thin films,” Ferroelectrics 23, 75 (1997).

53) C. D. Gutleben, “Band alignments of the platinum/$SrBi_2Ta_2O_9$ interface,” Applied Physics Letters, 71, 3444 (1997).

54) “Handbook of Chemistry and Physics,” edited by R. C. Weast (CRC, Boca Raton, FL, 1978).

55) J. Roberton, C. W. Chen, W. L. Warren and C. D. Gutleben, “Electronic structure of the ferroelectric layered perovskite $SrBi_2Ta_2O_9$,” Applied Physics Letters, 69, 1704 (1996).

56) P. Pertosa, G. Hollinger and F. M. Michel-Calendini, “Covalency effects in transition-metal perovskitelike compounds: Partial densities of *p* and *d* states and photoelectron valence-band spectra,” Physical Review B 18**,** 5177 (1978).

57) A. J. Hartmann, R. N. Lamb, J. F. Scott, P. N. Johnston, M. E. Bouanani, C. W. Chen and J. Robertson, “Surface characterisation of strontium-bismuth tantalate (SBT) thin films,” Integrated Ferroelectrics, 23, 113 (1999).

58) K. Komorita, T. Nishinaga and M. Nisio, "Oxidation of the Bismuth Thin Films," Shinku, 21, 196 (1978), in Japanese.

59) A. Li, D. Wu, H. Ling, T. Yu, M. Wang, X. Yin, Z. Liu and N. Ming, "Effects of processing on the characteristics of $SrBi_2Ta_2O_9$ films prepared by metalorganic decomposition," Journal of Applied Physics, 88, 1035 (2000).

60) M. Takahashi, M. Noda and M. Okuyama, "Photoyield and x-ray-photoelectron spectroscopic studies of O_2-annealing effects on $SrBi_2Ta_2O_9$ thin films prepared by pulsed laser deposition," Journal of Applied Physics, 94, 1912 (2003).

61) J. S. Kim, C. H. Yang, S. G. Yoon, W. Y. Choi and H. G. Kim, "The low temperature processing for removal of metallic bismuth in ferroelectric $SrBi_2Ta_2O_9$ thin films," Applied Surface Science, 140, 150 (1999).

62) J. F. Scott, "Dielectric breakdown in high-ε films for ulsi DRAMs: III. Leakage current precursors and electrodes," Integrated Ferroelectrics, 9, 1 (1995).

63) I. Pasti and S. Mentus, "DFT study of adsorption of hydrogen and carbon monoxide on Pt_xBi_{1-x}/Pt(111) bimetallic overlayers: correlation to surface electronic properties," Physical Chemistry Chemical Physics, 11, 6225 (2009).

64) Y. Huang, L. Mi, X. Liu, S. Bi and H. J. Seo, "Band structure, photochemical properties and luminescence characteristics of (Ni,F)-doped α-Bi_2O_3 nanorods via facile hydrothermal synthesis," Journal of Physics D: Applied Physics, 52, 025101 (2019).

65) B. M. Melnick, J. Abrokwah, J. Hallmark and B. Ooms, “Bismuth based layered perovskite thin films as a charge storage material for low power nonvolatile GaAs memory applications,” Integrated Ferroelectrics, 15, 221 (1997).

66) V. Joshi, C. P. Dacruz, J. D. Cuchiaro, C. A. Araujo and R. Zuleeg, “Analysis of C-V and I-V data of BST thin films,” Integrated Ferroelectrics, 14, 133 (1997).

67) E. Tokunaga and H. Ishiwara, “Operation Principle and Development Trend of Transistor-Type Ferroelectric Memories,” Hyomen Gijutsu 51, 7, p.669 (2000), in Japanese.

68) W. Zhang, M. Takahashi, Y. Sasaki, M. Kusuhara and S. Sakai, “3.3 V write-voltage Ir/$Ca_{0.2}Sr_{0.8}Bi_2Ta_2O_9$/$HfO_2$/Si ferroelectric-gate field-effect transistors with 10^9 endurance and good retention,” Japanese Journal of Applied Physics 56, 04CE04 (2017).

69) Z. Song, G. Li, Y. Xiong, C. Cheng, W. Zhang, M. Tang, Z. Li and J. He, “Multistate storage nonvolatile memory device based on ferroelectricity and resistive switching effects of $SrBi_2Ta_2O_9$ films,” Semiconductor science and technology, 33, 055009 (2018).

70) E. A. Eliseev, A. V. Semchenko, Y. M. Fomichov, M. D. Glinchuk, V. V. Sidsky, V. V. Kolos, Y. M. Pleskachevsky, M. V. Silibin, N. V. Morozovsky and A. N. Morozovska, “Surface and finite size effects impact on the phase diagrams, polar, and dielectric properties of (Sr,Bi)Ta_2O_9 ferroelectric nanoparticles,”

Journal of Applied Physics, 119, 204104 (2016).

71) M. Takahashi, W. Zhang and S. Sakai, “High-Endurance Ferroelectric NOR Flash Memory Using (Ca,Sr)$Bi_2Ta_2O_9$ FeFETs,” Proceeding of 2018 IEEE 10th International Memory Workshop, p.58-61.

72) W. Zhang, M. Takahashi and S. Sakai, “Investigation of Ferroelectric Grain Sizes and Orientations in Pt/$Ca_xSr_{1-x}Bi_2Ta_2O_9$/Hf–Al–O/Si High Performance Ferroelectric-Gate Field-Effect-Transistors,” Materials 12, 399 (2019).

73) R. R. Das, P. Bhattacharya, W. PE´ REZ and R. S. Katiyar, “Influence of Ca on Structural and Ferroelectric Properties of Laser Ablated $SrBi_2Ta_2O_9$ Thin Films,” Japanese Journal of Applied Physics 42, 162 (2003).

74) T. Tsukamoto and S. Ando, Chapter 2 Section 7 of “Kyouyudentai hakumaku no gousei to debaisu kaihatsu,” (TIC, Kyoto, 2014), in Japanese.

75) T. S. Boscke, J. Muller, D. Brauhaus, U. Schroder and U. Bottger, “Ferroelectricity in hafnium oxide thin films,” Applied Physics Letters, 99, 102903 (2011).

76) M. H. Park, H. J. Kim, Y. J. Kim, W. Lee, H. K. Kim and C. S. Hwang, “Effect of forming gas annealing on the ferroelectric properties of $Hf_{0.5}Zr_{0.5}O_2$ thin films with and without Pt electrodes,” Applied Physics Letters, 102, 112914 (2013).

77) A. Chernikova, M. Kozodaev, A. Markeev, D. Negrov, A. Gruvermann and A. Zenkevich, “Ultrathin $Hf_{0.5}Zr_{0.5}O_2$ Ferroelectric Films on Si,” ACS Applied Materials & Interfaces, 8, 7232 (2016).

78) T. Mikolajick, U. Schroeder, P. D. Lomenzo, E. T. Breyer, H. Mulaosmanovic,

M. Hoffmann, T. Mittmann, F. Mehmood, B. Max and S. Slesazeck, “Next Generation Ferroelectric Memories enabled by Hafnium Oxide,” IEDM Technical Digest, 15.5.1-4 (2019).

79) X. Sang, E. D. Grimley, T. Schenk, U. Schroeder, and J. M. LeBeau, “On the structural origins of ferroelectricity in HfO_2 thin films,” Applied Physics Letters, 106, 162905 (2015).

80) T. Shimizu, K. Katayama, T. Kiguchi, A. Akama, T. Konno, O. Sakata and H. Funakubo, “The demonstration of significant ferroelectricity in epitaxial Y-doped HfO_2 film,” Scientific Reports 6, 32931 (2016).

81) K. Katayama, T. Shimizu, O. Sakata, T. Shiraishi, S. Nakamura, T. Kiguchi, A. Akama, T. Konno, H. Uchida and H. Funakubo, “Growth of (111)-oriented epitaxial and textured ferroelectric Y-doped HfO_2 films for downscaled devices,” Applied Physics Letters, 109, 112901 (2016).

82) J. Muller, T. S. Boscke, U. Schroder, S. Mueller, D. Brauhaus, U. Bottger, L. Frey and T. Mikolajick, “Ferroelectricity in Simple Binary ZrO_2 and HfO_2,” Nano Letters, 12, 4318 (2012).

83) S. Mueller, J. Muller, A. Singh, S. Riedel, J. Sundqvist, U. Schroeder and T. Mikolajick, “Incipient Ferroelectricity in Al-Doped HfO_2 Thin Films,” Advanced Functional Materials, 22, 2412 (2012).

84) T. Yu, Z. X. Shen, W. S. Toh, J. M. Xue and J. Wang, “Size effect on the ferroelectric phase transition in $SrBi_2Ta_2O_9$ nanoparticles,” Journal of Applied Physics, 94, 618 (2003).

85) H. Huang, C. Q. Sun, Z. Tianshu and P. Hing, "Grain-size effect on ferroelectric $Pb(Zr_{1-x}Ti_x)O_3$ solid solutions induced by surface bond contraction," Physical Review B, 63, 184112 (2001).

86) T. Mihara, H. Yoshimori, H. Watanabe and C. A. Paz de Araujo, "Characteristics of Bismuth Layered $SrBi_2Ta_2O_9$ Thin-Film Capacitors and Comparison with $Pb(Zr, Ti)O_3$," Japanese Journal of Applied Physics 34, 5233 (1995).

87) J. F. Scott, "Device Physics of Ferroelectric Thin-Film Memories," Japanese Journal of Applied Physics 38, 2272 (1999).

88) A. Kumar, S. Mondal and K. S. R. K. Rao, "Tunable band alignment and dielectric constant of solution route fabricated $Al/HfO_2/Si$ gate stack for CMOS applications," J. Appl. Phys. 121, 85301 (2017).

89) X. Zhang, M. Takahashi, K. Takeuchi and S. Sakai, "64 kbit Ferroelectric-Gate-Transistor-Integrated NAND Flash Memory with 7.5 V Program and Long Data Retention," Japanese Journal of Applied Physics 51, 04DD01 (2012).

90) J. A. Rodriguez, C. Zhou, T. Graf, R. Bailey, M. Wiegand, T. Wang, M. Ball, H.C. Wen, K.R. Udayakumar, S. Summerfelt, T. San and T. Moise, "High Temperature Data Retention of Ferroelectric Memory on 130nm and 180nm CMOS," Proceeding of 2016 IEEE 8th International Memory Workshop, p.5-8.

91) M. Trentzsch, S. Flachowsky, R. Richter, J. Paul, B. Reimer, D. Utess, S. Jansen, H. Mulaosmanovic, S. Müller, S. Slesazeck, J. Ocker, M. Noack, J. Müller, P. Polakowski, J. Schreiter, S. Beyer, T. Mikolajick and B. Rice, "A

28nm HKMG super low power embedded NVM technology based on ferroelectric FETs," IEDM Technical Digest, 11.5.1-4 (2016).

92) T. Francois, L. Grenouillet, J. Coignus, P. Blaise, C. Carabasse, N. Vaxelaire, T. Magis, F. Aussenac, V. Loup, C. Pellissier, S. Slesazeck, V. Havel, C. Richter, A. Makosiej, B. Giraud, E. T. Breyer, M. Materano, P. Chiquet, M. Bocquet, E. Nowak, U. Schroeder and F. Gaillard, "Demonstration of BEOL-compatible ferroelectric $Hf_{0.5}Zr_{0.5}O_2$ scaled FeRAM co-integrated with 130nm CMOS for embedded NVM applications," IEDM Technical Digest, 15.7.1-4 (2019).

93) M. Kobayashi, "Current status and challenges of emerging ferroelectric-HfO_2 based memory devices," OYO BUTURI, 89, 6, p.314 (2020), in Japanese.

94) T. Schenk, M. Pesic, S. Slesazeck, U. Schroeder and T. Mikolajick, "Memory technology—a primer for material Scientists," Reports on Progress in Physics, 83, 086501 (2020).

List of Journals

Journal that published the main part of this thesis

1. K. Watanabe, A. J. Hartmann, R. N. Lamb, R. P. Craig, S. M. Thurgate and J. F. Scott, “Valence Band and Bandgap States of Ferroelectric $SrBi_2Ta_2O_9$ Thin Films,” Japanese Journal of Applied Physics, 39, L309 (2000).
2. K. Watanabe, A. J. Hartmann and J. F. Scott, “A novel fabrication method for stoichiometric strontium bismuth tantalate thin films for memory devices,” Applied Physics A, 70, 243 (2000).
3. K. Watanabe, A. J. Hartmann, R. N. Lamb and J. F. Scott, “Electronic Characteristics of the $SrBi_2Ta_2O_9$-Pt Junction,” Journal of Applied Physics, 84, 4, 2170 (1998).
4. K. Watanabe, A. J. Hartmann, R. N. Lamb and J. F. Scott, “A Comparison of Schottky-Limited and Space-Charge-Limited Currents in $SrBi_2Ta_2O_9$ Thin Films,” Integrated Ferroelectrics, 21, 241 (1998).
5. K. Watanabe, M. Tanaka, N. Nagel, K. Katori, M. Sugiyama, H. Yamoto, and H. Yagi, “Development of a New Annealing Process to Allow New Top Electrode Materials for $SrBi_2Ta_2O_9$ Capacitors,” Integrated Ferroelectrics, 17, 451 (1997).

Other journals

6. K. Watanabe, M. Tanaka, E. Sumitomo, K. Katori and H. Yagi, "Spin-coated ferroelectric $SrBi_2Nb_2O_9$ thin films," Applied Physics Letters, 73, 1, 126 (1998).
7. K. Watanabe, M. Ami and M. Tanaka, "Properties of Polycrystalline $SrRuO_3$ Thin Films on Si Substrates," Materials Research Bulletin, 32, 1, 83 (1997).
8. K. Watanabe, J. F. Tressler, M. Sadamoto, C. Isobe and M. Tanaka, "Characterization of Solution Derived RuO_2 Electrodes for $Pb(Zr, Ti)O_3$ Microcapacitors," Journal of The Electrochemical Society, 143, 9, 3008 (1996).

Conference presentation list

1. K. Watanabe, A. J. Hartmann, R. N. Lamb, R. P. Craig, S. M. Thurgate and J. F. Scott, "Electronic structure of layered perovskite $SrBi_2Ta_2O_9$ thin films," 13th National Congress of the Australian Institute of Physics, Fremantle, Western Australia, Australia, September 27 - October 2, 1998
2. K. Watanabe, A. J. Hartmann, R. N. Lamb and J. F. Scott, "A Comparison of Schottky-Limited and Space-Charge-Limited Currents in $SrBi_2Ta_2O_9$ Thin Films," The 10th International Symposium on Integrated Ferroelectrics, Monterey, California, USA, March 1 - March 4, 1998
3. K. Watanabe, M. Tanaka, N. Nagel, K. Katori, M. Sugiyama, H. Yamoto, and H. Yagi, "Development of a New Annealing Process to Allow New Top Electrode Materials for $SrBi_2Ta_2O_9$ Capacitors," The 9th International Symposium on Integrated Ferroelectrics, Santa Fe, New Mexico, USA, March 3 - March 5, 1997